COMPUTATIONAL
INFRASTRUCTURE FOR
GEODYNAMICS

Computational Infrastructure for Geodynamics 2016-2020 Part II: Appendices

Submitted to NSF EAR - Geoinformatics

July 1, 2015

Submitted by:

Louise H. Kellogg
University of California, Davis

22119 EPS, One Shields Avenue
University of California
530.752.2889
Davis, CA 95616
geodynamics.org

A. Research Highlights

ASPECT

Jacqueline Austermann, Jerry X. Mitrovica, Wolfgang Bangerth, and Timo Heister: *Correcting Paleo Sea Level Records for Dynamic Topography* 7

Juliane Dannberg, Zach Eilon, Rene Gassmoeller, Pritwiraj Moulik, Robert Myhill, Ulrich Faul, and Paul Asimow: *Grain size evolution in the mantle and its effect on geodynamics, seismic velocities and attenuation* 8

Juliane Dannberg and Timo Heister: *3D Compressible Melt Transport with Adaptive Mesh Refinement* 9

Juliane Dannberg and Stephan V. Sobolev: *Geodynamic modeling of low-buoyancy thermo-chemical plumes* 10

Menno R.T. Fraters, Anne C. Glerum, Cedric Thieulot, and Wim Spakman: *Thermo-mechanically coupled subduction with ASPECT: coupling AMR, nonlinear rheology and a free surface* 11

H. Fuqua, P. Bremner, M. Diamond, G. Garapic, S. Lock, A. Mallik, Y. Nishikawa, S. Panovska, A. Shahar, P. Lognonné, W. Paner, U. Faul, M. Panning, H. Jimenez-Perez, and N. Schmerr: *Consequences and Resolution of Lunar Mantle Partial Melt* 12

Anne C. Glerum, Cedric Thieulot, Menno Fraters, and Wim Spakman: *Four-dimensional Modeling of Thermo-mechanically coupled, Visco-plastic Subduction* 13

Ian Rose, Bruce Buffet, and Timo Heister: *The figure, rotation, and gravity of convecting planet*....14

Bernhard Steinberger, Rene Gassmöller, Juliane Dannberg, and Eva Bredow: *Models and observations of plume-ridge interaction in the South Atlantic and their implications for crustal thickness variations* 15

Sanne Cottaar, Timo Heister, Bob Myhill, Ian Rose, and Cayman Unterborn: *Constraining a family of allowable lower mantle compositions within seismic constraints*....16

CALYPSO

Bruce Buffett and Hiroaki Matsui: *A Power Spectrum for the Geomagnetic Dipole Moment* 17

CITCOMCU

Maxim D. Ballmer, Clinton P. Conrad, Nicholas Harmon, and Eugene I. Smith: *Non-hotspot volcano chains produced by migration of shear-driven upwelling toward the East Pacific Rise* 18

Maxim D. Ballmer, Clinton P. Conrad, and Eugene I. Smith: *Intraplate volcanism at the edges of the Colorado Plateau sustained by edge-driven convection and shear-driven upwelling* 19

Maxim D. Ballmer, Garrett Ito, and Cheng Cheng*: Double Layering and Bilateral Asymmetry of a Thermochemical Plume in the Upper Mantle beneath Hawaii* 20

Maxim D. Ballmer, Garrett Ito, Jeroen van Hunen, and Paul Tackley: *Spatial and temporal variability in Hawaiian hotspot volcanism induced by small-scale convection* 21

Maxim D. Ballmer, Todd A. Bianco, Clinton P. Conrad, and Eugene I. Smith: *The time-dependence of shear-driven upwelling* 22

Tobias Höink, Adrian Lenardic, and Mark Jellin: *Poiseuille–Couette flow in the asthenosphere and viscous coupling at the lithosphere-asthenosphere boundary* 23

Margarete A. Jadamec: *Slab driven mantle weakening and rapid mantle flow* 24

Margarete A. Jadamec and Magali Billen: *Reconciling surface plate motions with rapid three-dimensional mantle flow around a slab edge* 25

Margarete A. Jadamec and Magali Billen: *The role of rheology and slab shape on rapid mantle flow: 3D numerical models of the Alaska slab edge* 26

Margarete A. Jadamec, Magali Billen, and Sarah Roeske: *Three-dimensional numerical models of flat slab subduction and the Denali fault driving deformation in south-central Alaska* 27

Matthew H. Motoki and Maxim D. Ballmer: *Intraplate volcanism due to convective instability of stagnant slabs in the mantle transition zone* 28

Margarete A. Jadamec, Magali Billen, and Oliver Kreylos: *Three-dimensional simulations of geometrically complex subduction with large viscosity variationis* 29

CITCOMS

Katrina M. Arredondo and Magali I. Billen: *Dynamic linkages between the transition zone & surface plate motion in 2D models of subduction* 30

Clinton P. Conrad and Mark D. Behn: *Using seismic anisotropy to constrain global mantle flow and lithosphere net rotation* 31

Clinton P. Conrad, Todd A. Bianco, Paul Wessel, and Eugene I. Smith: *Asthenospheric shear controls patterns of intraplate volcanism* 32

Clinton P. Conrad, Todd A. Bianco, Benjun Wu, Eugene I. Smith, and Ashley Tibbetts: *Shear-driven upwelling: a mechanism for intraplate volcanism* 33

Clinton P. Conrad, Bernhard Steinberger, and Trond H. Torsvik: *Past mantle flow revealed by plate motion net characteristics* 34

Tobias Höink, Adrian Lenardic, and Mark Richards: *The role of the asthenosphere in maintaining plate tectonics* 35

Svetlana I. Natarov and Clinton P. Conrad: *Poiseuille flow and the depth-variation of asthenospheric shear* 36

Craig O'Neill, Adrian Lenardic, Tobias Höink, and Nicoas Coltic: *Mantle convection and outgassing on terrestrial planets* 37

Pavithra Sekhar and Scott D. King: *3D spherical models of Martian mantle convection constrained by melting history* 38

Vlada Stamenković, Tobias Höink, and Adrian Lenardic: *Temporal stress patterns in episodic plate tectonics models with implications for the initiation of plate tectonics on terrestrial planets* 39

Joost van Summeren, Clinton P. Conrad, and Eric Gaidos: *Mantle convection, tectonics, and volcanism on hot exo-Earths* 40

Joost van Summeren, Clinton P. Conrad, and Eric Gaidos: *Magnetodynamo lifetimes in rocky planets with contrasting mantle convection regimes* 41

CONMAN

Scott D. King, Daniel J. Frost, and David C. Rubie: *Why cold slabs stagnate in the transition zone* 42

GALE

Catherine M. Cooper, Meghan S Miller, Louis Moresi, and Steve Quenette: *Coupled continental-lithosphere and mantle dynamics simulation using Underworld/GALE* 43

Marcus W. Haynes, Anthony R. Budd, Ed J. Gerner, Chris Harris-Pascal and Alison L. Kirkby: A*ssessing subsurface temperatures in Australia from a geothermal systems perspective*.....44

PYLITH

Brad T. Aagaard, Charles A. Williams, and Bill Fry: *Factors contributing to multi-segment rupture in the 2010 M7.1 Darfield, New Zealand, earthquake* 45

William D. Barnhart and Rowena B. Lohman: *Evaluation of effect of salt diapirs on fault source inversions*.....46

Susan Ellis and Charles Williams: *Combining short-term and long-term stress models to evaluate stress perturbations during the 2010 Darfield, New Zealand, earthquake* 47

Scott T. Henderson and Matthew E. Pritchard: *Finite element modeling of a voluminous active intrusion in Bolivia* 48

B. Jha, F. Bottazz, R. Wojcik, M. Coccia, N. Bechor, D. McLaughlin, T. Herring, B. H. Hager, S. Mantica, and R. Juanes: *Reservoir characterization in an underground gas storage field using joint inversion of flow and geodetic data* 49

Eric O. Lindsey, Yuri Fialko, Valerie. J. Sahakian, Yehuda Bock, Sylvain Barbot, Thomas. K. Rockwell, and Roger Bilham: *High-resolution geodetic observations of fault zone deformation on the San Andreas and San Jacinto faults in southern California* 50

Douilly Roby, Hideo Aochi, Eric Calais, and Andrew M. Freed: *3D dynamic rupture simulations across interacting faults: the Mw7.0, 2010, Haiti earthquake* 51

Jeanne Sauber, Shin-Chan Han, Scott Luthcke, Natasha Ruppert, and Ron Bruhn: *Measurement and modeling of cryosphere-geosphere interactions in south central, Alaska* 52

Adrian Shelley, Martha Savage, Charles Williams, Yosuke Aoki, and Boris Gurevich: *Modeling shear wave splitting due to stress-induced anisotropy, with an application to Mount Asama Volcano, Japan* 53

Charles A. Williams and Laura M. Wallace: *Effects of material property variations on slip estimates for subduction interface slow slip events* 54

RELAX

Sylvain Barbot: *Relax: unified models of postseismic relaxation* 55

Oliver Boyd, Robert Smalley, Jr., and Yuehua Zeng: *Crustal deformation in the New Madrid seismic zone and the role of postseismic processes* 56

SELEN

Daniele Melini, Nicola Piana Agostinetti, and Giorgio Spada: *Bayesian inference of late Pleistocene deglaciation models* 57

SPECFEM2D

Ryan Modrak and Jeroen Tromp: *Nonlinear optimization algorithms for large-scale seismic waveform inversion* 58

Ping Tong, Wu Chen, Dimitri Komatitsch, Piero Basini, and Qinya Liu: *High-resolution seismic array imaging based on a SEM-FK hybrid method* 59

Yanhua O. Yuan, Frederik J. Simons, and Ebru Bozdag: *Full-waveform-difference adjoint tomography based on a wavelet multiscale analysis* 60

SPECFEM3D

Ping Tong, Dimitri Komatitsch, Tai-Lin Tseng, Shu-Huei Hung, Chin-Wu Chen, Piero Basini, and Qinya Liu: *A 3D spectral-element and frequency-wavenumber (sem-fk) hybrid method for high-resolution seismic array imaging* 61

P. Galvez, J.-P. Ampuero, L.A. Dalgue, S.N. Somala, and T. Nissen-Meyer: *Dynamic earthquake rupture and the 2011 M9 Tohoku earthquake* 62

Herurisa Rusmanugroho, Ryan Modrak, and Jeroen Tromp: *Seismic imaging for TTI based on adjoint methods* 63

Dimitri Komatitsch and Paul Cristini: *Use of acoustic wave modeling for ocean acoustics and for non-destructive testing of materials* 64

Carene S. Larmat, Monica Maceira, Robert W. Porritt, David M. Higdon, Charlotte A. Rowe, and Richard M. Allen: *Validation of western North America models based on finite-frequency and ray theory imaging methods*.....65

Ulrika Miller and Carl Tape: *The effect of topography on the seismic wavefield* 66

Youyi Ruan, Samuel Bell, and Donald Forstyh: *Toward adjoint tomography of 3D structure of the Juan de Fuca plate and Cascadia Trench* 67

Carl Tape and Emanuele Casarotti: *Numerical resolution of seismic wavefield simulations in southern California* 68

Carl Tape and Vipul Silwal: *Seismic wavefield simulations of earthquakes within a complex crustal model for Alaska* 69

SPECFEM3D CARTESIAN

Carene S. Larmat and David W. Steedman, Esteban Rougier, and Chris R. Bradley: *Coupling hydrodynamic and wave propagation modeling for waveform modeling of SPE* 70

SPECFEM3D GLOBE

Ebru Bozdag, Matthieu Lefebvre, Wenjie Lei, Daniel Peter, James Smith, Dimitri Komatitsch, and Jeroen Tromp: *Global adjoint tomography* 71

Hom Nath Gharti and Jeroen Tromp: *Efficient numerical solution of global dynamic and quasistatic problems using a spectral-infinite-element method* 72

Matthieu Lefebvre: *High-performance I/O for large scale seismic imaging computations* 73

Wenjie Lei, Youyi Ruan, Ebru Bozdag, Matthieu Lefebvre, James Smith, and Jeroen Tromp: *Global structure of the crust and upper mantle based on adjoint tomography* 74

Michael Afanasiev, Andreas Fichtner, Daniel Peter, Laura Ermert, Korbinian Sager, and Saulé Zukauskaité: *Towards a comprehensive seismic earth model across the scales* 75

Brian Savage, Chistina Mornecy, Jeroen Tromp, and Arthur Rodgers: *Short-period, anelastic and anisotropic, waveform-based 3D Middle East model* 76

James Smith, Wenjie Lei, Jeroen Tromp, Lion Krischer, and Ludwig Maximillian: *An adaptable seismic data format suitable for large seismic inversions including global adjoint tomography* 77

SW4

Andrea Chiang, Douglas S. Dreger, Arben Pitarka, and Sean R. Ford: *The effects of 3D heterogeneity on regional moment tensor source-type discrimination* 78

TERRAFERMA

Marc Spiegelman, Dave May, and Cian Wilson: *Brittle Solvers: Lessons and insights into effective solvers for visco-plasticity in geodynamics* 79

Cian Wilson and Marc Spiegelman: *TerraFERMA: The transparent finite element rapid model assembler* 80

Cian Wilson, Marc Spiegelman, Peter van Keken, and Brad Hacker: *Advanced fluid flow modeling in subduction zones using TerraFERMA: The role of solid rheology and compaction pressure* 81

VIRTUALQUAKE

Kasey W. Schultz, Michael K. Sachs, Eric M. Heien, John B. Rundle, and Don L. Turcotte: *Simulating gravity changes and InSAR interferograms in topologically realistic driven fault networks* 82

Yi-Hsuan Wu, Chein-Chih Chen, Eric M. Heien, and John B. Rundle: *An earthquake model for studying interaction of faults and earthquake simulations in Taiwan* 83

M.R. Yoder, K.W. Schultz, E.M. Heien, J.B. Rundle, D.L. Turcotte, J.W. Parker, and A. Donnellan: *The Virtual Quake earthquake simulator: A simulation based forecast of the El Mayor-Cucapah region and evidence of earthquake predictability*.....84

Correcting Paleo Sea Level Records for Dynamic Topography

Jacqueline Austermann, Jerry X. Mitrovica, Wolfgang Bangerth, Timo Heister

Changes in the global mean sea level (GMSL) during the ice age are crucial indicators of climate variability. Reconstructions of GMSL are widely based on local sea level records, which have to be corrected for glacial isostatic adjustment (GIA) and dynamic topography (DT) to calculate the GMSL.

We are particularly interested in the GMSL during the mid-Pliocene warm period (MPWP, ~3 Ma), which was characterized by slightly elevated temperatures and is therefore an ideal testing ground for investigating ice sheet stability in a warmer world. GMSL change since the MPWP has been a source of contention and has been estimated anywhere in the range 0-50m. Improved models of Earth deformation are needed to refine this estimate and bring it in agreement with dynamic ice sheet models. Rowley et al. (2013) have shown that models of mantle convection can reproduce dynamic topography changes that are visible in the elevation of a mid-Pliocene shoreline along the US East coast; however, a robust inference of GMSL from the GIA and DT corrected shoreline was not possible. To address this issue – both for the US shoreline and an increasing database of mid-Pliocene shorelines from other locations (Australia, South Africa and Argentina) – we are using ASPECT to revisit dynamic topography changes over the past 3 Myr.

To date, we have used ASPECT to compute dynamic topography and have benchmarked our results using a simple 2-D box model case. We have also computed dynamic topography on a spherical shell with the Gypsum tomography model (see Figure) and are currently working on benchmarking this prediction with the results shown in Rowley et al. (2013). In the next step, ASPECT will allow us to explore a much wider parameter space of viscosity in an attempt to reconcile the ancient shoreline records using a single GMSL value.

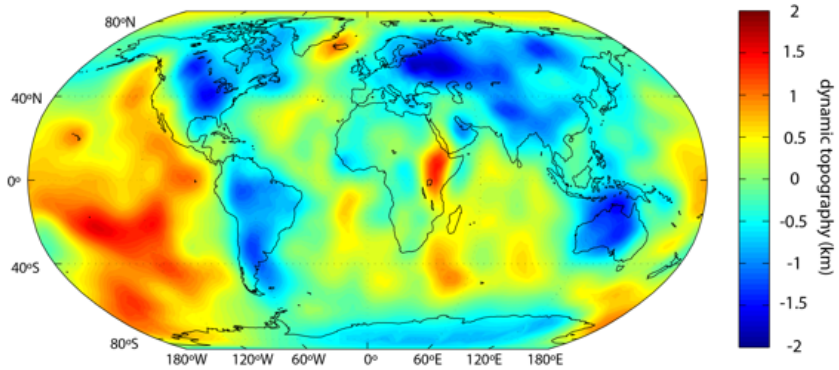

Present-day dynamic topography calculated from the density converted Gypsum tomography model (without crustal correction) and Earth-like values for viscosity, thermal expansivity and conductivity.

CIG Code: ASPECT

References:

Rowley, D. B., Forte, A.M.,Moucha, R.,Mitrovica, J. X., Simmons, N. A., & Grand, S. P., 2013. Dynamic topography change of the eastern United States since 3 million years ago. Science, 340, 1560–1563.

Grain size evolution in the mantle and its effect on geodynamics, seismic velocities and attenuation

Juliane Dannberg, German Research Centre for Geosciences Potsdam GFZ, Zach Eilon, Lamont-Doherty Earth Observatory, Rene Gassmoeller, German Research Centre for Geosciences Potsdam GFZ, Pritwiraj Moulik, Lamont Doherty Earth Observatory, Robert Myhill, Bayerisches Geoinstitut, Universitaet Bayreuth, Ulrich Faul, Massachusetts Institute of Technology, Paul Asimow, California Institute of Technology

Dynamic models of Earth's convecting mantle usually implement flow laws with constant grain size, stress-independent viscosity and a limited treatment of variations associated with changes in mineral assemblage. These simplifications greatly reduce computational requirements but preclude effects such as shear localisation and transient changes in rheology associated with phase transitions, which have the potential to fundamentally change flow patterns in the mantle.

Here we use the finite-element code ASPECT to model grain size evolution and the interplay between grain size, stress and strain rate in the convecting mantle. We include the simultaneous and competing effects of dynamic recrystallisation resulting from work done by dislocation creep, grain growth in multiphase assemblages and recrystallisation at phase transitions. Grain size variations also affect seismic properties of mantle materials. We use several published formulations to relate intrinsic variables (P, T, and grain size) from our numerical models to seismic velocity (Vs) and attenuation (Q).

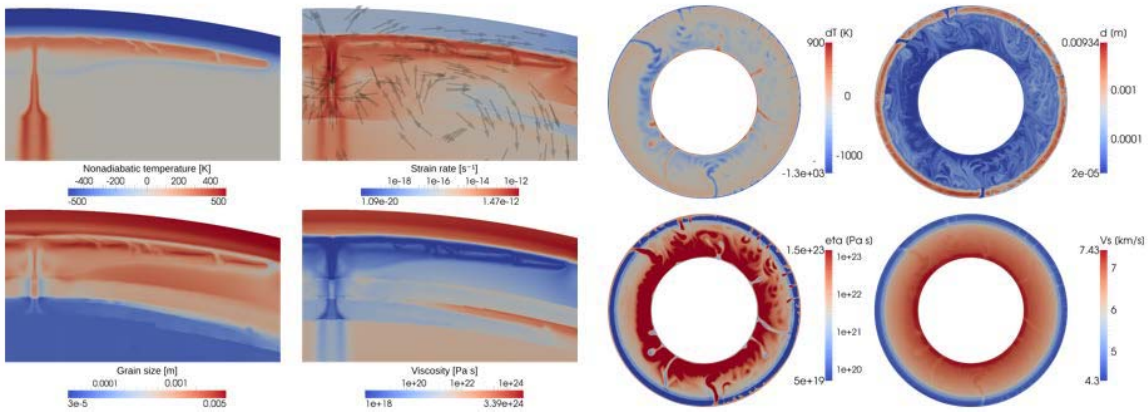

Figure 1: Images of the temperature, velocities, grain size and viscosity in a regional (left) and a global (right) mantle convection model incorporating grain size evolution.

Our models show that rapid metamorphic reactions in mantle upwellings and downwellings lead to high lateral viscosity contrasts, as a result of gradual grain size evolution. Positive feedback between grain size reduction and viscosity reduction results in shear localization (Fig. 1). As a result, the edges of thermal plumes have smaller grain sizes and lower viscosities than their cores. Dynamic recrystallisation in subducting slabs results in lower seismic velocities and Q than would be predicted from purely thermal models.

CIG Code(s): ASPECT

Acknowledgements: This work is based on a project started at the CIDER 2014 summer program.

3D Compressible Melt Transport with Adaptive Mesh Refinement

Juliane Dannberg, German Research Centre for Geosciences Potsdam GFZ, Timo Heister, Clemson University

Melt generation and migration have been the subject of numerous investigations, but their typical time and length-scales are vastly different from mantle convection, which makes it difficult to study these processes in a unified framework. In addition, modeling magma dynamics poses the challenge of highly non-linear and spatially variable material properties, in particular the viscosity. Applying adaptive mesh refinement to this type of problems is particularly advantageous, as the resolution can be increased in mesh cells where melt is present and viscosity gradients are high, whereas a lower resolution is sufficient in regions without melt. In addition, considering volume changes due to compressibility in both the solid and the fluid phase ensures self-consistency of models that strive to link melt generation to processes in the deeper mantle.

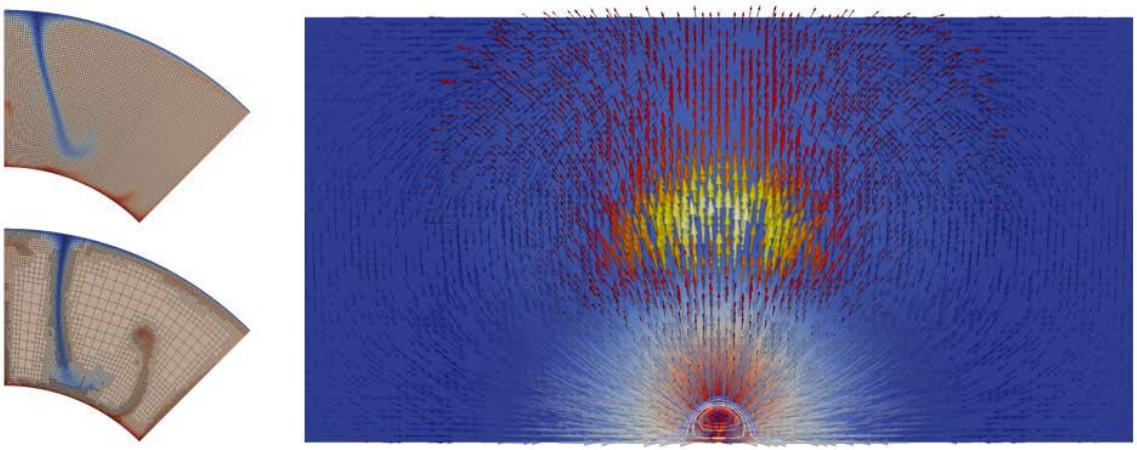

Left: Model of mantle convection without (top) and with (bottom) adaptive mesh refinement, illustrating how the resolution is increased where the gradients of a field (in this case the temperature) are high. Right: Image of a rising diapir, showing the porosity (background color), the region where melt is generated (isocontours) and solid (blue arrows) and melt (red and yellow arrows) velocities.

Our extension of the finite-element mantle convection code ASPECT allows for solving additional equations describing the behaviour of silicate melt percolating through and interacting with a viscously deforming host rock. We use the original compressible formulation of the McKenzie equations, augmented by an equation for the conservation of energy and including both melt migration and melt generation.
Our model of magma dynamics will provide a framework for modeling processes on different scales and investigating links between processes occurring in the deep mantle and melt generation and migration. This approach could prove particularly useful applied to modeling the generation of komatiites or other melts originating in greater depths.

CIG Code(s): ASPECT

References: Dannberg, J., Dynamics of thermo-chemical mantle plumes and plume-lithosphere interaction. PhD thesis, in preparation.

Geodynamic modeling of low-buoyancy thermo-chemical plumes

Juliane Dannberg, Stephan V. Sobolev, German Research Centre for Geosciences Potsdam GFZ

The Earth's biggest magmatic events that form Large Igneous Provinces are believed to originate from massive melting when hot mantle plumes rising from the lowermost mantle reach the base of the lithosphere. Classical models of thermal mantle plumes predict a flattening of the plume head to a disk-like structure, a kilometer-scale surface uplift just before the initiation of LIPs and thin plume tails (see figure, left panel). However, there are seismic observations and paleo-topography data that are difficult to explain with this classical approach. Here, using numerical models, we show that the issue can be resolved if major mantle plumes are thermo-chemical rather than purely thermal and contain recycled oceanic crust in the form of dense eclogite, which drastically decreases their buoyancy and makes it depth-dependent.

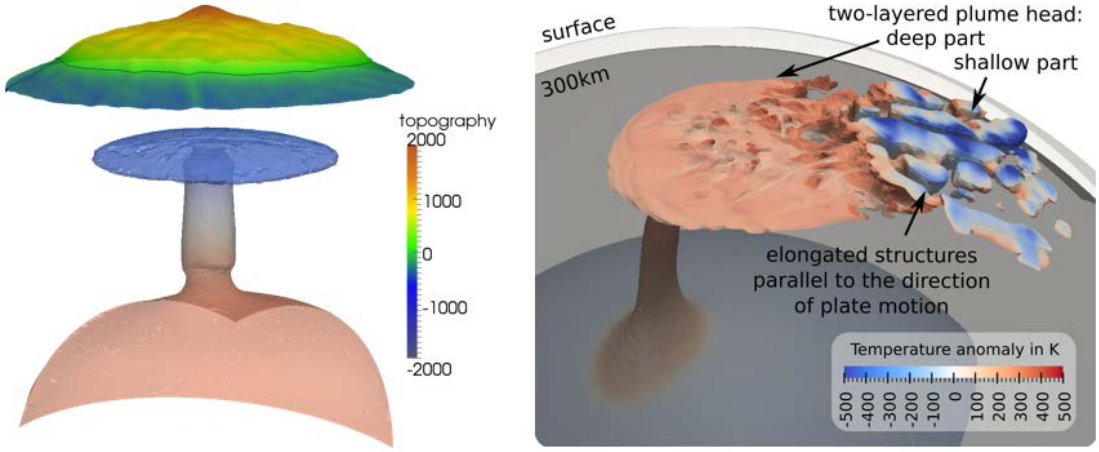

Images of the temperature field of a thermal mantle plume, together with the generated surface uplift (left), and the excess temperature of a thermochemical plume (right) showing a two-layered plume head and elongated finger-like structures parallel to the direction of plate motion.

We perform numerical experiments in a 3D spherical shell geometry to investigate the dynamics of the plume ascent, the interaction between plume- and plate-driven flow and the dynamics of melting in a plume head. For this purpose, we use the finite-element code ASPECT, which allows for complex temperature-, pressure- and composition-dependent material properties. Moreover, our models incorporate phase transitions (including melting) with the accompanying rheological and density changes.

We demonstrate that despite their low buoyancy, such plumes can rise through the whole mantle causing only negligible surface uplift. While high plume buoyancy results in plumes directly advancing to the base of the lithosphere, plumes with slightly lower buoyancy pond in a depth of 300-400 km and form pools or a second layer of hot material. These structures become asymmetric and finger-like channels begin to form when the plume gets entrained by a quickly moving overlying plate (see figure, right panel).

CIG Code(s): ASPECT

Thermo-mechanically coupled subduction with ASPECT: coupling AMR, nonlinear rheology and a free surface

Menno R.T. Fraters[1], Anne C. Glerum[1], Cedric Thieulot[1,2] and Wim Spakman[1,2], (1) Utrecht University, Earth Sciences, Utrecht, Netherlands and (2) Centre of Earth Evolution and Dynamics, Oslo, Norway

Subduction is one of the main tectonic processes on the Earth and is still under extensive investigation due to its complex nature. We investigate the link between the crust and upper mantle in these rheologically and dynamically complex zones (Fraters, 2014) using the new CIG code ASPECT, which is built on deal.II. We use a strongly nonlinear rheology which includes diffusion creep, dislocation creep and visco-plasticity (Glerum et al., in prep.) to simulate realistic lithosphere and mantle processes. To simulate topography we are using both the sticky air method (numerically challenging due to high viscosity contrast), and a true free surface, as implemented in ASPECT, as shown in the figure. We are now working to extend this to complex 3D regions like the Caribbean region.

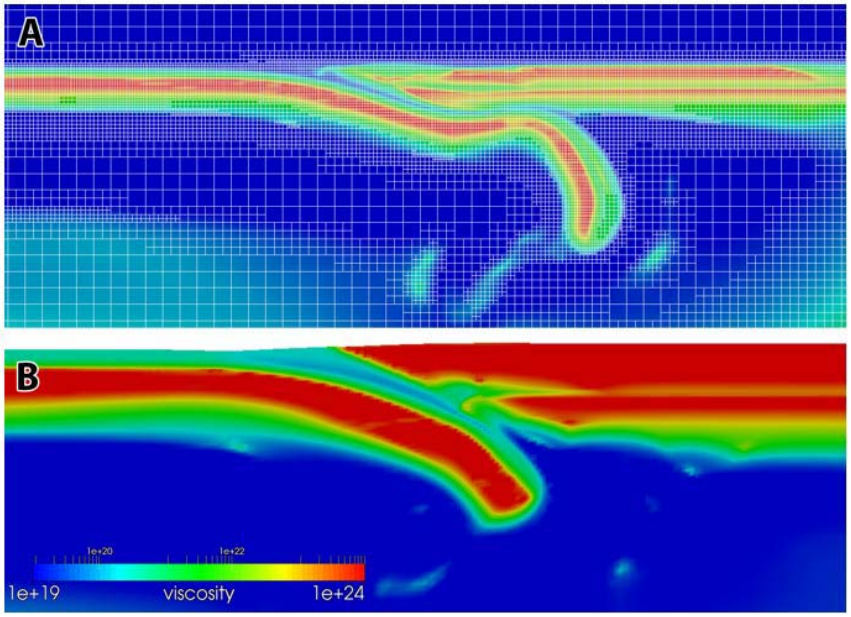

Images of the viscosity fields of two subduction models. Figure A shows a subduction model with a sticky air layer on top, showing the grid in white. Figure B shows a subduction model with a true free surface.

CIG Code(s): ASPECT and deal.ii

Acknowledgements: This research has been funded by The Netherlands Organisation for Scientific Research (NWO) and the Centre of Earth Evolution and Dynamics (CEED), University of Oslo.

References

Fraters, M.R.T. (2014), Thermo-mechanically coupled subduction modelling with ASPECT. Master's thesis, Utrecht University, Utrecht, Netherlands, http://dspace.library.uu.nl/handle/1874/297347.

Glerum, A.C., Thieulot, C., van der Berg, A., Spakman, W., Geodynamic modeling using ASPECT: Implementation and benchmarking of viscoplasticity and an application to subduction, in prep, 2015.

Consequences and Resolution of Lunar Mantle Partial Melt

H. Fuqua[1], P. Bremner[2], M. Diamond[1], G. Garapic[3], S. Lock[4], A. Mallik[5], Y. Nishikawa[6], S. Panovska[7], A. Shahar[8], P. Lognonné[6], W. Panero[9], U. Faul[10], M. Panning[2], H. Jimenez-Perez[6], N. Schmerr[11]. [1]EPS Dept., UC Berkeley; [2]Dept. of Geological Sciences, UF; [3]Dept of Geology, SUNY; [4]EPS Dept., UC Davis; [5]Dept of Earth Science, Rice; [6]Université Paris Diderot, IPGP; [7]Scripps, UCSD; [8]Geophysical Lab., Carnegie Inst. of Washington; [9]School of Earth Sciences, OSU; [10]Dept. of EAPS, MIT; [11]Dept. of Geology, UM.

Existence of a partially molten layer at depth has been proposed to explain the lack of observed far side deep moonquakes, the observation of reflected phases from deep moonquakes, and the dissipation of tidal energy within the lunar interior. However, subsequent models explore the possibility that dissipation due to elevated temperatures alone can explain the observed dissipation factor (Q) and tidal love numbers. We have explored the hypothesis that high titanium melt compositions associated with lunar mantle overturn may sink to the base of the mantle, locally or regionally. We have performed forward calculations varying composition and thickness of layers to evaluate if a partially molten layer at the base of the mantle is well constrained by the observational data. Self-consistent physical parameters are calculated for each compositional model that is then compared against the observed data to determine a subset of permissible models. The data constraints considered by this study include bulk density, moment of inertia, real and imaginary parts of the Love numbers, seismic travel times, and electrical conductivity. Dynamic calculations using ASPECT have also been considered to determine the implications of early lunar mantle convection for the survivability of the partially molten layer. Finally, and as a perspective for a future NASA New Frontiers Geophysical Network, we present 1D synthetic seismograms calculated for each proposed structure of the Moon to investigate the future seismological resolution of these deep lunar structure features.

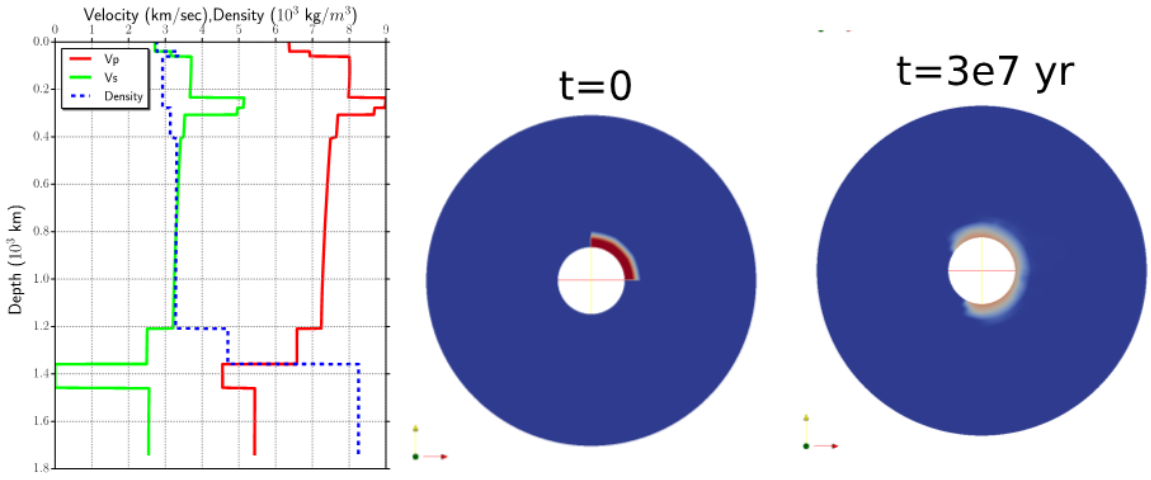

Left: Self consistent velocity (Vp,Vs) and density profiles calculated in BurnMan modified for the Moon's conductive mantle. Right: Survivability of this partial melt layer against lunar convection tested in Aspect.

CIG Codes: ASPECT, BurnMan

Acknowledgements: This project originated at the 2014 CIDER program.

Reference: Fuqua, H., et al. (2014). AGU 2014 Fall Meeting. San Francisco, California.

Four-dimensional Modeling of Thermo-mechanically coupled, Visco-plastic Subduction

Anne C. Glerum[1], Cedric Thieulot[1,2], Menno Fraters[1] and Wim Spakman[1,2]
[1]Utrecht University and [2]University of Oslo

Increasing computational resources enable investigations into modeling geodynamic processes in 3-D. For example, 3-D process modeling has been shown to be of great importance in generic subduction models (e.g. Crameri and Tackley, 2014) as well as in specific regional problems (e.g. Chertova et al., 2014). The state-of-the-art computational methods of the easily extendable Finite Element (FE) code ASPECT, such as Adaptive Mesh Refinement (AMR) and efficient solvers, make ASPECT a promising tool for our studies of regional-global subduction dynamics. We have developed, added, and benchmarked a nonlinear, visco-plastic, multi-material rheology including diffusion and dislocation creep as well as frictional plasticity (Glerum et al., in prep, 2015.). This allows us to construct thermo-mechanically coupled models of 3-D time-dependent subduction with self-consistently evolving weak zones.

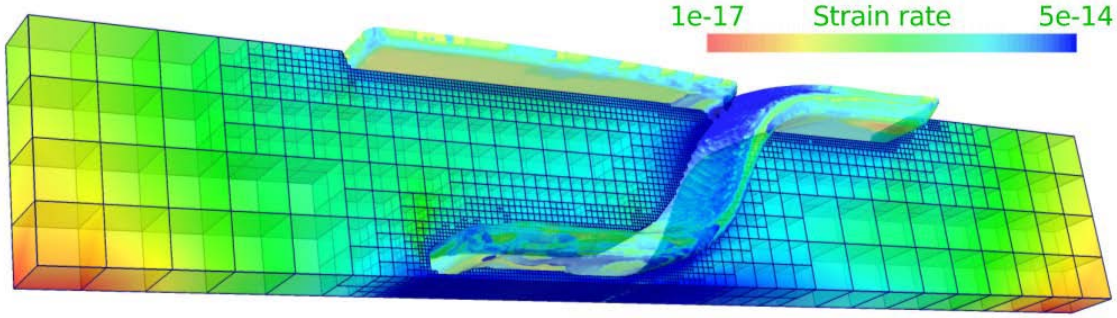

The strain rate field of an intraoceanic subduction setting after 17.5 My of subduction. The initial model set-up is based on Schellart and Moresi (2013). The Finite Element grid is shown to demonstrate ASPECT's AMR, focusing computationally expensive high resolution in and around the plates.

CIG Codes: ASPECT (built on deal.II)

Acknowledgements: This research has been funded by The Netherlands Research Centre for Integrated Solid Earth Science (ISES) and the Centre of Earth Evolution and Dynamics (CEED), University of Oslo.

References

Glerum, A., Thieulot, C., van den Berg, A. P. and Spakman, W., Geodynamic modeling using ASPECT: Implementation and benchmarking of viscoplasticity and an application to subduction, in prep.

Schellart, W. P. and Moresi, L., A new driving mechanism for backarc extension and backarc dynamic subduction models with an overriding plate, J. Geophys. Res. Solid Earth, 2013 (118), 1-28.

Chertova, M. V., Spakman, W., Geenen, T., van den Berg, A. P. and van Hinsbergen, D. J. J., Underpinning tectonic reconstructions of the western Mediterranean region with dynamic slab evolution from 3-D numerical modeling, J. Geophys. Res. Solid Earth, 2014 (119), 5876–5902.

Crameri, F. and Tackley, P. J., Spontaneous development of arcuate single-sided subduction in global 3-D mantle convection models with a free surface, J. Geophys. Res. Solid Earth, 2014 (119), 5921–5942.

The Figure, Rotation, and Gravity of Convecting Planets

Ian Rose and Bruce Buffett, University of California, Berkeley; Timo Heister, Clemson University

The low-order structure of mantle convection controls the rotational dynamics of a planet. Most previous models investigating this control have relied on Earth models with radially varying mantle rheology. We have been developing a version of ASPECT with a free surface which allows us to self-consistently calculate the figure and the geoid of a convecting mantle with lateral material properties.
In particular, this extension to ASPECT uses an arbitrary-Lagrangian-Eulerian (ALE) approach to allowing deformation of the planet, as well as dynamic remeshing of the domain to preserve mesh regularity. We have done this in a way which is agnostic to the model rheology, gravity, and geometry, so it should be applicable to other situations which call for a free surface.

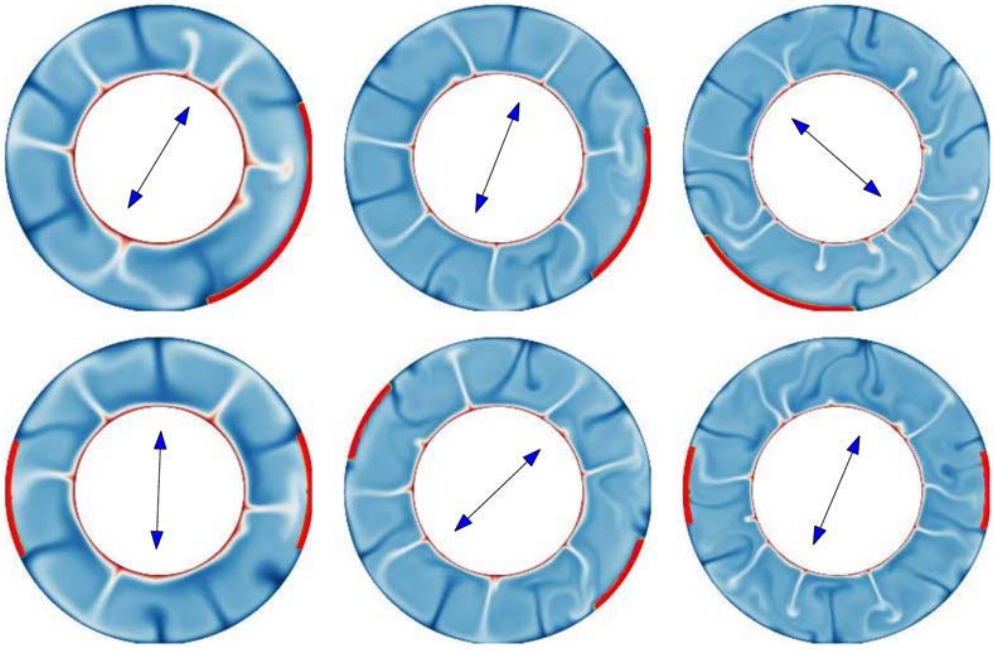

Exploring the effect of continents on the planform of convection for various sizes of continents and different Rayleigh numbers. Continents (red surface features) are represented as highly viscous, buoyant blocks which rise isostatically. The size and location of the continents control the low-order structure of mantle convection, which in turn determines the spin axis (central arrow).

We are performing numerical simulations to explore the shape, gravity, and rotation of Earth and other planetary bodies in a range of parameter space. These simulations are accompanied by scaling analyses.

CIG Code(s): ASPECT

References

Rose, I., and Buffett, B., Rates of true polar wander on convecting planets. (In preparation).
Rose, I. The figure, rotation, and gravity of convecting planets. PhD thesis.

Models and observations of plume-ridge interaction in the South Atlantic and their implications for crustal thickness variations

Bernhard Steinberger, Rene Gassmöller, Juliane Dannberg, Eva Bredow

Mantle plumes are thought to originate at thermal or thermo-chemical boundary layers, and since their origin is relatively fixed compared to plate motion they produce hotspot tracks at the position of their impingement. When plumes reach the surface close to mid-ocean ridges, they generate thicker oceanic crust due to their increased temperature and hence higher degree of melting. Observations of these thickness variations allow estimates about the buoyancy flux and excess temperature of the plume. One example is the interaction of the Tristan plume with the South Atlantic Mid-Ocean Ridge, however, conclusions about the plume properties are complicated by the fact that the Tristan plume track has both on- and off-ridge segments. In these cases, where a plume is overridden by a ridge, it is assumed that the plume flux has a lateral component towards the ridge (the plume is "captured" by the ridge). Additionally, sea floor spreading north of the Florianopolis Fracture Zone did not start until 112 Ma – at least 15 Ma after the plume head arrival – while the Atlantic had already opened south of it. Therefore, the plume is influenced by the jump in lithosphere thickness across the Florianopolis Fracture Zone. We investigate crustal thickness and plume tracks of a three-dimensional regional convection model of the upper mantle for the Tristan-South Atlantic ridge interaction. The model is created with the convection code ASPECT, which allows for adaptive finite-element meshes to resolve the fine-scale structures within a rising plume head in the presence of large viscosity variations. The boundary conditions of the model are prescribed from a coarser global mantle convection model and the results are compared against recently published models of crustal thickness in the South Atlantic and hotspot tracks in global moving hotspot reference frames.

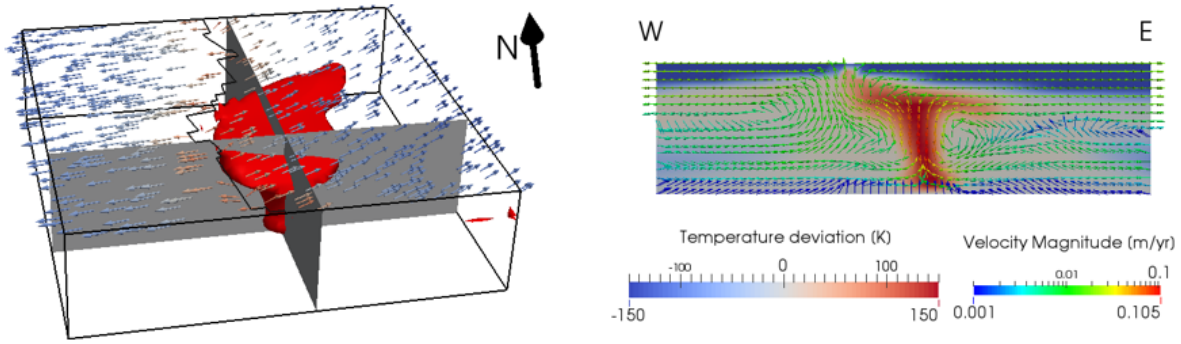

Images of the temperature and velocity field of the Tristan-Plume-South-Atlantic-Ridge interaction at a present-day state. The spreading of the plume material is strongly asymmetrical due to the 3D shape of the nearby ridge

CIG Code(s): ASPECT

Constraining a family of allowable lower mantle compositions within seismic constraints

Sanne Cottaar, University of Cambridge, Timo Heister, Clemson University, Bob Myhill, University Bayreuth, Ian Rose , University of California, Berkeley, and Cayman Unterborn, Ohio State University

The present-day bulk composition of the mantle is a topic of continuing debate and depends largely on constraining the composition of the lower mantle. While the composition of the upper mantle yields Mg/Si (atomic ratio) of ~1.3 by analyzing MORB samples (e.g. Salters and Stracke, 2004), constraining the Mg/Si ratio for the lower mantle is difficult . This uncertainty has also led to discussion of the primordial material of which the Earth is made, with proposals ranging from pyrolitic models (e.g. McDonough & Sun, 1995) to more reduced, enstatite chondrite models (e.g. Javoy et al., 2010).

Our main constraint in determining the composition of the lower mantle lies in the analysis of seismic velocities. Unfortunately, fitting a seismic velocity profile with a composition and geothermal gradient is a severely undetermined system and one needs to incorporate many more models in order to constrain the possible range of input variables in an inverse model. Some work has been done in this area (e.g. Matas et al., 2007; Cobden et al. 2009), but we plan to extend beyond fitting a 1D radial velocity model, and gather additional constraints from 3D velocity modes.

We are implementing a Bayesian inversion adopting the BurnMan code (Cottaar et al. 2014) as a forward model to include the latest results from mineral physcis as well as uncertainties on mineral physical parameters and seismic velocities.

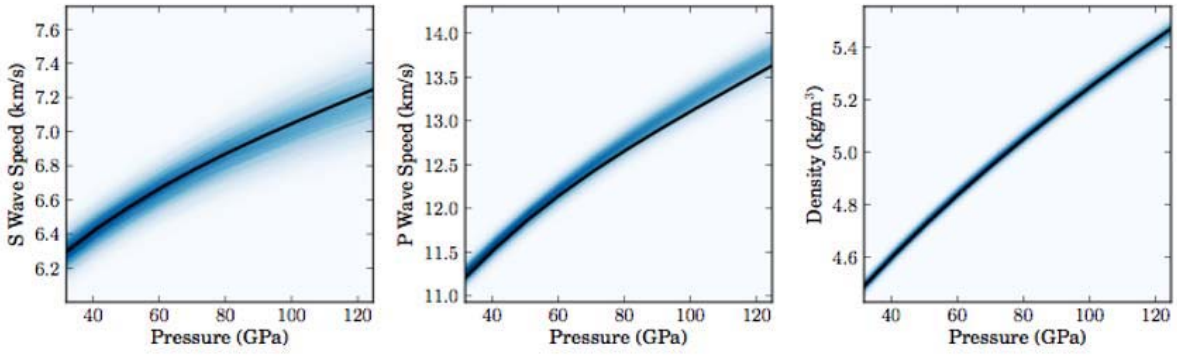

Example of 10000 realizations of seismic velocity and density using BurnMan (blue) compared to PREM (black). The composition is fixed with 67% perovskite with 7% Fe and 33% ferropericlase with 21% Fe and the temperature profile is adiabatic. The mineral physical parameters and their errors are from Stixrude and Lithigow-Bertelloni (2011) and Zhang et al. (2013). The variation results from a random perturbation of each mineral physical parameter within error bars.

CIG Code(s): BurnMan, ASPECT

Acknowledgements: This project originated at the 2012 CIDER program

References: Cottaar S., T. Heister, I. Rose and C. Unterborn, BurnMan: A lower mantle mineral physics toolkit, Geochem. Geophys. Geosys. 15(4), p. 1164–1179 (2014)

A Power Spectrum for the Geomagnetic Dipole Moment

Bruce Buffett, Department of Earth and Planetary Science, University of California, Berkeley
Hiroaki Matsui, CIG, University of California, Davis, CA 95616

A power spectrum for the geomagnetic field quantifies the observed variability and offers insights into the underlying processes. However, a quantitative interpretation requires physical models for the generation of magnetic field. Numerical geodynamo models offer insights, but concerns about unrealistic model parameters invariably complicate a direct comparison with observations. We propose an alternative approach that uses stochastic models for the axial dipole moment to construct a theoretical power spectrum. The parameters of a stochastic model can be recovered from a realization of the process, so it is possible to use paleomagnetic observations to guide the construction of a power spectrum. The same procedures can also be applied to the output of geodynamo models. By comparing the theoretical power spectrum from the stochastic model with that computed directly from the geodynamo model, we build confidence in the approach and attach physical significance to features in the resulting power spectrum. Extending these ideas to paleomagnetic observations provides a physical basis for interpreting the geomagnetic power spectrum.

The figure show a comparison of the theoretical power spectrum with the spectrum computed directly from the output of the numerical geodynamo model **Calypso**. When the theoretical spectrum for the axial dipole moment is computed with a white noise source we obtain the spectrum $S_\varepsilon(f)$. Allowing for correlated noise in the stochastic model gives the spectrum $S_e^c(f)$. Here the correlation time is tuned to fit the spectrum computed directly from Calypso. Good agreement indicates that the simple stochastic model is capable of reproducing the dipole fluctuations in the numerical dynamo model.

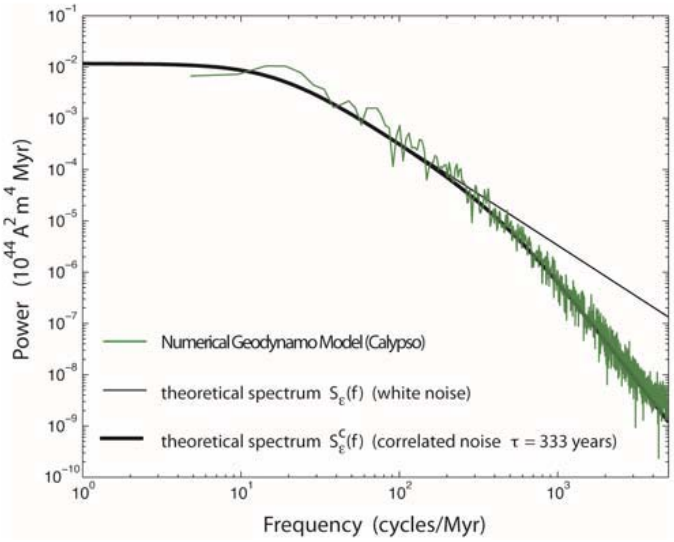

Applying stochastic model to the power spectrum from paleomagnetic observations provides constraints on dynamo processes. Based on inferences from the numerical model, we associate the corner frequency in the spectrum with the dipole decay time. Paleomagnetic observations yield a decay time of 29 kyr. The correlation time in the noise model is associated with the lifetime of convective eddies in the core. The best-fitting value inferred from paleomagnetic observations is several hundred years.

*Comparison of theoretical power spectra for dipole moment with the spectrum computed directly from the output of the numerical geodynamo model **Calypso**.*

CIG Code(s): Calypso

References: Buffett and Matsui, Earth and Planetary Science Letters, 411, 20-26, 2015.

Non-hotspot volcano chains produced by migration of shear-driven upwelling toward the East Pacific Rise

Maxim D. Ballmer, Earth-Life Science Institute, Tokyo Tech, Japan
Clinton P. Conrad, University of Hawaii
Eugene I. Smith, University Nevada Las Vegas
Nicholas Harmon, University of Southampton, UK

While most oceanic volcanism is associated with the passive rise of hot mantle beneath the spreading axes of mid-ocean ridges (MOR), volcanism occurring off-axis reflects intra-plate upper-mantle dynamics and composition, yet is poorly understood. Off the southern East Pacific Rise (SEPR), volcanism along the Pukapuka, Hotu-Matua, and Sojourn ridges has been attributed to various mechanisms, but none can reconcile its spatial, temporal, and geochemical characteristics. Our three-dimensional numerical models show that asthenospheric shear can excite upwelling and decompression melting at the tip of low-viscosity fingers that are propelled eastward by vigorous sublithospheric flow. This shear-driven upwelling is able to sustain intraplate volcanism that progresses toward the MOR, spreads laterally close to the axis, and weakly continues on the opposite plate. Thus, it can explain patterns of volcanism observed near the SEPR. Our study highlights the role of horizontal asthenospheric flow and mantle heterogeneity in producing linear chains of intraplate volcanism independent of a (deep-rooted) buoyancy source.

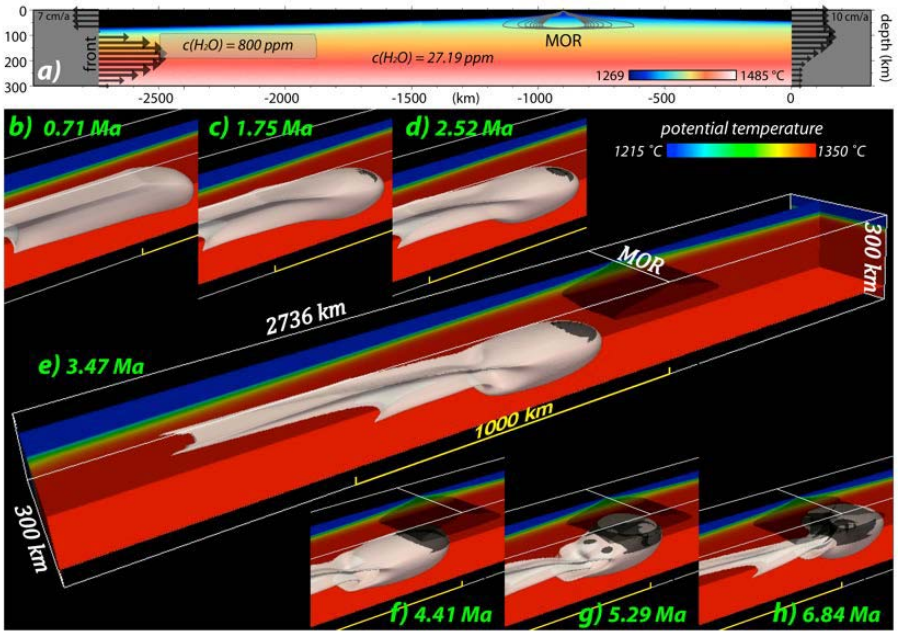

Time series of temperature (colors) and melting (black) for a numerical model of a low-viscosity pocket (grey) being drawn toward the SEPR by Poiseuille flow. Initial and boundary conditions are shown in (a). Significant melting occurs at the tip of the finger, and increases as the finger approaches the mid-ocean ridge (MOR) or SEPR.

CIG Code(s): CitcomCU

References

Ballmer, M.D., C.P. Conrad, E.I. Smith, and N. Harmon (2013), Non-hotspot volcano chains produced by migration of shear-driven upwelling toward the East Pacific Rise, *Geology, 41*, 479-482.

Intraplate volcanism at the edges of the Colorado Plateau sustained by edge-driven convection and shear-driven upwelling

Maxim D. Ballmer, Earth-Life Science Institute, Tokyo Tech, Japan
Clinton P. Conrad, University of Hawaii
Eugene I. Smith, Racheal Johnson, University Nevada Las Vegas

Although volcanism in the southwestern US has been studied extensively, its origin remains controversial. Various mechanisms such as mantle plumes, upwelling in response to slab sinking, and small-scale convective processes have been proposed, but have not been evaluated within the context of rapidly shearing asthenosphere that is thought to underlie this region. Using geodynamic models that include this shear, we here explore spatio-temporal patterns of mantle melting and volcanism near the Colorado Plateau for comparison with observations. We show that the presence of viscosity heterogeneity within an environment of asthenospheric shearing can give rise to decompression melting along the margins of the Colorado Plateau. Eastward shear flow advects pockets of asthenospheric mantle with anomalously low viscosity toward the edges of thickened lithosphere beneath the plateau, where they can induce magmatism in two ways. First, the arrival of the pockets critically changes the effective viscosity near the plateau to trigger small-scale edge-driven convection and associated decompression melting. Second, they can excite shear-driven upwelling, in which shear flow can become focused and redirected upward by the low-viscosity pocket. We find that a combination of both mechanisms can explain volcanism along the margins of the Colorado Plateau, its encroachment toward the plateau's southwestern edge, and the association of volcanism with slow seismic anomalies in the asthenosphere.

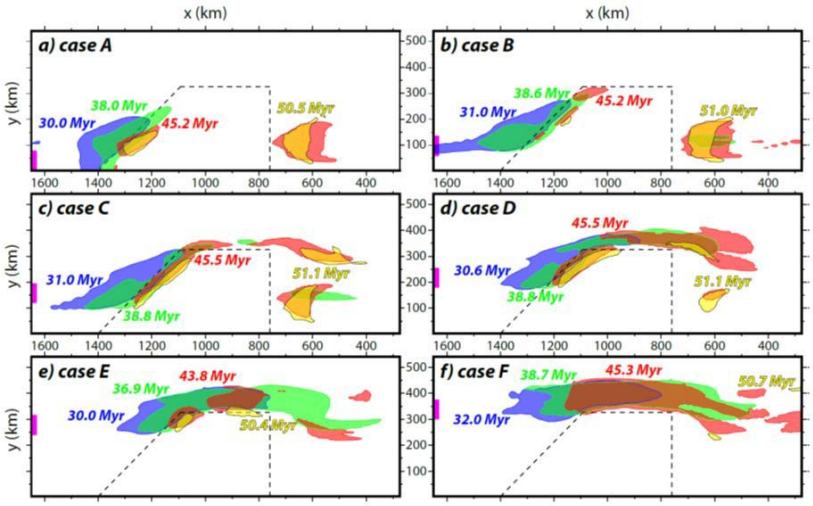

Patterns of volcanism predicted by numerical models in which a low-viscosity pocket is driven toward the thickened lithosphere of Colorado Plateau (dotted line) by east-ward mantle flow. Volcanism occurs off of the leading and trailing edges of the plateau (A-D), and along the lateral sides (D-F), depending on the impact location of the pocket into the plateau (initial y-position of the pocket is shown by pink bar). Volcanism occurring off of the leading edge slowly encroaches toward the plateau (colors).

CIG Code(s): CitcomCU

References

Ballmer, M.D., C.P. Conrad, E.I. Smith, and R. Johnsen (2015), Intraplate volcanism at the edges of the Colorado Plateau sustained by a combination of triggered edge-driven convection and shear-driven upwelling, *G-cubed,* doi:10.1002/2014GC005641.

Double Layering and Bilateral Asymmetry of a Thermochemical Plume in the Upper Mantle beneath Hawaii

Maxim D. Ballmer, Earth-Life Science Institute, Tokyo Tech, Japan; Garrett Ito, University of Hawaii; and Cheng Cheng, UC Berkeley

Classical plume theory describes purely thermal upwellings that rise through the entire mantle, pond beneath the lithospheric plate in a thin "pancake," and generate hotspot volcanism. High-resolution regional seismic tomography supports the concept of a deep-rooted mantle plume beneath the Hawaiian hotspot, but also challenges traditional concepts inasmuch as it indicates a broad low-velocity body in the upper mantle that is much thicker and more asymmetric than a thermal pancake predicted from purely thermal plume models. Geochemical observations also argue against a purely thermal (i.e., isochemical) mantle source for Hawaiian lavas and instead indicate a heterogeneous plume involving mafic lithologies such as eclogite. To explore the dynamical and melting behavior of hot plumes that also contain eclogite, we perform three-dimensional numerical simulations of thermochemical convection. The models simulate eclogite with an excess density relative to ambient-mantle peridotite that peaks at depths of 410–300 km due to solid phase changes in the quartz and olivine systems. Because of the effects of these phase transitions, a mantle plume containing >12% eclogite pools as a wide body (hundreds of kilometers wide) at depths of 450–300 km (the "deep eclogite pool", or DEP). From the top of the DEP rises a shallow and narrow plume, which supplies material into a thin sublithospheric pancake and feeds hotspot volcanism. Seismic resolution tests indicate that the double layering of hot plume material (DEP and shallow pancake) is consistent with the broad body of slow velocity material imaged by regional tomography. A more recent joint tomography model can even resolve two slow layers at depths that agree well with predicted by our numerical models. A subset of numerical models predicts pulsations in plume ascent and variations in magmatic activity over timescales of ~10 Myr, as are observed. In these models, the complex upper-mantle dynamics of the eclogitic plume moreover give rise to intermittent bilateral asymmetry in the contribution of mafic materials to partial melting, a prediction that is consistent with the geochemical distinction between the Loa and Kea trends among Hawaiian volcanoes. Therefore, a deep origin of characteristic Loa and Kea sources, as previously suggested, may not be required. Furthermore, any deep-rooted asymmetry in eclogite content of the plume is shown to be veiled by the complex dynamics of the DEP and the shallow plume. Our results reveal that phase transitions exert important effects on thermochemical convection in the upper mantle that influence the overall dynamics of mantle plumes, the genesis of intraplate volcanism, and ocean-island geochemistry.

CIG Code(s): CitcomCU

References

Ballmer, M. D., G. Ito, C. Cheng (2015), Thermochemical convection of bilaterally asymmetric plumes and implications for Hawaiian lava composition. in: Hawaiian Volcanism, From Source to Surface, edited by Carey, Poland, Cayol & Weis; AGU Monograph 208, in press

Cheng, C., R. M. Allen, R. W. Porritt, and M. D. Ballmer (2015), Seismic constraints on a double-layered asymmetric whole-mantle plume beneath Hawaii, in: Hawaiian Volcanism, From Source to Surface, edited by Carey, Poland, Cayol & Weis; AGU Monograph 208, in press

Ballmer, M. D., G. Ito, Wolfe, C. J., and Solomon, S. C. (2013): Double layering of a thermochemichal plume in the upper mantle beneath Hawaii, Earth and Planetary Science Letters, 376, 155-164, doi:10.1016/j.epsl.2013.06.022

Spatial and Temporal Variability in Hawaiian Hotspot Volcanism induced by small-scale convection

Maxim D. Ballmer, Earth-Life Science Institute, Tokyo Tech, Japan
Garrett Ito (Univ. Hawaii), Jeroen van Hunen (Durham Univ.), Paul J. Tackley (ETH Zurich)

Volcanism far from plate boundaries is often attributed to an underlying mantle plume. However, enigmatic observations of Hawaiian volcanism, such as variations in the volume of erupted volcanic material through time, a geographical asymmetry in the geochemistry of the lavas and secondary volcanism that occurs far away from the hotspot, cannot be explained by the classical mantle plume concept. Here we present a numerical model of mantle plume upwelling beneath Hawaii. We find that small-scale convection in the ambient mantle can erode the base of the lithosphere, creating a washboard topography on the underside of the plate. As the plate migrates over the upwelling plume, the plume interacts with alternating thicker and thinner sections of lithosphere to generate temporal variations in the flux of erupted volcanic material. The pre-existing washboard topography also causes the plume to spread and melt asymmetrically. In our simulations, this asymmetry in mantle flow generates an asymmetry in the chemistry of the erupted lavas. Finally, a more vigorous type of small-scale convection develops within the spreading plume, generating localized zones of upwelling well away from the hotspot. The associated magmatism is fed by chemically distinct material originating from the edges of the plume conduit. Our results show that shallow processes have an important influence on the character of volcanism fed by deep-rooted mantle plumes.

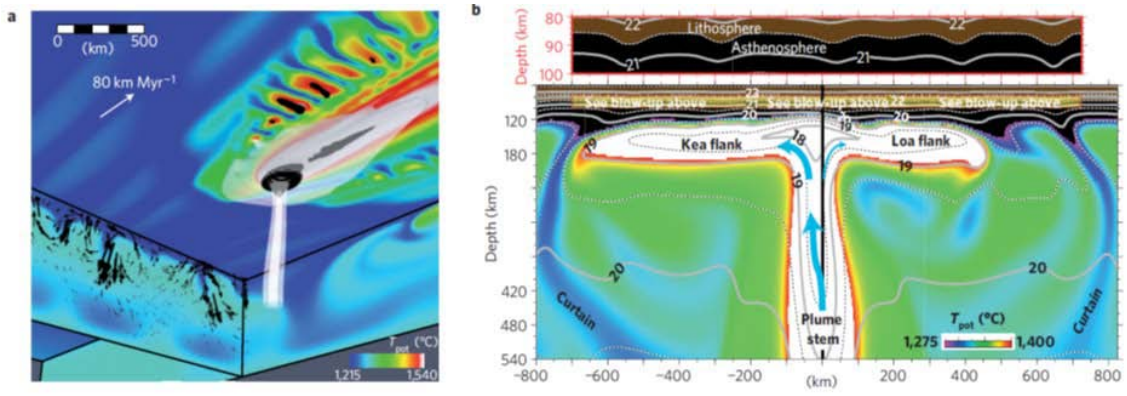

Visualization of model results. (a) Horizontal and vertical cross-sections are colored by temperature. The hotspot and secondary melting zones are in black. Isotherms of 1,550 and 1,620 °C are white. Black arrows show the direction and strength of ambient-mantle convection rolls 800 km upstream of the plume. (b) Vertical cross-section of temperature and viscosity through the upwelling plume oriented perpendicular to plate-motion. Upper panel shows a blow-up of the yellow-shaded area. Light blue arrows show the schematic flow field indicating that the plume pancake spreads asymmetrically as guided by undulations in lithospheric thickness.

CIG Code(s): CitcomCU

References

Ballmer, M. D., G. Ito, J. van Hunen, and P. J. Tackley (2011): Spatial and temporal variability in Hawaiian hotspot volcanism induced by small-scale convection, *Nature Geoscience*, *4,* 7, 457-460, doi:10.1038/ngeo1187

The Time-Dependence of Shear-Driven Upwelling

Todd A. Bianco, Clinton P. Conrad, University of Hawaii
Eugene I. Smith, University Nevada Las Vegas

Although volcanism far from tectonic boundaries is likely due to upwelling near the lithospheric base, the convective processes that induce upwelling are unclear. Numerical models show that asthenospheric shear can be deflected upward by lateral viscosity variations within the asthenosphere, producing "shear-driven upwelling" (SDU). To constrain the rate, duration, and surface expression of intraplate volcanism caused by SDU, we simulated 2D flow and peridotite melting in the upper 200 km of the mantle. Asthenospheric shear is driven by lithospheric plates with different thicknesses moving at 3-9 cm/yr, and the initial low-viscosity region is a rectangular–shaped pocket with an imposed viscosity that is two orders of magnitude smaller than the surrounding asthenosphere. Melting decreases as the pocket deforms, and reaches steady state after 3-12 Myr. The age progression of surface volcanism is nearly stationary in the reference frame of the plate, which distinguishes SDU from hotspot volcanism. Similar behavior occurs if the viscosity heterogeneity is induced by variations in the water content of mantle peridotite. If the pocket's low viscosity is caused by excess temperature, buoyant upwelling of the entire pocket dominates volcanism. We suggest that asthenospheric shear induced by plate motions and global mantle flow, by exciting SDU, drives much of the non-hotspot small-scale volcanism that occurs away from plate boundaries.

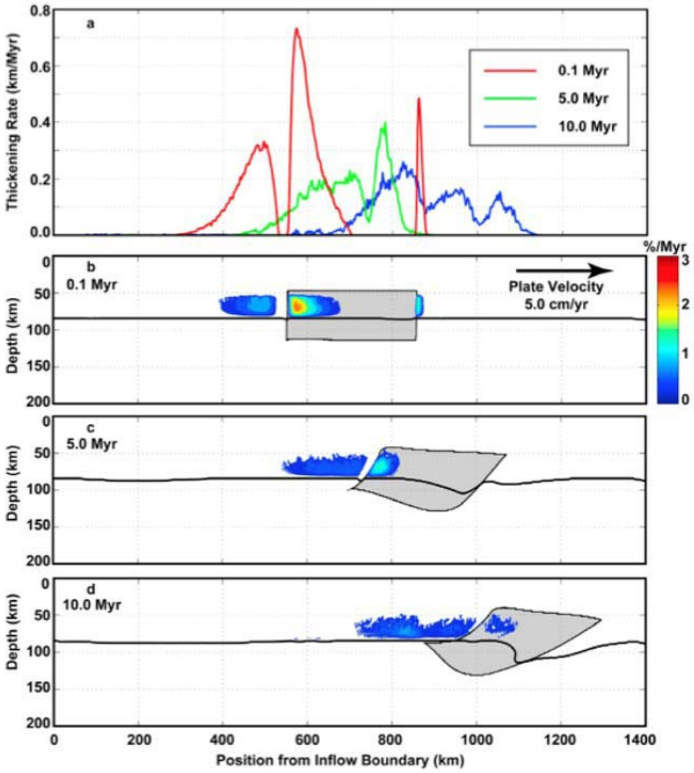

The rate of melt emplacement at the surface at 0.1 (red line), 5.0 (green line), and 10.0 (blue line) Myr due to evolving shear-driven upwelling (SDU). (b) Shear driven upwelling at 0.1 Myr. Black line is the base of residual mantle layer, gray region is the low viscosity pocket, which is two orders of magnitude less viscous than the ambient mantle. Color contours are melting rate in %/Myr. (c) As in (b) at 5.0 Myr. (d) As in (b) for 10.0 Myr.

CIG Code(s): CitcomCU

References

Bianco, T.A., C.P. Conrad, and E.I. Smith (2011), Time-dependence of intraplate volcanism caused by shear-driven upwelling of low-viscosity regions within the asthenosphere, *Journal of Geophysical Research, 116*, B11103, doi:10.1029/2011JB008270.

Poiseuille–Couette Flow In The Asthenosphere And Viscous Coupling At The Lithosphere-Asthenosphere Boundary

Tobias Höink and Adrian Lenardic, Rice Univ., and Mark Jellinek, Univ. of British Columbia

Mixed heated 3-D mantle convection simulations with a low-viscosity asthenosphere show that mantle flow in the lithosphere–asthenosphere region is a Poiseuille–Couette flow. Our simulations establish a connection between the strength of plate margins, solid-state flow in the asthenosphere and the wavelength of mantle convection, which suggests that plate tectonics in the sluggish lid mode is wavelength dependent and potentially more robust than previously envisioned.

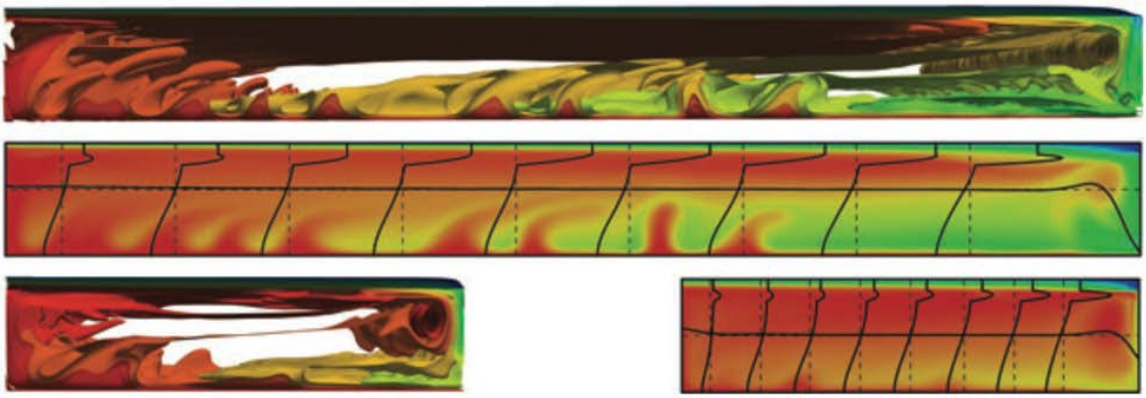

Typical flow field for 3D simulations with low-viscosity asthenosphere. Shown are temperature contours and velocity profiles.

Viscous coupling at the lithosphere-asthenosphere boundary leads to an additional plate driving force, which contributes to the observed plate velocity. The extent to which asthenosphere-drive contributes to plate motions depends on the lateral dimension of plates and on the relative viscosities and thicknesses of the lithosphere and asthenosphere.

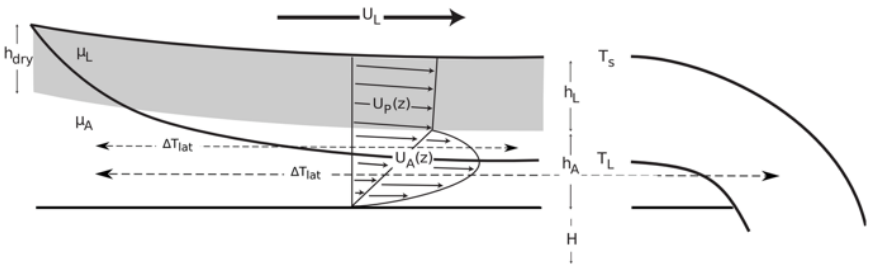

Sketch of the lithosphere-asthenosphere model used for scaling analysis.

CIG Code(s): CitcomCU

References

Höink, T. and A. Lenardic, Long wavelength convection, Poiseuille–Couette flow in the low-viscosity asthenosphere and the strength of plate margins, Geophys. J. Int., 180, 23-33, 2010, doi: 10.1111/j.1365-246X.2009.04404.x

Höink, T., A. Mark Jellinek and A. Lenardic, Viscous coupling at the lithosphere - asthenosphere boundary, Geochem. Geophys. Geosys., 12 (10), Q0AK02, doi:10.1029/2011GC003698

Slab driven mantle weakening and rapid mantle flow

Margarete A. Jadamec, University of Houston

Numerical models of subduction are presented to investigate the relative role of a Newtonian versus composite viscosity, maximum yield stress, and the initial slab dip on the upper mantle viscosity structure and velocity. The results show that using the experimentally derived flow law to define the Newtonian viscosity (diffusion creep deformation mechanism) and the composite viscosity (both diffusion creep and dislocation creep deformation mechanisms) has a first order effect on the viscosity structure and flow velocity in the upper mantle. Models using the composite viscosity formulation produce a zone of subduction induced mantle weakening that results in reduced viscous support of the slab. The maximum yield stress, which places an upper bound on the slab strength, can also have a significant impact on the viscosity structure and flow rates induced in the upper mantle, with maximum mantle weakening and mantle flow rates occurring in models with a lower maximum yield stress and shallower slab dip. In all cases the magnitude of induced mantle flow is larger in the models using the composite viscosity formulation. The laterally variable viscosity that develops in the upper mantle leads to lateral variability in coupling of the mantle to the base of the surface plates.

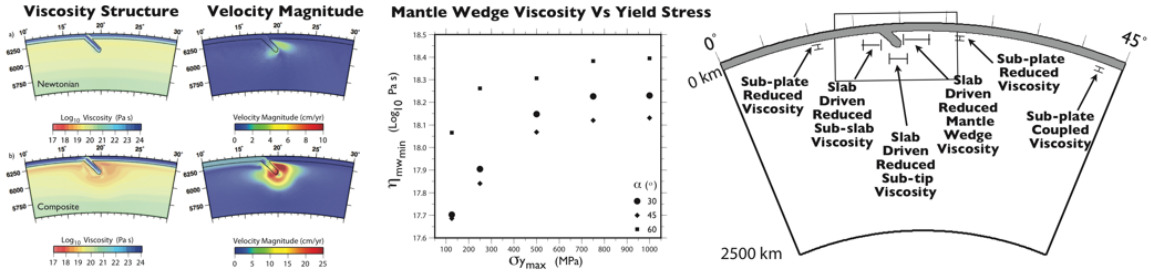

(Left) Zoomed in view of subduction model showing viscosity and velocity magnitude for model using Newtonian viscosity (upper left) and composite viscosity (lower left). (Center) Minimum mantle wedge viscosity as a function of maximum yield stress for models using the composite viscosity. (Right) Conceptual diagram of subduction driven mantle weakening based on two-dimensional models of subduction with a strain-rate dependent viscosity.

CIG Code(s): CitcomCU

Acknowledgements: This work was supported by National Science Foundation grant EAR-1316416 awarded to M. Jadamec. Models were run on Lonestar, at the Texas Advanced Computing Center, through XSEDE allocations TG-EAR120010 and TG-TRA110020. The models were run with a modified version of the CIG supported code CitcomCU.

References:

Jadamec, M. A., In Press 2014, Slab driven mantle weakening and rapid mantle flow. In AGU Geophysical Monograph Series, Subduction Dynamics, Eds. G. Morra, D. Yuen, S. King, S. Lee, and S. Stein. AGU Wiley

Reconciling surface plate motions with rapid three-dimensional mantle flow around a slab edge

Margarete A. Jadamec and Magali I. Billen, UC Davis, *Now at Univ. of Houston*

The direction of tectonic plate motion at the Earth's surface and the flow field of the mantle inferred from seismic anisotropy are well correlated globally, suggesting large-scale coupling between the mantle and the surface plates. The fit is typically poor at subduction zones, however, where regional observations of seismic anisotropy suggest that the direction of mantle flow is not parallel to and may be several times faster than plate motions. Here we present three-dimensional numerical models of buoyancy-driven deformation with realistic slab geometry for the Alaska subduction–transform system and use them to determine the origin of this regional decoupling of flow. We find that near a subduction zone edge, mantle flow velocities can have magnitudes of more than ten times the surface plate motions, whereas surface plate velocities are consistent with plate motions and the complex mantle flow field is consistent with observations from seismic anisotropy. The seismic anisotropy observations constrain the shape of the eastern slab edge and require non-Newtonian mantle rheology. The incorporation of the non-Newtonian viscosity results in mantle viscosities of 10^{17} to 10^{18} Pa s in regions of high strain rate (10^{-12} s^{-1}), and this low viscosity enables the mantle flow field to decouple partially from the motion of the surface plates. These results imply local rapid transport of geochemical signatures through subduction zones and that the internal deformation of slabs decreases the slab-pull force available to drive subducting plates.

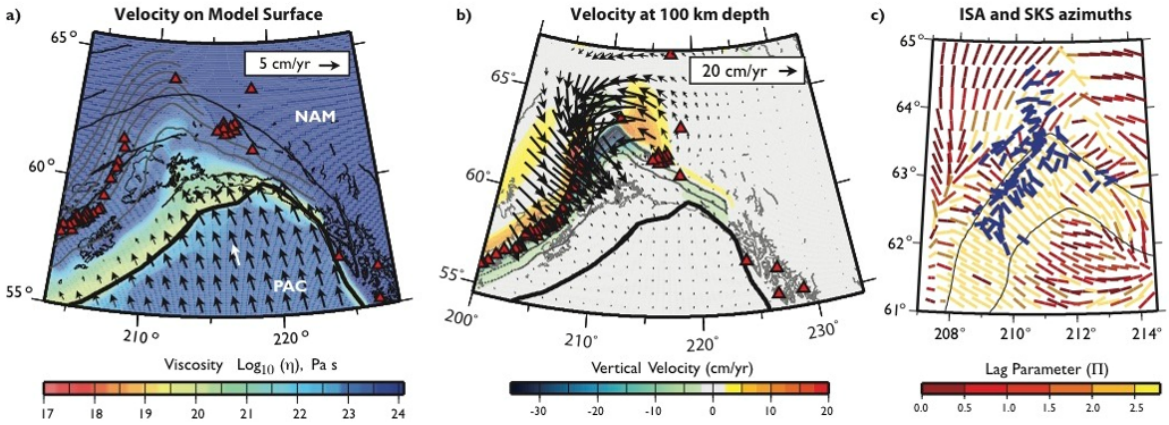

(left) Predicted Pacific plate motion and composite viscosity, (middle) predicted rapid velocity around eastern Alaska slab edge in same model, (right) comparison of predicted ISA to observed SKS fast axis. SKS data from Christensen and Abers (2010). Plots show subset of model domain.

CIG Code(s): CitcomCU

Acknowledgements: High resolution models were run TG-EAR080015N. This work was supported by National Science Foundation grants EAR-0537995 and EAR-1049545. We thank Oliver Kreylos and the UC Davis Keck Center for Active Visualization in the Earth Sciences (KeckCAVES).

References:

Jadamec, M.A., and Billen, M.I., 2010, Reconciling surface plate motions with rapid three-dimensional mantle flow around a slab edge. Nature, 465, p. 338-342.

The role of rheology and slab shape on rapid mantle flow: 3D numerical models of the Alaska slab edge

Margarete A. Jadamec and Magali I. Billen, UC Davis, *Now at Univ. of Houston*

Away from subduction zones, the surface motion of oceanic plates is well correlated with mantle flow direction, as inferred from seismic anisotropy. However, this correlation breaks down near subduction zones, where shear wave splitting studies suggest the mantle flow direction is spatially variable and commonly non-parallel to plate motions. This implies local decoupling of mantle flow from surface plate motions, yet the magnitude of this decoupling is poorly constrained. We use 3D numerical models of the eastern Alaska subduction-transform plate boundary system to further explore this decoupling, in terms of both direction and magnitude. Specifically, we investigate the role of the slab geometry and rheology on the mantle flow velocity at a slab edge. The subducting plate geometry is based on Wadati-Benioff zone seismicity and tomography, and the 3D thermal structure for both the subducting and overriding plates, is constrained by geologic and geophysical observations. In models using the composite viscosity, a laterally variable mantle viscosity emerges as a consequence of the lateral variations in the mantle flow and strain rate. Spatially variable mantle velocity magnitudes are predicted, with localized fast velocities (greater than 80 cm/yr) close to the slab where the negative buoyancy of the slab drives the flow. The same models produce surface plate motions of less than 10 cm/yr, comparable to observed plate motions. These results show a power law rheology, i.e., one that includes the effects of the dislocation creep deformation mechanism, can explain both observations of seismic anisotropy and decoupling of mantle flow from surface motion.

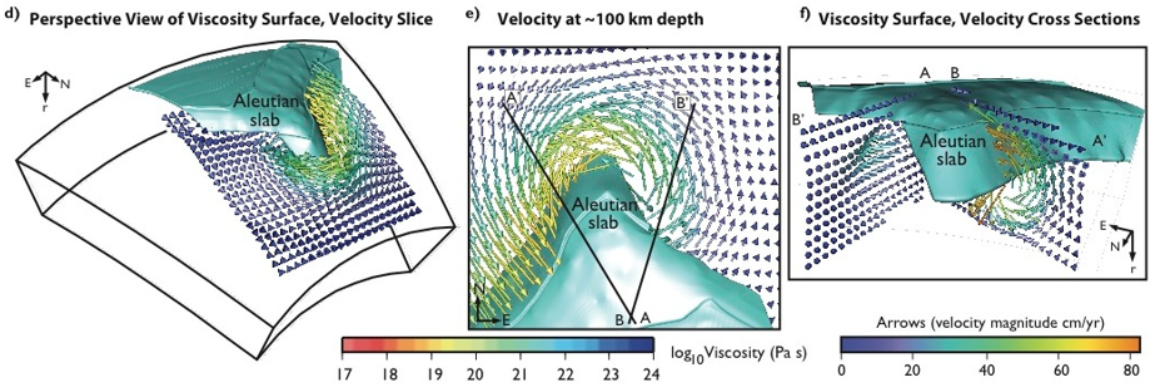

(left) Oblique view of predicted mantle velocity beneath south central Alaska, including 3D flow around eastern Alaska slab edge, (middle) map view of toroidal flow, (right) cross sections through poloidal flow.

CIG Code(s): CitcomCU

Acknowledgements: High resolution models were run TG-EAR080015N. This work was supported by National Science Foundation grants EAR-0537995 and EAR-1049545. We thank Oliver Kreylos and the UC Davis Keck Center for Active Visualization in the Earth Sciences (KeckCAVES).

References:

Jadamec, M.A., and Billen, M.I., 2012, The role of rheology and slab shape on rapid mantle flow: 3D numerical models of the Alaska slab edge. Journal of Geophysical Research, 117, B02304.

Three-dimensional numerical models of flat slab subduction and the Denali fault driving deformation in south-central Alaska

Margarete A. Jadamec, Magali Billen, and Sarah Roeske, UC Davis, *Now at Univ. of Houston*

Early theories of plate tectonics assumed plates were rigid with deformation limited to within a few tens of kilometers of the plate boundary. However, observations indicate most continental plates defy such rigid behavior with deformation extending over 1000 kilometers inboard. We construct 3D numerical models of the boundary between the Pacific and North American plates in Alaska to investigate the relative controls of flat slab subduction, continental scale faulting, and a non-linear rheology on deformation in the overriding plate. The models incorporate a realistic slab shape based on seismic data and a variable thermal structure for both the subducting and overriding plates based on geologic and geophysical observables. The inclusion of the Denali fault allows for the portion of south-central Alaska between the Denali fault and the trench to partially decouple from the rest of North America, forming an independently moving region that correlates to what has been described from geologic and geodetic studies as the Wrangell block. The motion of the Wrangell block tracks the motion of the flat slab indicating the subducting plate is driving the motion of the Wrangell block. Models using a composite (Newtonian and non-Newtonian) viscosity predict compressional motion along the northern bend in the Denali fault, consistent with thermochronologic data that show significant late Neogene exhumation in the central Alaska Range, including at Mt. McKinley, the tallest mountain in North America. These 3D numerical models show the subducting slab is the main driver of overriding plate deformation in south-central Alaska and combined with the Denali fault can reproduce several first order tectonic features of the region including the motion of the Wrangell block, uplift in the central Alaska Range, subsidence in the Cook Inlet-Susitna Basins, and upwelling at the slab edge beneath the Wrangell volcanics.

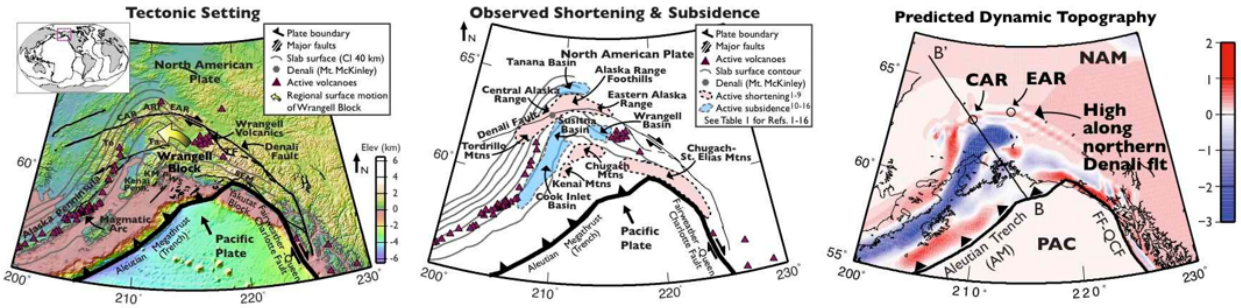

(left) Alaska tectonic setting, (b) regions of active uplift-subsidence, (c) predicted dynamic topography.

CIG Code(s): CitcomCU

Acknowledgements: National Science Foundation Postdoctoral Fellowship EAR-1049545 awarded to M. Jadamec and National Science Foundation grant EAR-0537995 awarded to M. Billen and S. Roeske. CIG for CitcomCU source code, and Oliver Kreylos and the UC Davis KeckCAVES for 3D visualization infrastructure and software.

References:

Jadamec, M.A., Billen, M.I., and Roeske, S. M., 2013, Three-dimensional numerical models of flat slab subduction and the Denali fault driving deformation in south-central Alaska. Earth and Planetary Science Letters, 376, p. 29-42.

Intraplate Volcanism due to convective instability of Stagnant Slabs in the Mantle Transition Zone

Matthew H. Motoki, University of Hawaii
Maxim D. Ballmer, Earth-Life Science Institute, Tokyo Tech, Japan

Continental intraplate volcanism commonly occurs above subducted slabs that stagnate in the Mantle Transition Zone (MTZ), such as in Europe, eastern China, and western North America. Here, we use two-dimensional numerical models to explore the evolution of stagnant slabs in the MTZ and their potential to sustain mantle upwellings that can support volcanism. We find that weak slabs may go convectively unstable within tens of Myr. Upwellings rise out of the relatively warm underbelly of the slab, are entrained by ambient-mantle flow and reach the base of the lithosphere. The first and most vigorous upwellings rise adjacent to lateral heterogeneity within the slab. Ultimately, convective instability also acts to separate the compositional components of the slab, harzburgite and eclogite, from each other with harzburgite ri-sing into the upper mantle and eclogite sinking into the lower mantle. Such a physical filtering pro-cess may sus-tain a long-term compositional gradient across the MTZ.

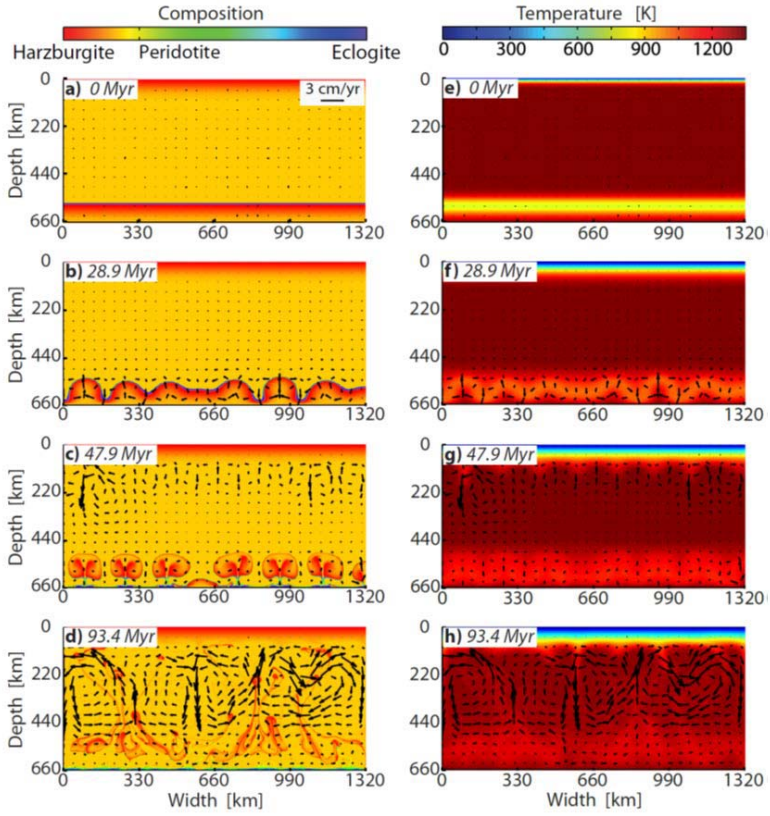

Time evolution (i.e., from top to bottom) of model results for an example case. Left column (a-d) shows compo-sition (colors) and velocity (arrows); right column (e-h) shows tempe-rature [°C].

CIG Code(s): CitComCU

References

Motoki, M.H., M.D. Ballmer (2015), Intraplate Volcanism due to convective instability of Stagnant Slabs in the Mantle Transition Zone, *G-cubed,* doi:10.1002/2014GC005608.

Three-dimensional simulations of geometrically complex subduction with large viscosity variations

Margarete A. Jadamec, Magali I. Billen, Oliver Kreylos, UC Davis, *Now at Univ. of Houston*

The incorporation of geologic realism into numerical models of subduction is becoming increasingly necessary as observational and experimental constraints indicate plate boundaries are inherently 3D and contain large viscosity variations. However, large viscosity variations occurring over short distances pose a challenge for computational codes, and models with complex 3D geometries require substantially greater numbers of elements, increasing the computational demands. We modified CitcomCU to model realistic subduction zones that use an arbitrarily shaped 3D plate boundary interface and incorporate the effects of a strain-rate dependent viscosity based on an experimentally derived flow law for olivine. Tests of this implementation on 3D models with a simple subduction zone geometry indicate that limiting the overall viscosity range in the model, as well as limiting the viscosity jump across an element, improves model runtime and convergence behavior, consistent with what has been shown previously. In addition, the choice of method and averaging scheme used to transfer the viscosity structure to the different levels in the multigrid solver can significantly improve model performance. These optimizations can improve model runtime by over 20%. 3D models of a subduction zone with a complex plate boundary geometry were then constructed, containing over 100 million FE nodes with a local resolution of 2.35 km, and run on XSEDE. The optimizations in solver parameters determined from the simple 3D models applied to the much larger and more complex models of an actual subduction zone improved model convergence behavior and reduced runtimes by on the order of 25%. While the solver parameter optimization can improve model performance, the results also demonstrate the need for new solvers to keep pace with the demands for increasingly complex numerical simulations.

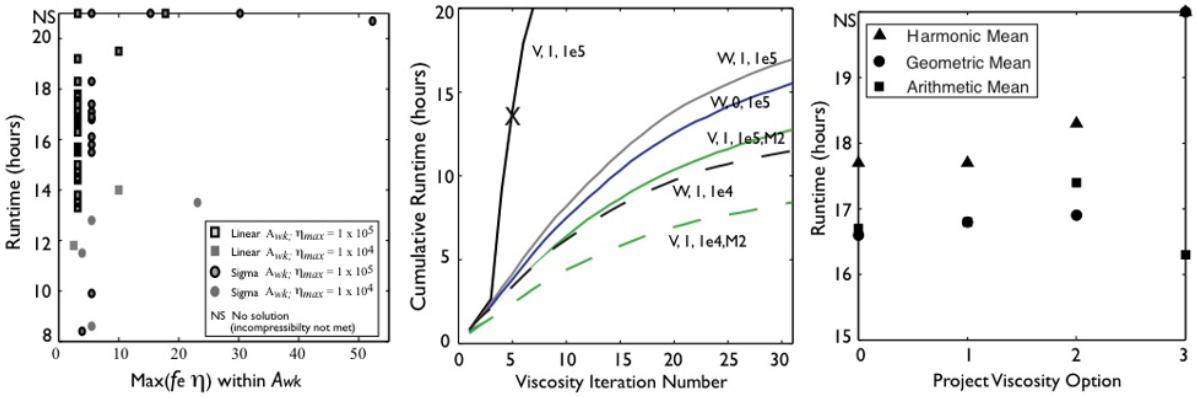

Runtime for simplified 3D model for (a) all multigrid parameters varied, (b) cycle type, viscosity maximum, projection type, and (c) averaging schemes within the full multigrid.

CIG Code(s): CitcomCU

Acknowledgements: NSF EAR-0537995 and EAR-1049545.

References:

Jadamec, M. A. , Billen, M. I., and Kreylos, O., 2012, Three-dimensional simulations of geometrically complex subduction with large viscosity variations. ACM Proceedings of the 2012 Conference on eXtreme Science and Engineering Discovery Environment.

Dynamic Linkages Between the Transition Zone & Surface Plate Motion in 2D Models of Subduction

Katrina M. Arredondo, Magali I. Billen, University of California, Davis

Subduction zones exhibit a wide range of behavior, from slab stagnation at 660 km to direct penetration into the lower mantle. Due to uncertainties in the tectonic history of individual subduction zones, such as trench velocities, potential mechanisms for controlling slab behavior in the transition zone are explored using numerical models. We have used CitcomS to complete numerical simulations of subduction zones to test the importance of a range of forces on subduction zone dynamics: the presence of shear, adiabatic and latent heating, compositional layering, composition-dependent phase transitions and explicit plate speeds versus dynamically evolving plate and trench velocities. Additionally the eight major, composition-dependent, phase transitions for pyrolite, harzburgite and eclogite may be an important influence on subducting slab dynamics due to the additional forces that are dependent on depth and compositional layering within the slab (e.g., Ricard et al., 2005). Preliminary results indicate that individual components have a relatively minor effect, but create important feedbacks when combined together. Also ignoring the additional phase transitions leads to overestimation of slab stagnation.

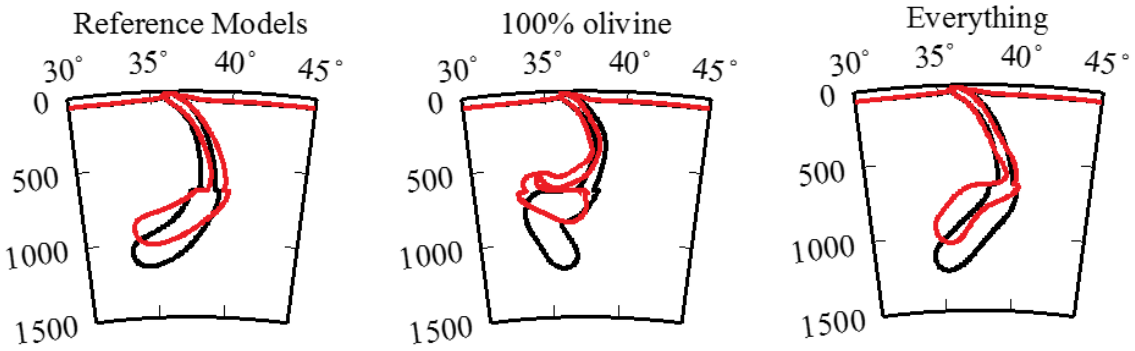

Selected kinematic models, where the red slab includes latent heat, shear heating and adiabatic heating and the black does not. The model on the left is a basic subduction zone with no added components, the middle is most similar to past studies that include the 410 and 660 km phase transitions and the right figure has all of the components chosen for this study.

Dynamic models with all seven composition-dependent phase transitions are very sensitive to the plate strength and weak zone viscosity, causing large changes in plate speed and higher incidence of slab detachment. A sufficient approximation for low-temperature plasticity (i.e. Peierl's creep) may be critical for realistic trench rollback. These feedbacks and parameter-sensitive behavior indicate that the wide range of observed slab behavior may result from subtle differences in plate and plate boundary properties. Two manuscripts on these results are in preparation for submission in April 2015.

CIG Code(s): CitcomS, ASPECT (planned)

References:

Ricard, Y., E. Mattern, and J. Matas, in Geophysical Monograph Series, vol. 160, American Geophysical Union, 2005.

Using Seismic Anisotropy to Constrain Global Mantle Flow and Lithosphere Net Rotation

Clinton P. Conrad, University of Hawaii
Mark D. Behn, Woods Hole Oceanographic Insitution

Although the motions of Earth's tectonic plates are well constrained, the interaction of these plate motions with viscous flow in Earth's dynamic interior is poorly understood. However, because this interaction deforms the rocks beneath the tectonic plates, observations of deformation can provide a constraint on how the plates interact with the Earth's mantle. We used a numerical model of mantle flow to predict seismic anisotropy, which is a property of deformed rocks that can be detected using seismological techniques. By using observations of seismic anisotropy from rocks beneath the tectonic plates, we were able to constrain certain aspects of the numerical model. For example, we determined that the plates are probably moving westward relative to the deep mantle in a net sense, but that this net motion of the plates is probably not faster than 1-2 cm per year. Further, we were able to constrain the general pattern of mantle flow beneath the plates, and determine some of the material properties of the upper mantle. These findings help us understand the interaction between Earth's dynamic interior and the tectonic motions of the surface plates. Understanding this interaction is particularly important because it ultimately generates the tectonic forces that cause earthquakes and geological deformation of the Earth's surface.

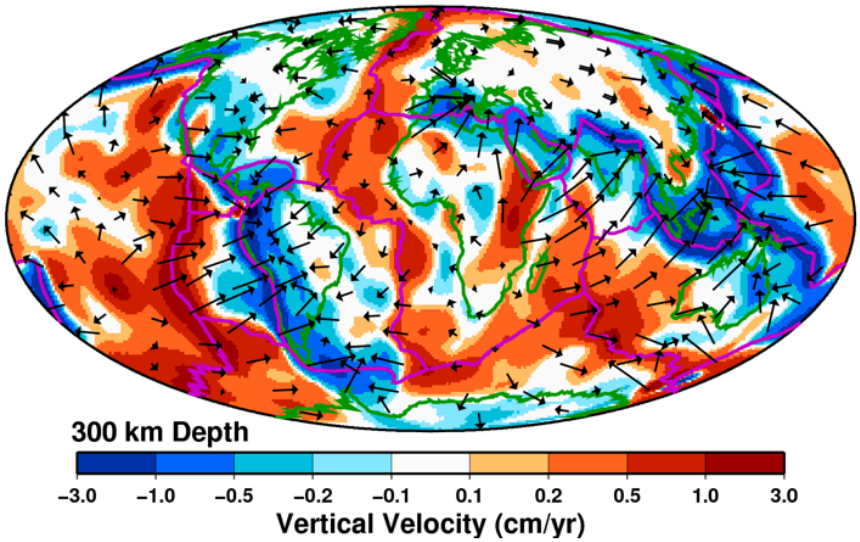

Calculated mantle flow field model at 300 km depth (beneath the tectonic plates). This model was constrained by observations of seismic anisotropy in the upper mantle. Colors and arrows show vertical and horizontal flow directions, respectively. Note that downward flow (blues) occurs around the edges of the Pacific basin, where tectonic plates come together and form subduction zones, and upward flow (reds) occurs in the middle of the ocean basins, where the plates are separating. The mantle at 300 km depth typically flows from regions of upwelling toward regions of downwelling.

CIG Code(s): CitComS

References

Conrad, C.P., and M.D. Behn, Constraints on lithosphere net rotation and asthenospheric viscosity from global mantle flow models and seismic anisotropy, *Geochemistry Geophysics Geosystems, 11,* Q05W05, doi:10.1029/2009GC002970, 2010.

Asthenospheric Shear Controls Patterns of Intraplate Volcanism

Clinton P. Conrad, Todd A. Bianco, Paul Wessel, University of Hawaii
Eugene I. Smith, University Nevada Las Vegas

Most of Earth's volcanism occurs at subducting and rifting plate boundaries, and at fewer than a dozen high-volume volcanic fields fed by upwelling plumes from the deep mantle. The remaining intraplate volcanism, which is typically basaltic, low-volume, and effusive, occurs away from plate boundaries on every continent and produces seamounts on the ocean floor. Although it has been attributed to various localized processes such as lithospheric cracking or sub-lithospheric small-scale convection, this effusive volcanism is ultimately driven by Earth's interior heat, which also drives mantle convection. To pursue links to interior convection, we compare intraplate volcanism locations with patterns of global mantle flow from a numerical model. We show, with high statistical confidence, that recent continental and oceanic intraplate volcanism occurs preferentially above rapidly-shearing regions of the asthenosphere. Basaltic volcanic fields in western North America, eastern Australia, southern Europe, and Antarctica exemplify this relationship, as does an area of dense seamount volcanism west of the East Pacific Rise that was more intense during periods of rapid Pacific spreading. These correlations indicate a control on intraplate volcanism from mantle-scale convection, and are most easily explained by melting induced by upward deflection of asthenospheric shear.

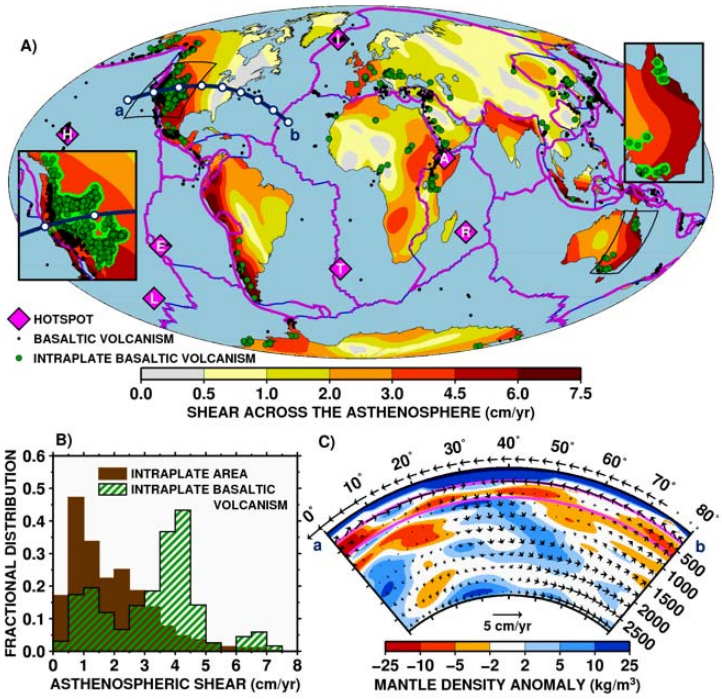

Spatial correlation between asthenospheric shear and continental intraplate volcanism. (A) Background colors show asthenospheric shear magnitude. Recent basaltic volcanism locations are denoted as continental intraplate (green circles) or other (black dots) Regions <100 km from intraplate volcanism are denoted (insets; green area), as are major hotspots[1] (pink diamonds) and volcanic plate boundaries (pink lines). (B) Asthenospheric shear distribution for all intraplate areas (brown) compared with the distribution for regions containing intraplate volcanism (green hatched). (C) Mantle density heterogeneity (colors), flow velocity (arrows in panel), and plate motions (arrows above panel) across western North America (section in A).

CIG Code(s): CitcomS

References

Conrad, C.P., T.A. Bianco, E.I. Smith, and P. Wessel (2011), Patterns of intraplate volcanism controlled by asthenospheric shear, *Nature Geoscience, 4*, 317-321.

Shear-Driven Upwelling: A Mechanism for Intraplate Volcanism

Clinton P. Conrad, Todd A. Bianco, University of Hawaii
Benjun Wu, Johns Hopkins University
Eugene I. Smith, Ashley Tibbetts, University Nevada Las Vegas

Low-volume volcanism occurring away from plate boundaries does not have an obvious plate tectonic explanation. We investigate a new mechanism for intraplate volcanism, the shear-driven upwelling (SDU), which generates upwelling solely through the action of asthenospheric shear flow on viscosity heterogeneity. Using a numerical flow model, we demonstrate that for certain geometries and viscosity ratios, circulatory flow develops within a "cavity" or "step" embedded into the lithospheric base, or within a low-viscosity "pocket" embedded within the asthenospheric layer. For asthenosphere shearing at 5 cm/yr, we estimate that SDU can produce upwelling rates of up to ~0.2 cm/yr within a continental rift, ~0.5 cm/yr along the vertical edge of a craton, or ~1.0 cm/yr within a "pocket" of low-viscosity asthenosphere. In the last case, the pocket must feature an aspect ratio of more than 5, occupy ~20-60% of the asthenosphere's thickness, and be at least 100 times less viscous than the surrounding asthenosphere. We estimate that SDU may generate up to 2.5 km/Myr of melt that is potentially eruptible as surface volcanism. We conclude that SDU could provide an explanation for intraplate volcanism occurring above rapidly shearing asthenosphere, for example in the Basin and Range region of North America.

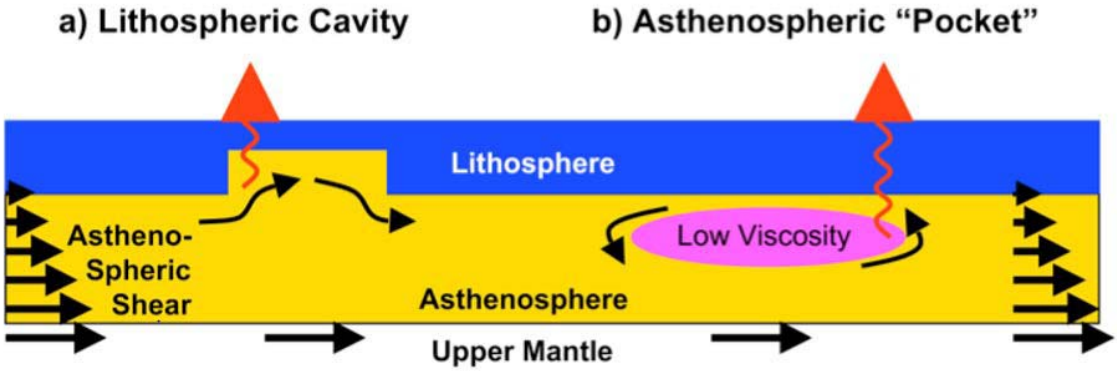

Diagram showing two mechanisms by which asthenospheric shear can act on lateral viscosity heterogeneity to induce Shear-Driven Upwelling (SDU). Asthenospheric shear is generated by relative motion between the mantle and the lithosphere, and is drawn here in a lithospheric reference frame. Shearing asthenosphere can induce (a) "shear-driven cavity flow" within a variation in lithospheric thickness or (b) circulatory flow within a "pocket" of low-viscosity asthenosphere. Both flows induce upwelling; if the asthenospheric mantle is fertile and near its solidus, melting and surface volcanism can result.

CIG Code(s): CitcomS

References

Conrad, C.P., B. Wu, E.I. Smith, T.A Bianco, and A. Tibbetts (2010), Shear-driven upwelling induced by lateral viscosity variations and asthenospheric shear: A mechanism for intraplate volcanism, *Physics of the Earth and Planetary Interiors, 178*, 162-175.

Past Mantle Flow Revealed by Plate Motion Net Characteristics

Clinton P. Conrad, University of Hawaii
Bernhard Steinberger, GFZ German Research Centre for Geosciences, Potsdam
Trond H. Torsvik, University of Oslo, Norway

Viscous convection within Earth's mantle is linked to tectonic plate motions and deforms Earth's surface across wide areas. Such close links between Earth's surface geology and its deep mantle dynamics presumably operated throughout Earth history, but are difficult to investigate for past times because the history of mantle flow is poorly known. We deduced the time-dependence of global-scale mantle flow from the net behavior of surface plate motions. In particular, we tracked the geographic locations of net convergence and divergence for harmonic degrees 1 and 2 by computing the dipole and quadrupole moments of plate motions from tectonic reconstructions extended back to the early Mesozoic. For present-day plate motions, we find dipole convergence in eastern Asia and quadrupole divergence in both central Africa and the central Pacific. These orientations are nearly identical to the dipole and quadrupole orientations of underlying mantle flow, which indicates that these "net characteristics" of plate motions reveal deeper flow patterns. The positions of quadrupole divergence have not moved significantly during the past 250 Myr, which suggests long-term stability of mantle upwelling beneath Africa and the Pacific. These upwelling locations are positioned above two compositionally- and seismologically-distinct regions of the lowermost mantle that may organize global mantle flow as they remain stationary over geologic time.

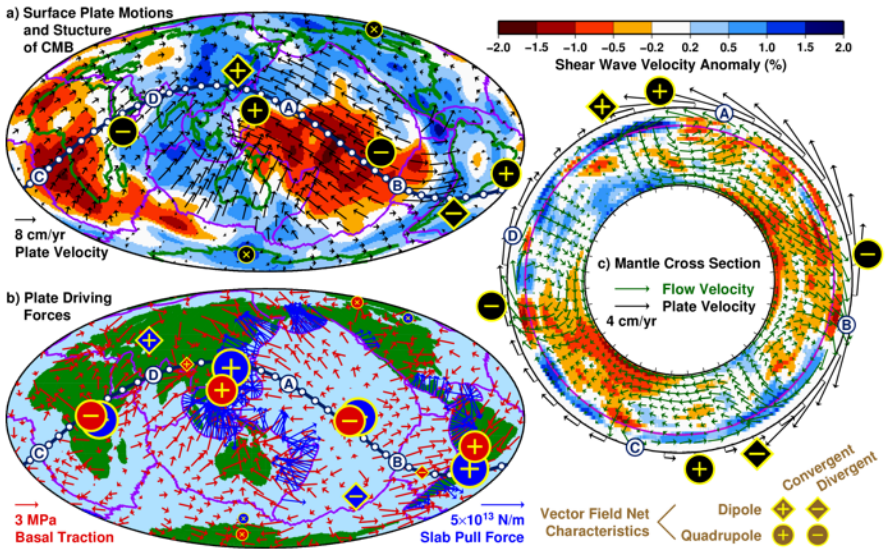

Dipole and quadrupole locations of (a) present-day plate motions (black) and (b) slab pull (blue) and basal tractions on plates (red). A mantle cross section (c) shows tomographic shear velocity anomaly (colors, also drawn in (a) at 2800 km), the associated mantle flow field (green arrows), surface plate motion (black arrows), and dipole and quadrupole locations for plate motions. The proximity of the plate tectonic dipole and quadrupole (a) to those of the plate tectonic driving forces (b) indicates that the net characteristics of plate tectonics reflect the mantle flow patterns at depth (c).

CIG Code(s): CitcomS

References

Conrad, C.P., B. Steinberger, and T.H. Torsvik (2013), Stability of active mantle upwelling revealed by net characteristics of plate tectonics, *Nature, 498*, 479-482.

The Role Of The Asthenosphere In Maintaining Plate Tectonics

Tobias Höink and Adrian Lenardic, Rice University, and Mark Richards, University of California, Berkeley

We use 3-D spherical shell simulations of mantle convection with temperature-, depth- and stress dependent rheology to test scaling trends from boundary layer theory. The simulations and theoretical scalings demonstrate that a low-viscosity layer (asthenosphere) can amplify convective stresses. If the level of convective stress plays a role in maintaining and/or reactivating plate boundaries, this suggests that a relatively thin low viscosity layer may help to maintain plate tectonics.

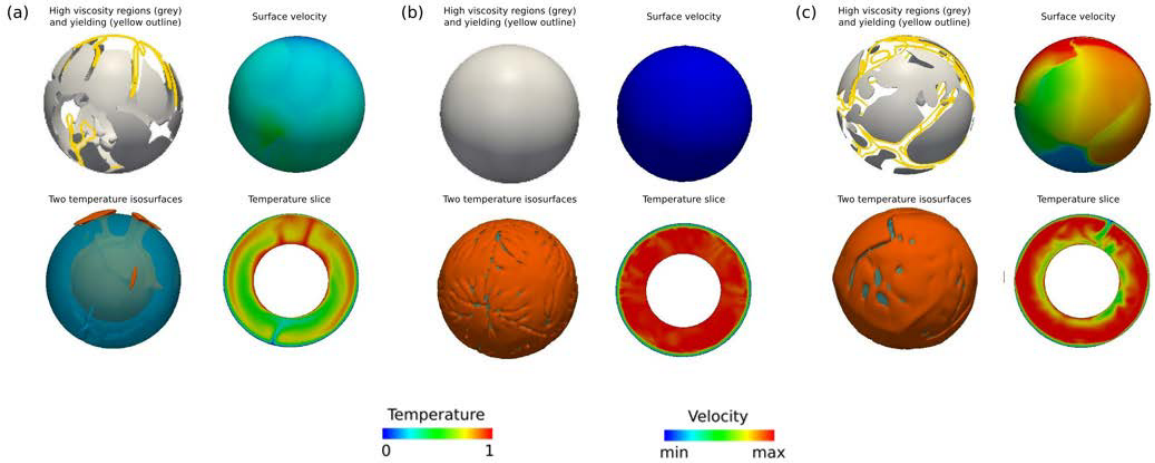

Snapshots of 3-D spherical mantle convection simulations. (a) Channelized lateral flow in a thin low-viscosity asthenosphere leads to long wavelength convection. Episodic behaviour occurs for higher yield stress and/or a thicker channel. In these cases (b) extended periods of stagnant lid convection are periodically interrupted by (c) planetary-scale lithospheric yielding, resulting in global surface mobilization and large surface heat flux excursions.

The numerical simulations support this suggestion as they show that an increase in the thickness of a low viscosity channel can cause the system to transition from an active-lid mode of convection to a stagnant lid state. Collectively, the simulations and theoretical scalings lead to the conclusion that the role of the asthenosphere in maintaining plate tectonics does not come principally from a basal lubrication effect, associated with a low absolute asthenosphere viscosity, but, instead, from a mantle flow channelization effect, associated with a high viscosity contrast from the asthenosphere to the mantle below.

CIG Code(s): CitcomS

Acknowledgements: Computations were carried out at Rice University and at the National Energy Research Scientific Computing Center (NERSC) at Lawrence Berkeley National Laboratory. This work was funded by NSF grant EAR-0944156 and in part by the Cyberinfrastructure for Computational Research funded by NSF under Grant CNS-0821727.

References

Höink, T., A. Lenardic, M. Richards, Depth-dependent viscosity and mantle stress amplification: implications for the role of the asthenosphere in maintaining plate tectonics, Geophys. J. Int., 191, 30-41, 2012

Poiseuille Flow and the Depth-Variation of Asthenospheric Shear

Svetlana I. Natarov, Clinton P. Conrad, University of Hawaii

Asthenospheric flow accommodates differential shear between plate and mantle motions (Couette flow) and hosts additional flow driven by horizontal pressure gradients (Poiseuille flow) that may be associated with mantle upwelling and subduction. Quantifying the relative contributions of these flows in Earth's asthenosphere could help discriminate among competing theories of asthenospheric origin and shed light on thermal history of the Earth. We develop a new method to constrain asthenospheric Poiseuille flow using observations of the depth-dependence of azimuthal seismic anisotropy, which can be obtained from frequency-dependent surface wave tomography models. In particular, we employ a simple 1-D Couette-Poiseuille flow model and analytically solve for depth-profiles of the strain axis orientations, which approximates the orientations of azimuthal seismic anisotropy. We show that Couette-Poiseuille flow induces rotation of azimuthal seismic anisotropy with depth provided that the horizontal pressure gradient has a component transverse to plate motion. We then construct an algorithm that uses depth rotations of azimuthal anisotropy to invert for horizontal pressure gradients everywhere in the asthenosphere and test it on a global numerical mantle flow model. A comparison of pressure gradients predicted using our method with those computed directly from the numerical model shows that our algorithm is stable and accurate. In the numerical model, we establish that Poiseuille flow drives ~40 per cent of the total flow velocity amplitude in the asthenosphere, which indicates that pressure gradients from mantle convection may be an important component of asthenospheric dynamics that can, in principle, be constrained seismically.

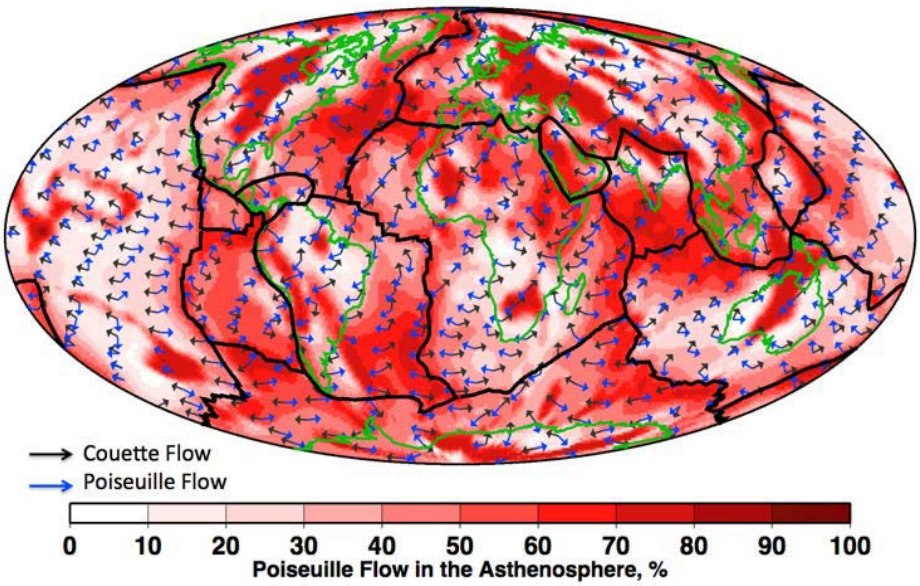

Magnitude of Poiseuille flow velocity in the asthenosphere constrained from a global mantle flow model and shown as a percentage of total flow velocity (colours). Arrows show the orientations of Couette (black) and Poiseuille (blue) flows.

CIG Code(s): CitcomS

References

Natarov, S.I., and C.P. Conrad (2012), The role of Poiseuille flow in creating depth-variation of asthenospheric shear, *Geophysical Journal International, 190,* 1297-1310.

Mantle Convection and Outgassing on Terrestrial Planets

Craig O'Neill, Macquarie University, Adrian Lenardic and Tobias Höink, Rice University, and Nicoas Coltice, École Normale Supérieure de Lyon

Argon-40 degassing from the mantle during volcanism places an important constraint on the tectonic evolution of a planet through time. While Earth has degassed approximately 50% of the ^{40}Ar produced over its history, Venus has only degassed ~24%. Here we explore the effect of tectonic style on ^{40}Ar degassing using numerical models of mantle convection. We find a strong sensitivity of mantle degassing rates to tectonic regime, but also to Rayleigh number and internal heating, such that stagnant-lid models may either degas far more or less than mobile-lid simulations, depending on the relative internal temperatures and lid thicknesses. Evolutionary models of degassing rates through time imply finite degassing efficiencies of terrestrial planets in any tectonic regime. Earth's canonical 50% ^{40}Ar degassing efficiency is in line with model predictions of a tectonically active planet over its lifetime, and Venus' low 40Ar atmospheric concentration is consistent with planetary modes with long periods of tectonic quiescence.

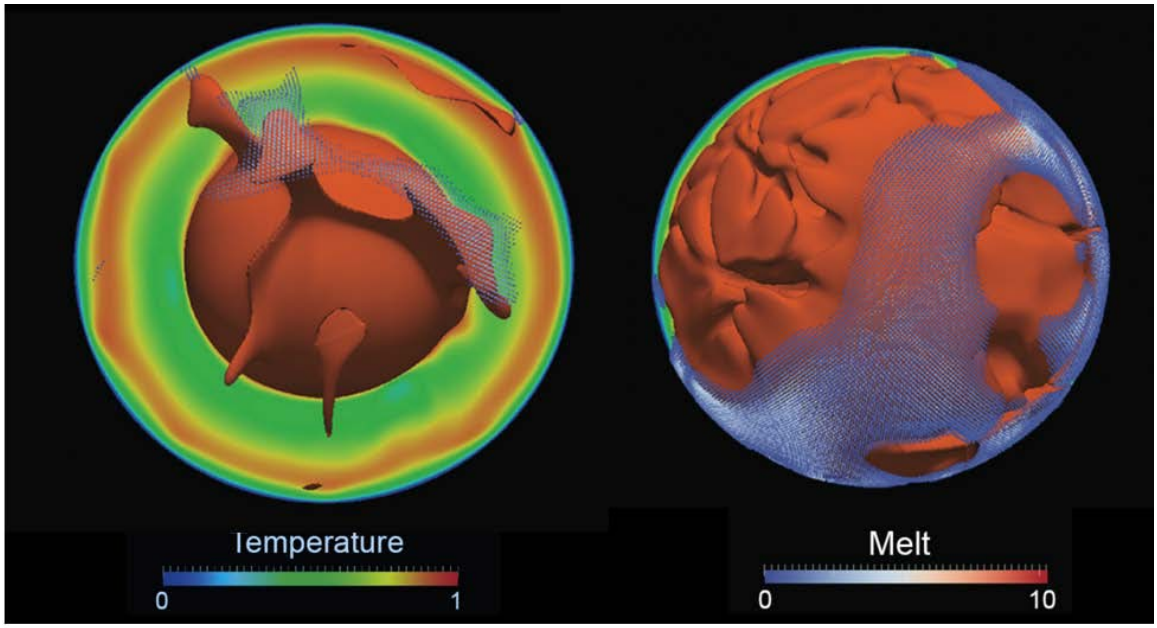

Temperature isosurface (T = 0.9, orange), temperature slice, and melt production (colored glyphs) in three-dimensional spherical mantle convection models using CitcomS. Mobile-lid convection (left) compared to an episodic convection model near overturn event (right), which shows elevated interior temperatures and melting rates.

CIG Code(s): CitcomS

Acknowledgements: C.O. acknowledges ARC support (DP0880801, DP110104 145, and FT100100717).

References

O'Neill C., Lenardic A., Höink T., and Coltice N. (2013) Mantle convection and outgassing on terrestrial planets. In *Comparative Climatology of Terrestrial Planets* (S. J. Mackwell et al., eds.), pp. 473–486. Univ. of Arizona, Tucson, DOI:10.2458/azu_uapress_9780816530595-ch19.

3D spherical models of Martian mantle convection constrained by melting history

Pavithra Sekhar, Scott D. King

While most of Tharsis rise was in place by end of the Noachian period, at least one volcano on Tharsis swell (Arsia Mons) has been active within the last 2 Ma, placing a constraint on the thermal evolution of Mars. The existence of recent volcanism on Mars implies that upwelling convective flow in the mantle remains important on Mars at present. The history of melt production, specifically generating sufficient melt in the first billion years of the planets history to produce Tharsis rise, can be used to constrain thermal history. In this work, mantle convection simulations were performed using finite element code CitcomS in a 3D sphere starting from a uniformly hot mantle and integrating forward in time for the age of the solar system. We implement constant and decaying radioactive heat sources; and vary the partitioning of heat sources between the crust and mantle, and consider decreasing core–mantle boundary temperature and latent heat of melting. The constant heat source calculations produce sufficient melt to create Tharsis early in Martian history and continue to produce significant melt to the present. Calculations with decaying radioactive heat sources generate excessive melt in the past, except when all the radiogenic elements are in the crust, and none produce melt after 2 Gyr. Producing a degree-1 or degree-2 structure may not be pivotal to explain the Tharsis rise: we present multi-plume models where not every plume produces melt. The Rayleigh number controls the timing of the first peak of volcanism while late-stage volcanism is controlled more by internal mantle heating. Decreasing the Rayleigh number increases the lithosphere thickness (i.e., depth), and increasing lithosphere thickness increases the mean mantle temperature. Increasing pressure reduces melt production while increasing temperature increases melt production; hence predicting melt production from convection parameters is not straightforward. Generating enough melt in the mantle to create Tharsis early on and also to explain recent volcanism may require other mechanisms such as small-scale convection or lowering the thermal conductivity of the crust.

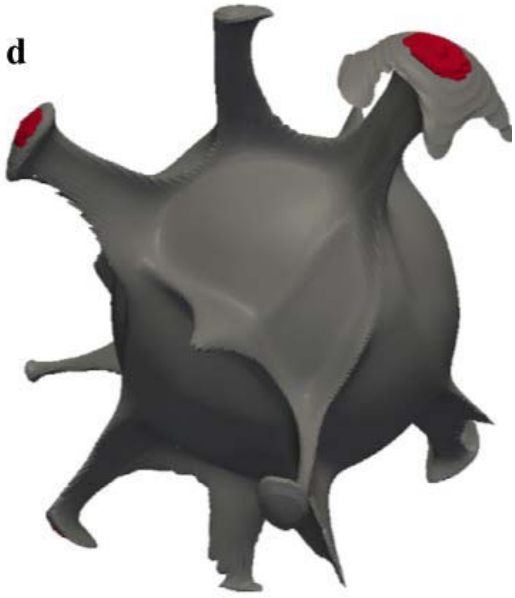

3D temperature and melt (red) for the constant heat sources during early formation, around 4 Ga and also during the late stages, around 0.08 Ga. The isothermal spherical plots for. All the early formation plots are taken at a non-dimensional temperature of approximately 1580 K.

CIG Code(s): CitcomS

References

Sekhar, P., and S. D. King, 3D spherical models of Martian mantle convection constrained by melting history, *Earth Planet. Sci. Lett.,* 388, 27-37, 2014.

Temporal Stress Patterns in Episodic Plate Tectonics Models with Implications for the Initiation of Plate Tectonics on Terrestrial Planets

Vlada Stamenković, MIT,
Tobias Höink and Adrian Lenardic, Rice University

We modeled mantle convection with a sub-lithospheric low-viscosity channel using CitcomS to explore which stress component initiates plate tectonics. The connection to the specific stress component that initiates failure ties to a debate regarding plate tectonics on exoplanets [Stamenković & Breuer, 2014]. We then combined our 3D numerical results with our 1D thermal evolution model to explore how the specific type of stress impacts the dependence of plate tectonics on planet mass and interior heat. This connection allowed us to also estimate the timing of the onset of plate tectonics on the Earth.

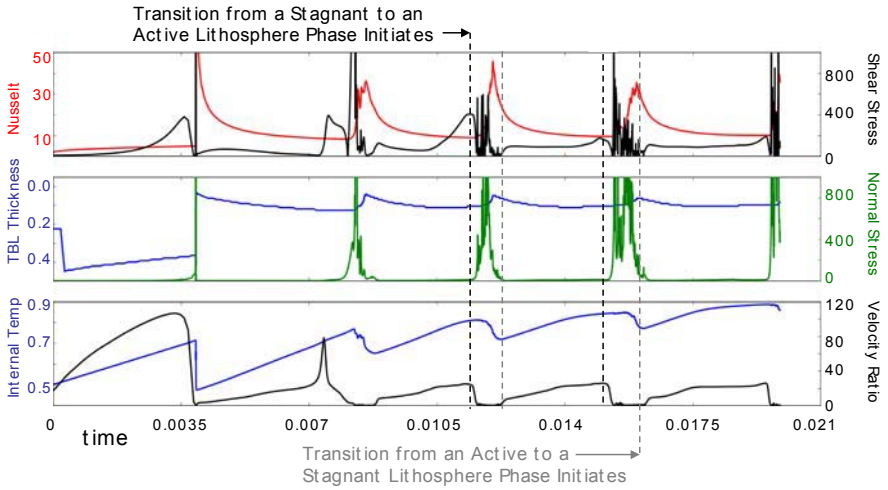

Time series diagnostics for transitions between periods of active and stagnant lid behavior from a 3D spherical numerical experiment that settled into an episodic mode of convection. Values are shown in dimensionless form.

We find that shear stresses are responsible for initiating plate tectonics from a stagnant lid state. We find also a reduced likelihood of initiating plate tectonics with increasing planet mass and interior heat. Moreover, our results indicate that for Earth an early (<500 Myr) or considerably later (0.5-3 Gyr after formation) start for plate tectonics are both possible. Once started, plate tectonics associated cooling of the interior can aid in its maintenance and our thermal evolution models suggest that in that situation the continuation for plate tectonics on Earth can be maintained for the lifetime of the sun as a main sequence star.

CIG Code(s): CitcomS

References

Stamenković, V., Höink, T., Lenardic A., Temporal Stress Patterns in Episodic Plate Tectonics Models with Implications for the Initiation of Plate Tectonics on Terrestrial Planets, In preparation.

Stamenković, V., Breuer, D., 2014, The tectonic mode of rocky planets: part 1 - driving forces, models, and parameters, Icarus, 234, 174-193.

Mantle Convection, Tectonics, and Volcanism on Hot Exo-Earths

Joost van Summeren, Clinton P. Conrad, Eric Gaidos, University of Hawaii

Recently discovered exoplanets on close-in orbits should have surface temperatures of hundreds to thousands of Kelvin. They are likely tidally locked and synchronously rotating around their parent stars and, if an atmosphere is absent, have surface temperature contrasts of many hundreds to thousands of Kelvin between permanent day and night sides. We investigated the effect of elevated surface temperature and strong surface temperature contrasts for Earth-mass planets on the (1) pattern of mantle convection, (2) tectonic regime, and (3) rate and distribution of partial melting, using numerical simulations of mantle convection with a composite viscous/pseudo-plastic rheology. Our simulations indicate that if a close-in rocky exoplanet lacks an atmosphere to redistribute heat, a ~400 K surface temperature contrast can maintain an asymmetric degree 1 pattern of mantle convection in which the surface of the planet moves preferentially toward subduction zones on the cold night side. The planetary surface features a hemispheric dichotomy, with plate-like tectonics on the night side and a continuously evolving mobile lid on the day-side with diffuse surface deformation and vigorous volcanism. If volcanic outgassing establishes an atmosphere and redistributes heat, plate tectonics is globally replaced by diffuse surface deformation and volcanism accelerates and becomes distributed more uniformly across the planetary surface.

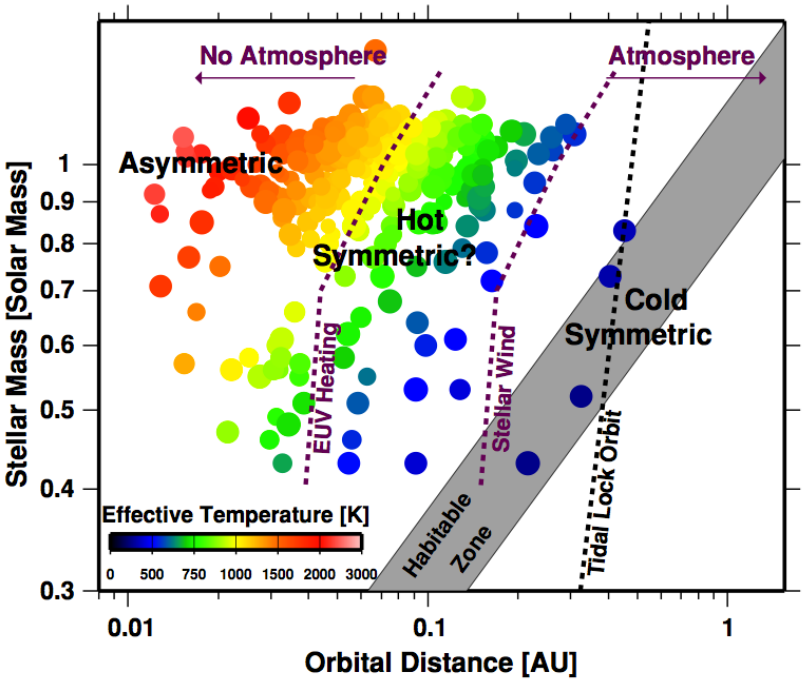

Possible occupation of planets in orbital distance–stellar-mass domain space. Tidal locking is likely at distances smaller than the tidal lock orbit (black dotted line). Colored dots show effective temperatures for recently-discovered exoplanets; dot size reflects variability in planet size. Tidally-locked planets without an atmosphere (stripped by EUV heating or stellar wind, purple dotted lines) can have estimated day-side temperatures twice the effective temperature a cold night side. We investigate global patterns of mantle convection, plate tectonics, and volcanism on such planets.

CIG Code(s): CitcomS

References

van Summeren, J., C.P. Conrad, and E. Gaidos (2011), Mantle convection, plate tectonics, and volcanism on hot exo-earths, *The Astrophysical Journal Letters, 736*, L15, doi:10.1088/2041-8205/736/1/L15.

Magnetodynamo Lifetimes in Rocky Planets with Contrasting Mantle Convection Regimes

Joost van Summeren, Clinton P. Conrad, Eric Gaidos, University of Hawaii

We used a thermal model of an iron core to calculate magnetodynamo evolution in Earth-mass rocky planets to determine the sensitivity of dynamo lifetime and intensity to planets with different mantle tectonic regimes, surface temperatures, and core properties. The heat flow at the core-mantle boundary (CMB) is derived from numerical models of mantle convection with a viscous/pseudoplastic rheology that captures the phenomenology of plate-like tectonics. Our thermal evolution models predict a long-lived (~8 Gyr) field for Earth and similar dynamo evolution for Earth-mass exoplanets with plate tectonics. Both elevated surface temperature and pressure-dependent mantle viscosity reduce the CMB heat flow but produce only slightly longer-lived dynamos (~8–9.5 Gyr). Single-plate ("stagnant lid") planets with relatively low CMB heat flow produce long-lived (~10.5 Gyr) dynamos. These weaker dynamos can cease for several billions of years and subsequently reactivate due to the additional entropy production associated with inner core growth, a possible explanation for the absence of a magnetic field on present-day Venus. We also show that dynamo operation is sensitive to the initial temperature, size, and solidus of a planet's core. These dependencies would severely challenge any attempt to distinguish exoplanets with plate tectonics and stagnant lids based on the presence or absence of a magnetic field.

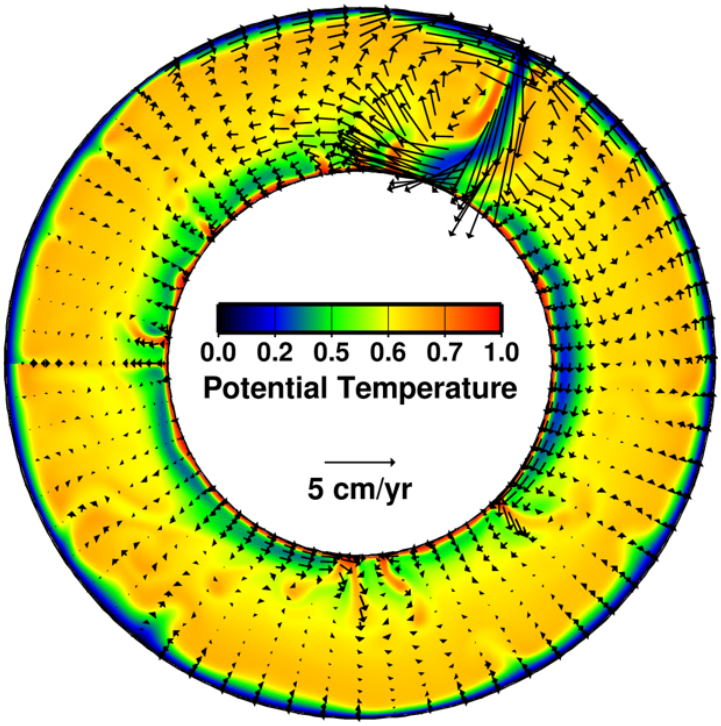

Typical convective flow field (arrows) and potential temperature (colors) in a 2-D, annular model of mantle convection. Both surface and CMB heat flow were measured from calculations like these to calibrate thermal evolution of planetary interiors. These models predict the time-dependence of CMB heat flow, which governs the magnetodynamo.

CIG Code(s): CitcomS

References

van Summeren, J., E. Gaidos, and C.P. Conrad (2013), Magnetodynamo lifetimes for rocky, Earth-mass exoplanets with contrasting mantle convection regimes, *Journal of Geophysical Research: Planets, 118*, 938-951, doi:10.1002/jgre.20077.

Why cold slabs stagnate in the transition zone

Scott D. King, Daniel J. Frost, and David C. Rubie

Oceanic lithosphere sinks, stagnates, and is deflected sub-horizontally beneath western Pacific island arcs, requiring buoyancy in the slab that is inconsistent with a thermal origin. The transformation of pyroxene to majoritic garnet occurs by extremely slow diffusion and pyroxene is therefore unlikely to transform at equilibrium pressures and temperatures in the cold interor of slabs. We present high-resolution numerical simulations using the finite element code ConMan, showing that when slow diffusion inhibits the dissolution of pyroxene into garnet, the slab becomes buoyant relative to the ambient mantle and stagnates whereas when the phase transformations occur in equilibrium, there is no effect on the slab. We test the model by comparing slab temperature and geometry and find that sub-horizontal slabs are more likely colder than average, consistent with our numerical simulations.

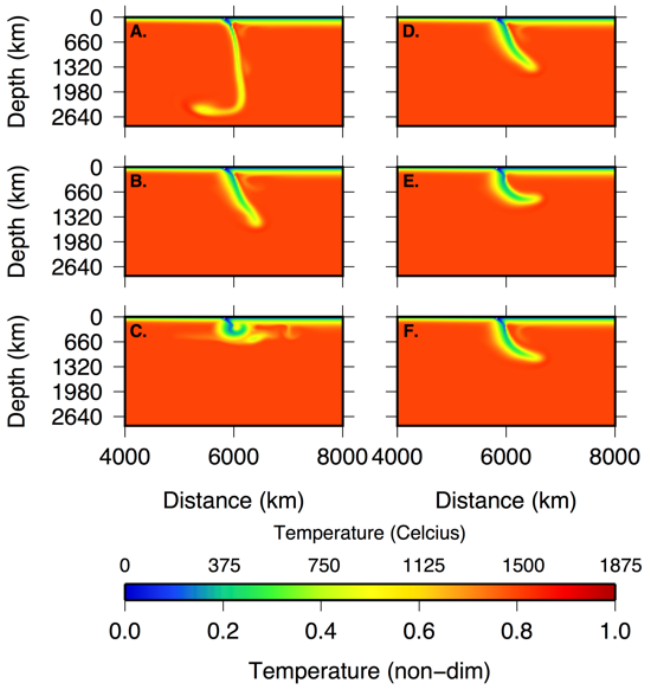

Temperature field from six subduction calculations illustrating the effects of phase transformations on slab geometry. Each result is shown 40 Myr after the initiation of subduction. A. Baseline case with no phase transformations; B. Same as A. except with the olivine to wadslayite (Clapyeron slope = 3.1 MPa/K) and ringwoodite to perovskite plus ferropericlase (Clapyeron slope = -2.8 MPa/K) transformations; C. same as B, except for a Clapeyron slope of -6 MPa/K for the ringwoodite phase transformation; D. Same as B. with the inclusion of the equilibrium pyroxene to majorite garnet transformation (see supplementary material for details); E. Same as D with the inclusion of slow diffusion of the pyroxene component into garnet majorite below 1200 K. F. Same as E with the inclusion of slow diffusion of the pyroxene component into garnet majorite below 1000 K.

CIG Code(s): ConMan

References:

Scott D. King, Daniel J. Frost, David C. Rubie. Why cold slabs stagnate in the transition zone. Geology. 43(3): 231-234. 2015

Coupled Continental-Lithosphere and Mantle Dynamics simulation using Underworld/GALE

Catherine M. Cooper, Washington State University; Meghan S Miller, University of Southern California; Louis Moresi, University of Melbourne, Steve Quenette, Monash University

A fundamental question in Earth evolution relates to the formation, deformation, evolution and preservation of the continental lithosphere in response to the evolving circulation of the plates and the deep mantle. To address such questions requires the ability to track the fluid dynamics of the deep interior, the solid mechanics of the lithosphere, and follow distinct compositional domains for multiple mantle overturns. The Underworld/GALE tool was developed with these problems in mind.

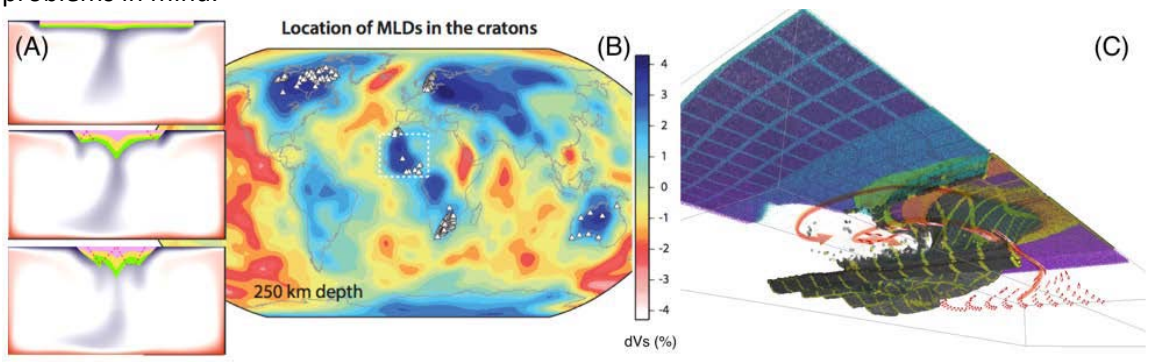

Models of the formation of mid-lithospheric discontinuities (MLDs) in the cratonic lithosphere (A) as localized deformation regions in the cratonic nucleus formed in response to convective thickening of the early continental lithosphere (Cooper & Miller, 2014). A compilation map of the MLDs imaged with receiver functions (B) and a model of the collision / accretion of continental ribbons in the modern Earth in which similar thickening and localization of deformation can occur (C) from Moresi et al. (2014).

Recent seismic imaging efforts of the continental lithosphere in North America, South Africa, Fennoscandia, West Africa, and Australia have produced images of deep, intra-cratonic features colloquially known as mid-lithospheric discontinuities. Geodynamic models using Underworld suggest that the mid-lithospheric discontinuities observed could be remnants of deformation structures produced during their formation as ancient oceans closed. The models demonstrate that ocean closure created a dynamic setting suitable for craton formation via the thickening of continental material over a mantle downwelling. This process subjected the thickening lithosphere to extensive deformation, forming internal structure that can be preserved over the lifetime of the craton, which we can now image with seismic methods.

CIG Code: Underworld/GALE

Acknowledgements: John Mansour, Julian Giordani, and Mirko Velic provided assistance in installing Underworld and running the simulations described in Figure 1A&C.

References

Cooper, C. M., and M. S. Miller (2014), Craton formation: Internal structure inherited from closing of the early oceans, *Lithosphere*, *6*(1), 35–42, doi:10.1130/L321.1.

Moresi, L., P. G. Betts, M. S. Miller, and R. A. Cayley (2014), Dynamics of continental accretion, *Nature*, *508*(7495), 245–248, doi:10.1038/nature13033.

Assessing Subsurface Temperatures in Australia from a Geothermal Systems Perspective

Marcus W. Haynes, Anthony R. Budd, Ed J. Gerner, Chris Harris-Pascal and Alison L. Kirkby, Geoscience Australia

Understanding the distribution of subsurface temperatures is an important early step in a geothermal exploration process. A new approach for developing a 3D temperature map of the Australian continent is being developed by Geoscience Australia, combining available proxy data using high-performance computing and large continental-scale datasets. The Underworld software package, with the Geothermal plug-in, is used to estimate the steady-state thermal profile of the Australian continent, and the uncertainties of this estimate, by modelling a suite of different scenarios. The geophysical properties of each scenario are determined using national-scale datasets including geological mapping and geochemical samples, amongst others. Although only in the early stages of development, the modelling has successfully demonstrated that there are greater amounts of geoscientific data available in Australia by which to estimate broad-scale subsurface temperatures than have previously been utilised.

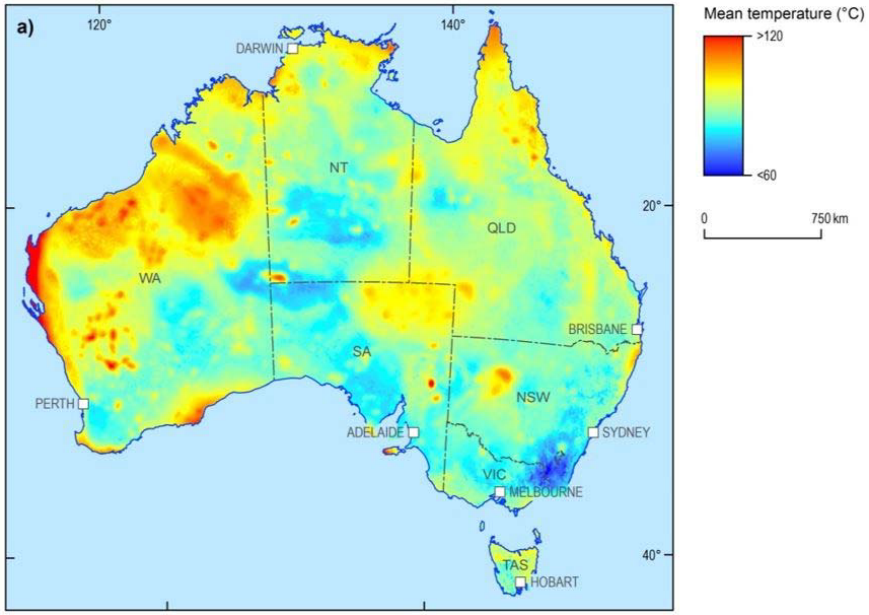

Early modelling results showing sub-surface temperature estimates at 4 km depth.

CIG Code(s): Underworld, with the Geothermal plug-in

Acknowledgements: This research was undertaken with the assistance of resources from the National Computational Infrastructure (NCI), which is supported by the Australian Government. This article is published with the permission of the CEO, Geoscience Australia

Reference:

Haynes, M. W., Budd, A. R., Gerner, E. J., Harris-Pascal, C. and Kirkby, A. L., TherMAP – Assessing Subsurface Temperatures in Australia from a Geothermal Systems Perspective, World Geothermal Congress. 19-25 April 2015, Melbourne, Australia, Submitted.

Factors Contributing to Multi-Segment Rupture in the 2010 M7.1 Darfield, New Zealand, Earthquake

Brad T. Aagaard (U.S. Geological Survey), Charles A. Williams and Bill Fry (GNS Science)

We use dynamic prescribed slip (kinematic) modeling to examine the factors contributing to multi-segment rupture in the 2010 M7.1 Darfield, New Zealand, earthquake. We consider fault geometry and slip distributions from inversions by Beavan et al. (2012) based on geodetic observations and by Elliott et al. (2012) based on geodetic and teleseismic observations. We invert for subevent origin times using strong-motion records and find complex rupture propagation across multiple fault segments. Our inversions suggest that the rupture began on one or two secondary faults with reverse/oblique slip near the hypocenter, consistent with the GNS first motion mechanism. The primary bilateral strike-slip rupture of the Greendale fault, consistent with centroid moment tensor solutions, occurred about 9-10 seconds after the origin time. The strong-motion records provide poor constraints on the timing of rupture of the reverse Hororata fault, which may have occurred about 16-17 seconds after the origin time. Denser strong-motion instrumentation would have provided stronger constraints on the timing of the complex rupture. The relative orientation of the regional stress field and the faulting regime explain the sense of motion and loading of these fault segments. Additionally, dynamic stress changes also created favorable conditions for triggering of the main rupture on the Greendale fault. Current work focuses on evaluating how well the UCERF3 (USGS Open File Report 2013-1165) criteria for forecasting multi-segment ruptures in California apply to this complex rupture in New Zealand.

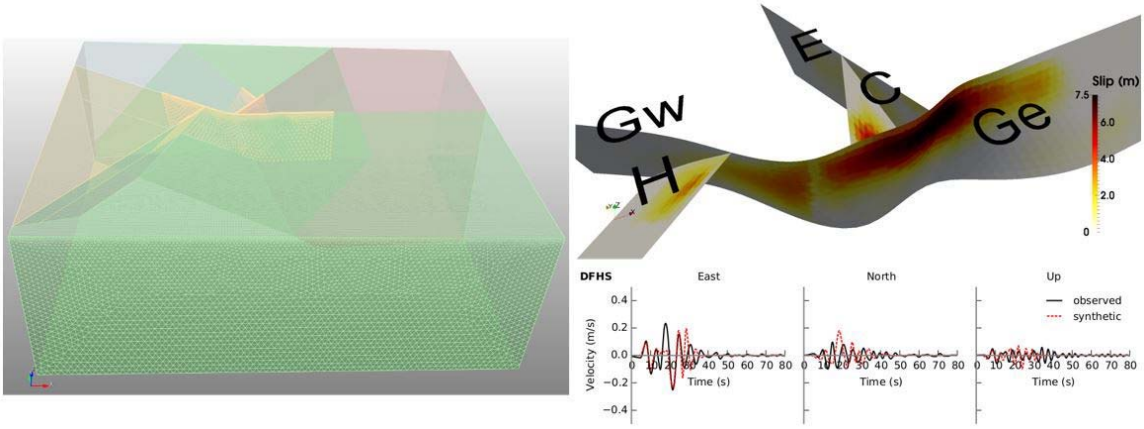

Image of the finite-element model (left), Elliott et al. slip model (upper right), and comparison of synthetic and observed T > 1s velocity waveforms at station DFHS with inverted subevent origin times.

CIG Code(s): PyLith

Evaluation of effect of salt diapirs on fault source inversions

William D. Barnhart and Rowena B. Lohman, Cornell University

Inversions of coseismic geodetic data, such as InSAR, for the orientation of a fault that ruptured during an earthquake, sense of motion along that fault, and earthquake magnitude, often use homogeneous elastic half spaces or layered spaces that do not necessarily well represent the 3D variation of material properties within the real earth. We examine a set of data spanning two magnitude 6 earthquakes that occurred in southern Iran within 3 years of eachother, on either side of one of the salt diapirs that occur throughout the region.

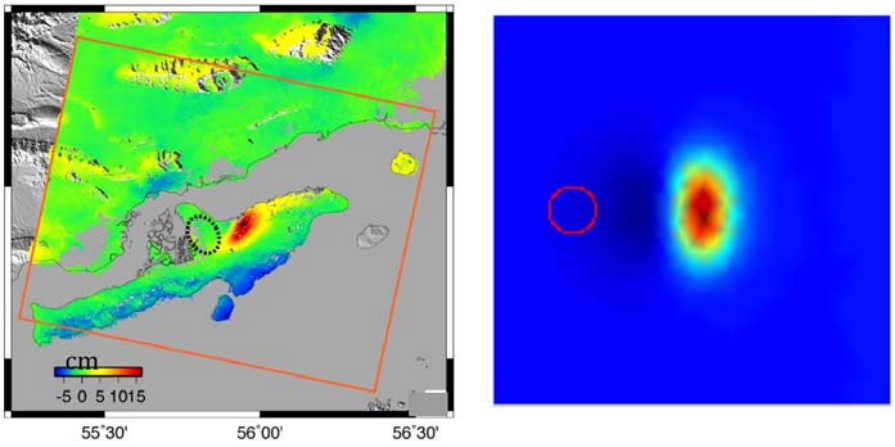

One of a series of magnitude 6 earthquake in southern Iran (left), with color indicating motion towards the satellite with a sense consistent with thrust faulting. Dashed line indicates extent of salt dome. Right – example of forward model using Pylith to simulate region of salt diapir (red circle) with different elastic parameters than surroundings – this synthetic data is then used in inversions to assess bias.

The goal of this work is to assess the impact that such heterogeneity will have on an inversion when it is neglected during the generation of a forward model – i.e., if we generate data with Pylith that contains heterogeneities, then invert it with an elastic half space, how much of a bias do we introduce. For this particular setting, the main effect is on the dip and rake of the inferred fault and slip distribution. The figure above shows an idealized setting where the diapir is immediately to the east of a N-S-dipping thrust fault. With the parameters used in this example, the diapir results in a very slight decrease in the amount of subsidence relative to the case with no diapir. In a nonlinear inversion for fault geometry using forward models within an elastic halfspace, this will perturb the solution in the direction of slightly shallower fault dips, but will also result in an inability for the inversion to fit the data exactly. In other words, there is a remaining residual that requires either a complicated slip distribution or more complicated fault geometry – this may be used as an indication of unmodeled material heterogeneities.

CIG Code(s): PyLith

Combining short-term and long-term stress models to evaluate stress perturbations during the 2010 Darfield, New Zealand, earthquake

Susan Ellis and Charles Williams, GNS Science, New Zealand

The Mw 7.1 Darfield earthquake in September 2010, was a complex event with nearly simultaneous ruptures on numerous fault surfaces. This event occurred in a region with little to no historical seismicity; however, since then the Canterbury earthquake sequence has been extremely active. In an attempt to understand the stress changes during this event, we have computed the long-term stress field using the SULEC finite element code (Ellis et al., 2011). Then, using the Darfield slip distribution inferred geodetically by Beavan et al. (2012), we used the PyLith finite element code to compute the stress changes induced by the earthquake. When we combine the stress fields, we observe rotations of the principal stress axes that are in general agreement with those observed from aftershock data. We hope to use these combined models to place constraints on the preexisting stress field for the Canterbury region.

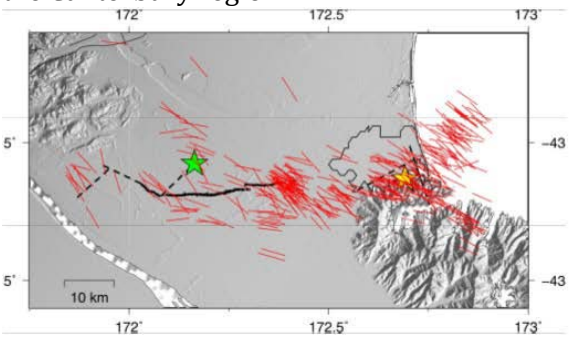

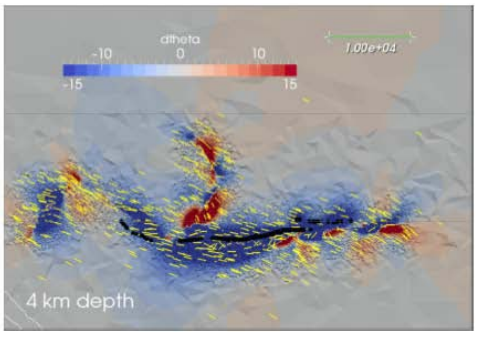

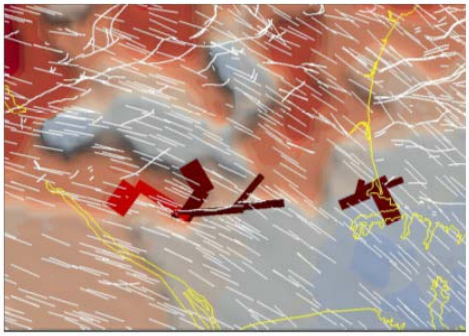

The upper left plot shows P-axis deflections inferred from aftershock data. On the lower left are the long-term maximum compressive stress directions computed by SULEC. At the upper right are the compressive stress orientations after including the coseismic stress changes computed by PyLith. Note the rotation of stress axes close to the faults, which are generally in agreement with those inferred from the aftershock data.

CIG Code(s): PyLith

References

Ellis, S. M., C. A. Williams, M. E. Reyners, D. Eberhart-Phillips, R. J. Beavan, and L. M. Wallace, Variations in mid-crustal density beneath northern Canterbury : the effect on stresses and postseismic strain-rates, p. 30-31 IN: Reid, C.M.; Wandres, A. (eds) Geosciences 2013 : Annual Conference of the Geoscience Society of New Zealand : abstracts. [Christchurch]: Geoscience Society of New Zealand. Geoscience Society of New Zealand miscellaneous publication 136A.

Finite element modeling of a voluminous active intrusion in Bolivia

Scott T. Henderson and Matthew E. Pritchard, Cornell University, Ithaca, NY

Uturuncu is a dacitic stratovolcano in southwest Bolivia, located at the center of a 3,800 km2 region currently uplifting at up to 1 cm/yr. Although the youngest lava flows from Uturuncu have been dated at 270 ka, the summit has active fumaroles, it is positioned in an area of intense silicic Miocene volcanism (the Altiplano Puna Volcanic Complex), and InSAR data shows that uplift has been occurring steadily since at least 1992. Combining two decades of InSAR data also shows evidence for a 'moat' of subsidence, up to 4 mm/yr over a 13,000 km^2 area. The unique combination of concentric surface uplift and subsidence could result from vertical ascent of magma from the lower crust (70 km) to the upper crust (20 km), or may result from the initiation of diapiric rise in the hot upper crust. Both mechanisms suggest magma migration at approximately 20 km depth, which coincides with a geophysically imaged zone of partial melt known as the Altiplano Puna Magma Body (APMB). Whether the current deformation is primarily due to the lateral migration of partial melt within the APMB toward a central diapir, due to the underplating of a recent intrusion, or due to an entirely different process, is an open question.

Surface deformation at Uturuncu can be replicated by vertically stacked finite pressure sources in a viscoelastic medium. However, rheological constraints imposed by compositional gradients, temperature gradients, and a layer of partial melt such as the APMB play a fundamental role in the transmission of shear and normal stresses from pressurization at depth. We therefore explore a range of realistic subsurface conditions with 3D finite element forward models using PyLith. Combing over 750 Envisat and ERS interferograms from two descending and two ascending tracks we calculate representative profiles of vertical and radial surface displacement to validate model output. Models are constrained by regional and local geophysical and petrological datasets including: seismic tomography, gravimetry, heat flow, and compositional analyses of surface deposits. Results are therefore tuned to the unique conditions at Uturuncu, but give general insight into volcanic deformation resulting from pressurization below the brittle-ductile transition.

CIG Code(s): PyLith

References

Henderson, S. T. and M. E. Pritchard, Viscoelastic finite element models of an active magmatic intrusion at Uturuncu Volcano, Bolivia: Insights into vertical ascent through stratified continental crust, IAVCEI 2013 scientific assembly, July 20-24, 2013, Japan.

Henderson, S. T., M. E. Prtichard, M. Diez and R. Del Potro, Geodetic observations and finite element models of a voluminous active intrusion: Uturuncu Volcano, Bolivia, AGU fall meeting, 2012, San Francisco.

Reservoir characterization in an underground gas storage field using joint inversion of flow and geodetic data

B. Jha[1,2], F. Bottazzi[3], R. Wojcik[1], M. Coccia[2], N. Bechor[2], D. McLaughlin[1], T. Herring[2], B. H. Hager[2], S. Mantica[3], R. Juanes[1,2],
[1]Civil and Environmental Engineering, Massachusetts Institute of Technology, USA
[2]Earth, Atmospheric and Planetary Sciences, Massachusetts Institute of Technology, USA
[3]Divisione E& P, Eni S.p.A., Italy

Characterization of reservoir properties like porosity and permeability in reservoir models typically relies on history matching of production data, well pressure data, and possibly other fluid-dynamical data. Calibrated (history-matched) reservoir models are then used for forecasting production, and designing effective strategies for improved oil and gas recovery. Here, we perform data assimilation of both flow data and deformation data for joint inversion of reservoir properties. Given the coupled nature of the process, joint inversion requires efficient simulation tools of coupled reservoir flow and mechanical deformation. We apply our coupled simulation tool to a real underground gas storage field in Italy. We simulate the initial gas production period, and several decades of seasonal natural gas storage and production. We perform a probabilistic estimation of rock properties by joint inversion of ground deformation data from geodetic measurements and fluid flow data from wells. Using an efficient implementation of the Ensemble Smoother as the estimator, and our coupled multiphase flow and geomechanics simulator as the forward model, we show that incorporating deformation data leads to a significant reduction of uncertainty in the prior distributions of rock properties such as porosity, permeability, and pore compressibility.

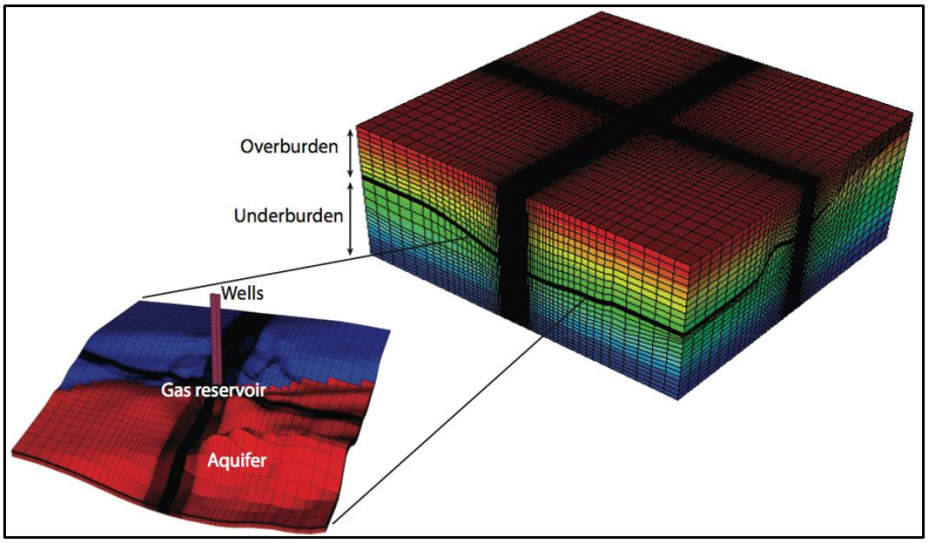

Geomechanical simulation grid (right) and a magnified view of the flow simulation grid (left). The flow domain appears sandwiched between the overburden and the underburden.

CIG Code(s): PyLith

References

Jha, B., F. Bottazzi, R. Wojcik, et al. Reservoir characterization in an underground gas storage field using joint inversion of flow and geodetic data. Int. J. Numer. Anal. Meth. Geomech., Submitted.

High-resolution geodetic observations of fault zone deformation on the San Andreas and San Jacinto faults in southern California

Eric O. Lindsey, Yuri. Fialko, Valerie. J. Sahakian, Yehuda Bock, Scripps Institution of Oceanography; Sylvain Barbot, Earth Observatory of Singapore; Thomas. K. Rockwell, San Diego State University; Roger Bilham, University of Colorado

We investigate the spatial pattern of surface creep and off-fault deformation along the southern segment of the San Andreas Fault using a combination of multiple interferometric synthetic aperture radar viewing geometries and survey-mode GPS occupations of a dense array crossing the fault. Radar observations from Envisat during the period 2003–2010 were used to separate the pattern of horizontal and vertical motion, providing a high-resolution image of uplift and shallow creep along the fault trace. Creep is localized on a well-defined fault trace only in the Mecca Hills and Durmid Hill areas, while elsewhere creep appears to be distributed over a 1–2 km wide zone surrounding the fault. The degree of strain localization is correlated with variations in the local fault strike. Using a two-dimensional boundary element model, we show that stresses resulting from slip on a curved fault can promote or inhibit inelastic failure within the fault zone in a pattern matching the observations. The occurrence of shallow, localized interseismic fault creep within mature fault zones may thus be partly controlled by the local fault geometry and normal stress, with implications for models of fault zone evolution, shallow coseismic slip deficit, and geologic estimates of long-term slip rates.

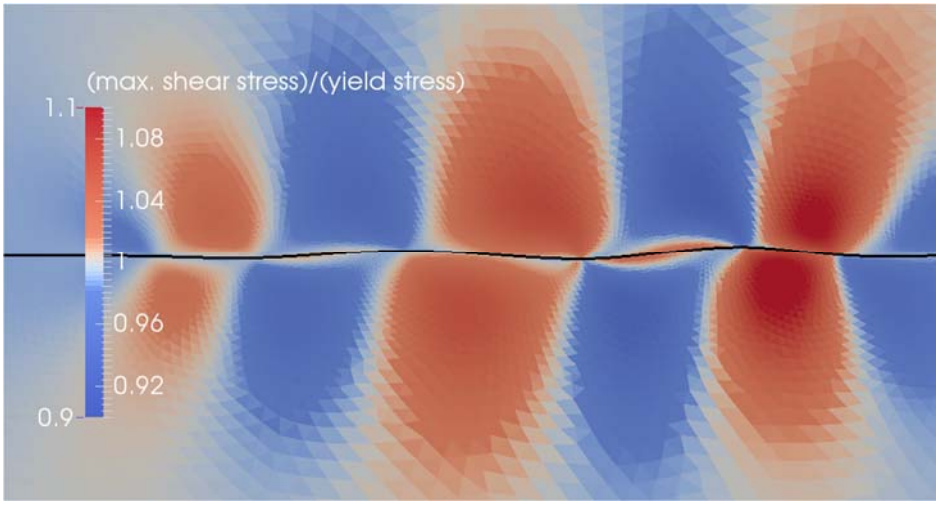

Ratio between the maximum shear stress and Coulomb failure criterion for uniform slip on a fault in a 2D elastic half space. Red areas indicate predicted off-fault yielding – future models will include plasticity to account for this effect.

CIG Code(s): PyLith

References:

High-resolution geodetic observations of fault zone deformation on the San Andreas and San Jacinto faults in southern California. E. O. Lindsey, V. J. Sahakian, Y. Fialko, Y. Bock, S. Barbot, and T. K. Rockwell. Abstract T21E-01 (invited) presented at 2013 AGU Fall Meeting, San Francisco, Calif., 9-13 Dec. 2013.

3D Dynamic Rupture Simulations Across Interacting Faults: The Mw7.0, 2010, Haiti Earthquake

Douilly Roby, Hideo Aochi, Eric Calais, Andrew M. Freed

The mechanisms controlling rupture propagation between fault segments during a large earthquake are key to the hazard posed by fault systems. Rupture initiation on a smaller fault sometimes transfers to a larger fault, resulting in a significant event (*e.g.i*, 2002 M7.9 Denali U.S.A and 2010 M7.1 Darfield New Zealand earthquakes. In other cases, rupture is constrained to the initial fault and does not transfer to nearby faults, resulting in events of more moderate magnitude. This was the case of the 1989 M6.9 Loma Prieta and 2010 M7.0 Haiti earthquakes, which initiated on reverse faults abutting against a major strike-slip plate boundary fault but did not propagate onto it. Here we investigate the rupture dynamics of the Haiti earthquake, seeking to understand why rupture propagated across two segments of the Léogâne fault but did not propagate to the adjacent Enriquillo Plantain Garden Fault, the major 200 km-long plate boundary fault cutting through southern Haiti. We use a finite element model to simulate propagation of rupture on the Léogâne fault, varying friction and background stress to determine the parameter set that best explains the observed earthquake sequence, in particular, the ground displacement. The two slip patches inferred from finite-fault inversions are explained by the successive rupture of two fault segments oriented favorably with respect to the rupture propagation, while the geometry of the Enriquillo fault did not allow shear stress to reach failure.

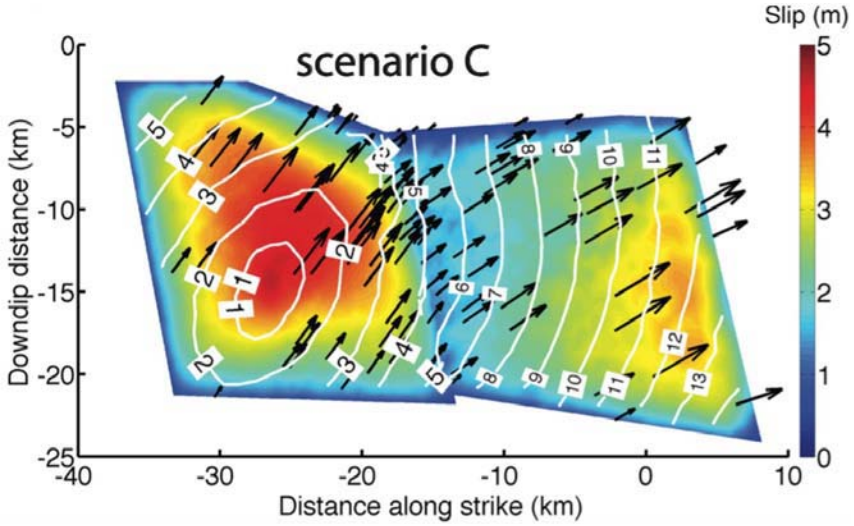

Distribution of final slip for scenario C. The colors denote the magnitude of the final slip. The arrows indicate the slip vectors at randomly selected point on the faults. The white lines indicate the rupture propagation, the time slip begins at each point on the faults.

CIG Code(s): PyLith

References

Douilly R., H. Aochi, E. Calais, A.M. Freed, 3D Dynamic Rupture Simulations Across Interacting Faults: The Mw7.0, 2010, Haiti Earthquake. Journal of Geophysical Research, in press.

Measurement and Modeling of Cryosphere-Geosphere interactions in South Central, Alaska

Jeanne Sauber, Shin-Chan Han, Scott Luthcke, NASA Goddard Space Flight Center, Natasha Ruppert, AEIC, GI, University of Alaska Fairbanks, and Ron Bruhn, University of Utah

The cryosphere interacts with the solid Earth and sea level over time scales varying from as short as geodetic observations to the span of the last interglacial. Modeling of the solid Earth response to variable cryosphere changes plays a critical role in decontaminating both regional and global geodetic signals for the studies of hydrologic, ice and ocean mass changes and is a critical factor in supporting interpretations of time-variable gravity (i.e. from the GRACE satellite mission). With the PyLith finite element modeling (FEM) code we calculated the predicted time-dependent displacements and stresses due to surface loading and unloading associated with snow accumulation and ice/snow wastage for alternate rheological structures. We used a 400 km X 400 km X 200 km FEM grid with 10 km cell spacing. For the results given below, we assumed a 30 km elastic layer over a 170 km isotopic Maxwell material layer with a linear viscous rheology and h = 10^{18} Pa s. The load was input over a 100 km East-West X 50 km North-South region in southern, coastal Alaska. The magnitude and timing of the accumulation and wastage cycle was estimated using a combination of the GRACE 1° x 1° degree mascon results, snow models and GPS reflectometry (K. Larson, 2012).

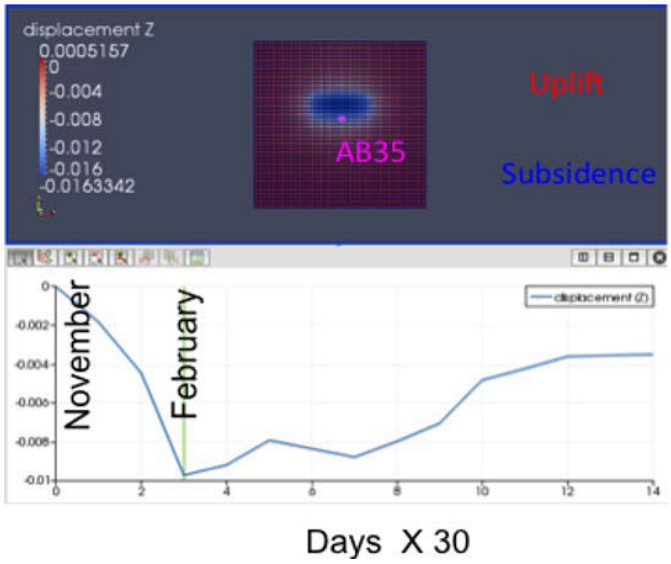

(Top) Our PyLith calculations show subsidence at the time of maximum snow loading in late Feb/early March just prior to snow melt onset. (Bottom) The Z displacement as a function of time. For a near-coastal central Gulf of Alaska GPS site such as AB35, most of the seasonal snow loading is north of the site and the Vertical and North (not shown) GPS position components would be predicted to see significant (> 2mm) seasonal position changes. For viscosities h < 10^{19} Pa s, the viscoelastic response to snow loading and unloading could influence estimates of the long-term trend used to estimate ongoing tectonic strain accumulation.

CIG Code(s): PyLith

Acknowledgements: Charles Williams, Brad Aagaard, and Matt Knepley

References Sauber, J., S. Han, S. Luthcke, N. Ruppert, and R. Bruhn, 2014, Measurement and modeling of Cryosphere-Geosphere interactions in South Central Alaska, 2014 Fall AGU, G51A-0338.

Modeling shear wave splitting due to stress-induced anisotropy, with an application to Mount Asama Volcano, Japan

Adrian Shelley and Martha Savage, Victoria University of Wellington, Charles Williams, GNS Science, Yosuke Aoki, Earthquake Research Institute, Tokyo, and Boris Gurevich, Curtin University of Technology, Perth

We use numerical modeling to investigate the proposed stress-based origin for changing anisotropy at Mount Asama Volcano, Japan. Stress-induced anisotropy occurs when deviatoric stress conditions are applied to rocks which are permeated by microcracks and compliant pore space, leading to an anisotropic distribution of open crack features. Changes to the local stress field around volcanoes can thus affect the anisotropy of the region. The 2004 eruption of Mount Asama Volcano coincided with time-varying shear wave splitting measurements, revealing changes in anisotropy that were attributed to stress changes associated with the eruption. To test this assertion, we create a model that incorporates knowledge of the volcanic stress, ray tracing, and estimation of the anisotropy to produce synthetic shear wave splitting results using a dyke stress model. Anisotropy is calculated in two ways, by considering a basic case of having uniform crack density and a case where the strength of anisotropy is related to dry crack closure from deviatoric stress. Our results show that this approach is sensitive to crack density, crack compliance, and the regional stress field, all of which are poorly constrained parameters. In the case of dry crack closure, results show that modeled stress conditions produce a much smaller degree of anisotropy than indicated by measurements. We propose that the source of anisotropy changes at Asama is tied to more complex processes that may precipitate from stress changes or other volcanic processes, such as the movement of pore fluid.

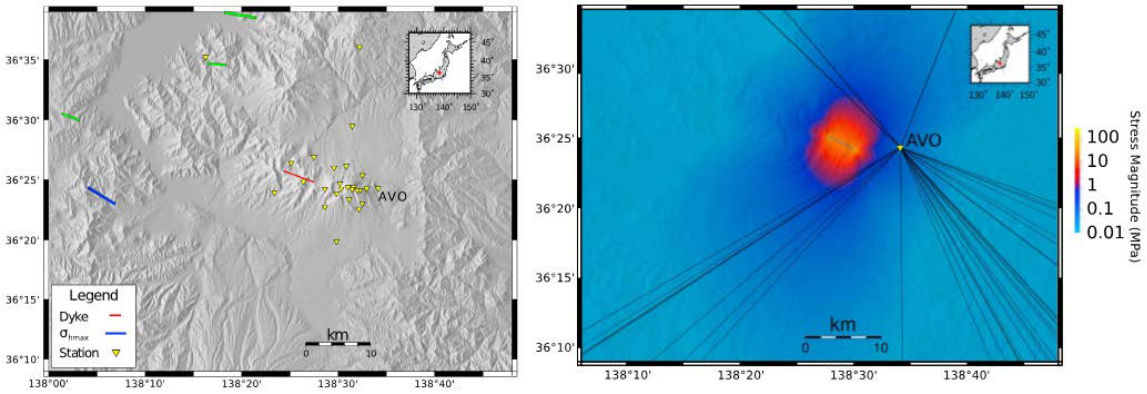

Asama region in central Japan (left), and stresses computed for dyke opening (right).

CIG Code(s): PyLith

References

Shelley, A., M. Savage, C. Williams, Y. Aoki, and B. Gurevich (2014), Modeling shear wave splitting due to stress-induced anisotropy, with an application to Mount Asama Volcano, Japan, *J. Geophys. Res. Solid Earth*, *119*, 4269–4286, doi:10.1002/2013JB010817.

Effects of material property variations on slip estimates for subduction interface slow slip events

Charles A. Williams, GNS Science, New Zealand and Laura M. Wallace, University of Texas

We investigate the influence of elastic heterogeneity on geodetic inversions of slow slip events (SSEs) by inverting for slip distributions of four events along the Hikurangi Margin, New Zealand. We generate Green's functions using a finite element code in conjunction with a New Zealand-wide seismic velocity model to assign elastic properties. We find that these heterogeneous models typically require ~20% less slip than homogeneous models in cases where the slip is deep or there is reasonable geodetic coverage above the slipping region. In cases where the slip is shallow (and mostly offshore) and there is little geodetic coverage directly above the slipping region, the heterogeneous models can predict significantly larger amounts of slip (42% in our study). These changes in the predicted amounts of slip have important implications for quantifying slip budgets accommodated by slow slip at subduction zones worldwide.

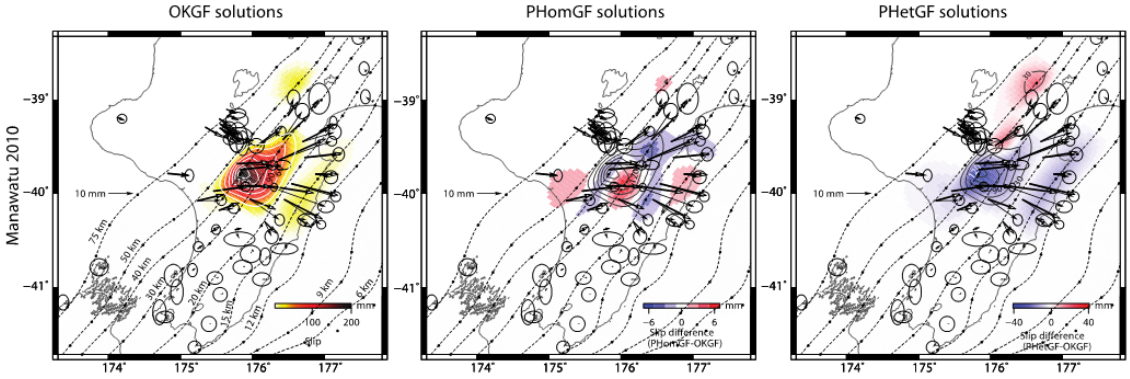

Inversion results for the 2010 Manawatu slow slip event. Leftmost plot shows results computed with Defnode (McCaffrey, 1995; 2002). Center plot shows slip using PyLith –generated Green's functions with homogeneous properties (line contours) and PyLith slip minus Defnode slip (color contours). The nearly identical solutions validate our technique. Rightmost plot shows slip inferred from PyLith-generated Green's functions and the New Zealand-wide seismic velocity model of Eberhart-Phillips et al. (2010) to assign elastic properties. Line contours are the inferred slip distribution, and color contours are the difference with the Defnode solution. Note the significant difference in the inferred slip distributions.

CIG Code(s): PyLith

References

McCaffrey, R. (1995), *DEF-NODE User's Guide*, Rensselaer Polytech. Inst., Troy.

McCaffrey, R. (2002), Crustal block rotations and plate coupling, in *Plate Boundary Zones, Geodyn. Ser.*, vol. 30, edited by S. Stein and J. Freymueller, pp. 100-122, AGU, Washington, D. C.

Eberhart-Phillips, D., M. Reyners, S. Bannister, M. Chadwick, and S. Ellis (2010). Establishing a versatile 3D seismic velocity model for New Zealand, *Seismol. Res. Lett.*, *81*, no. 6, 992-1000, doi:10.1785/ gssrl.81.6.992.

Williams, C. A. and L. M. Wallace, Effects of material property variations on slip estimates for subduction interface slow slip events, Geophys. Res. Lett., accepted, 2015.

Relax: unified models of postseismic relaxation

Sylvain Barbot, Earth Observatory of Singapore, Nanyang Technological University.

Postseismic deformation is a mechanism of relaxation of the rapid stress changes in the crust and mantle that incur due to earthquakes. This phenomenon offers a window into the mechanics of off-fault deformation and allows us to probe the mechanical properties of the lithosphere and mantle. The sources of postseismic deformation include afterslip the fault that ruptured coseismically or nearby faults, poroelastic deformation and viscoelastic flow in the lower crust and asthenosphere. Depending on the pressure and temperature conditions, the viscoelastic flow can be controlled by a linear or a non-linear stress/strain rate relationship. The aseismic creep on faults is controlled by rate and state friction. Relax simulates the postseismic relaxation accounting for both viscoelastic flow and afterslip. Furthermore, both linear and nonlinear viscoelastic flow can both take place in the models.

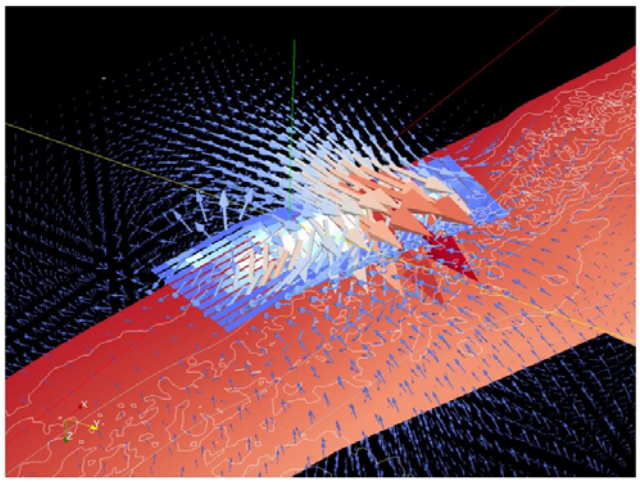

Visualization of the three-dimensional displacements occurring one year after the 2010 Mw 8.8 Maule earthquake. The model includes afterslip down-dip of the main shock and viscoelastic flow in the oceanic mantle and in the mantle wedge. We model the effect of the elastic slab using SLAB 1.0 (Hayes et al., 2010).

Relax is a semi-analytic model whereby the inelastic processes of deformation are represented by fictitious equivalent body forces. The displacement and stress are evaluated using an analytical solution in the Fourier domain. The coseismic displacements are also represented by equivalent body forces. This greatly simplifies the description of the model, as the difficult and often labor-intensive meshing step is not needed. The model can account for arbitrary distributions of viscosity in three dimensions. The Relax package also comes with a database of published slip distributions for earthquakes and slow-slip events just shy of one hundred cases.

CIG Code: Relax

Acknowledgements: Earth Observatory of Singapore

References

Barbot, Sylvain, and Yuri Fialko. "A unified continuum representation of post-seismic relaxation mechanisms: semi-analytic models of afterslip, poroelastic rebound and viscoelastic flow." *Geophysical Journal International* 182.3 (2010): 1124-1140.

Crustal Deformation in the New Madrid Seismic Zone and the Role of Postseismic Processes

Oliver Boyd, USGS, Robert Smalley, Jr., University of Memphis, and Yuehua Zeng, USGS

Global Navigation Satellite System data across the New Madrid seismic zone (NMSZ) in the central United States over the period from 2000 through 2014 are analyzed and modeled with several deformation mechanisms including: (1) subsurface creep; (2) postseismic frictional afterslip and viscoelastic relaxation from the 1811–1812 and 1450 earthquakes in the NMSZ; and (3) regional shear. Postseismic frictional afterslip and viscoelastic relaxation are modeled with the program Relax. In agreement with previous studies, a dislocation creeping at about 5 mm/yr between 12 and 20 km depth along the downdip extension of the Reelfoot fault reproduces the observations well. We find that the predictions of this kinematic creep model can be reproduced by a dynamic model of postseismic frictional afterslip from the 1450 and February 1812 Reelfoot fault events. Creep and afterslip on the downdip extension of the Cottonwood Grove fault and models of viscoelastic relaxation following the 1811–1812 earthquakes provide minimal predictive power. This is likely due to the smaller size of the December event and a distribution of stations better suited to constrain localized strain across the Reelfoot fault. Regional shear is found to be less than 0.3 mm/yr. If in fact much of the present-day surface deformation results from afterslip, it is likely that many of the earthquakes we see today in the NMSZ are aftershocks from the 1811–1812 New Madrid earthquakes. Despite this conclusion, our results are consistent with observations and models of intraplate earthquake clustering. Given this and the recent paleoseismic history of the region, we suggest that seismic hazard is likely to remain significant.

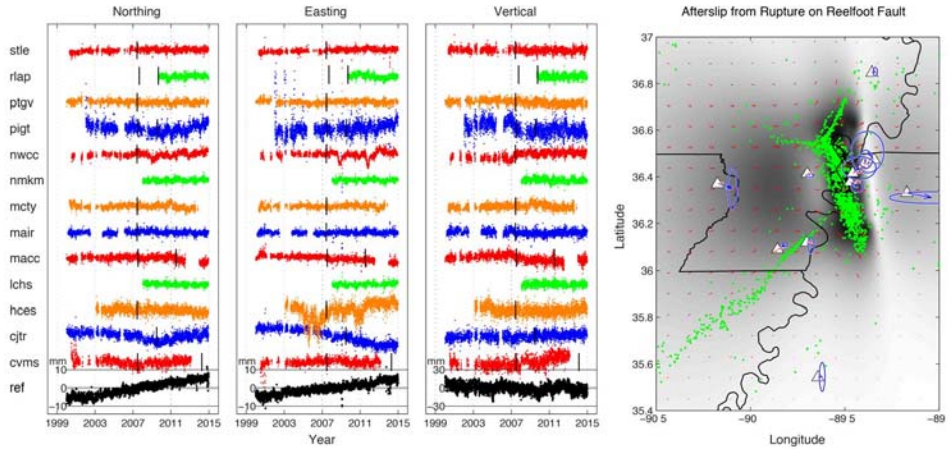

Position time series for stations of the GPS Array for Mid America network (left), and observed horizontal velocities (blue vectors) and model results (red vectors and gray shading) for afterslip from the February 1812 earthquake on the Reelfoot fault.

CIG Code: Relax

Acknowledgements: Sylvain Barbot provided important feedback on the use of the program Relax. Paul Segall, Michael Hamburger, John Langbein, Fred Pollitz, and Rob Williams provided feedback that helped improve the clarity and significance of our work.

References

Boyd, O.S., R. Smalley Jr., and Y. Zeng, Crustal Deformation in the New Madrid Seismic Zone and the Role of Postseismic Processes, Submitted to Journal of Geophysical Research.

Bayesian inference of Late Pleistocene deglaciation models

Daniele Melini, Istituto Nazionale di Geofisica e Vulcanologia, Roma, Italy
Nicola Piana Agostinetti, Dublin Institute for Advanced Studies, Dublin, Ireland
Giorgio Spada, Dipartimento di Scienze di Base e Fondamenti, University of Urbino, Italy

Glacial Isostatic Adjustment (GIA) contributes significantly to observed geodetic velocities in regions formerly covered by late-Pleistocene ice sheets. Modeling the response of the crust to the melting of ice sheets is therefore a crucial aspect for the correct interpretation of present-day geodetic observations. An accurate GIA modeling depends both on the knowledge of the Earth's viscosity structure and of the melting history of the ice sheets. These can be inferred on the basis of observed relative sea-level histories. The development of Bayesian inference methods potentially allows solving this kind of inverse problems, simultaneously providing information on tradeoffs between model parameters and sensitivities. We plan to build on the deglaciation models that have been proposed in literature (see e.g., Peltier, 2004) by exploring in a Bayesian framework the relationship between the ice deglaciation history and the Earth's viscosity profile.

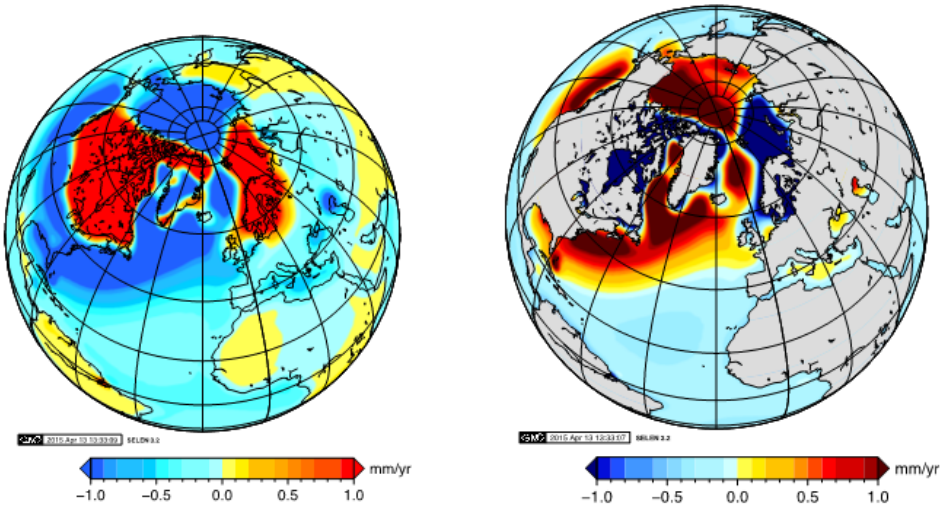

Rates of present-day uplift (left) and relative sea-level variation (right) computed with the SELEN code according to the ICE-5G deglaciation model (Peltier, 2004).

Bayesian inference is based on the repeated sampling of the model space and requires the computation of the surface deformations (i.e. the forward problem) for an ensemble of coupled Earth and ice models. We plan to implement a new functionality in the SELEN code, aimed at a quick evaluation of the misfit between observed and predicted relative sea-level histories, minimizing the disk I/O and eliminating all unnecessary output. The inverted models will be used to improve the GIA corrections to gravity observations obtained by GRACE (the Gravity Recovery And Climate Experiment) and trends of sea-level change observed from altimetry missions.

CIG Code(s): SELEN

Acknowledgements (optional):

References

W.R. Peltier, 2004. Global Glacial Isostasy and the Surface of the Ice-Age Earth: The ICE-5G (VM2) Model and GRACE, Ann. Rev. Earth and Planet. Sci., 32, 111-149.

Nonlinear optimization algorithms for large-scale seismic waveform inversion

Ryan Modrak and Jeroen Tromp, Princeton University

With the increasing scale of waveform inversion problems in seismology, attention to the details of an inversion's underlying nonlinear optimization procedure is becoming essential. To help practitioners in this regard, we compare the efficiency of optimization algorithms through regional, global, and exploration test cases. In all these experiments, quasi-Newton algorithms provided the best performance. Newton and Gauss Newton methods, which can be implemented in a matrix free manner to avoid storing the Hessian or Jacobian, were not quite competitive, though promising improvements are demonstrated. Nonlinear conjugate gradient methods, which are still perhaps the most widely used type of algorithm, were least efficient and least robust, requiring monitoring to avoid numerical stagnation. Overall, the combination of a quasi-Newton algorithm and a backtracking line search was found to be particularly effective, providing computational savings of 30 to 60 percent over the next closest competitors.

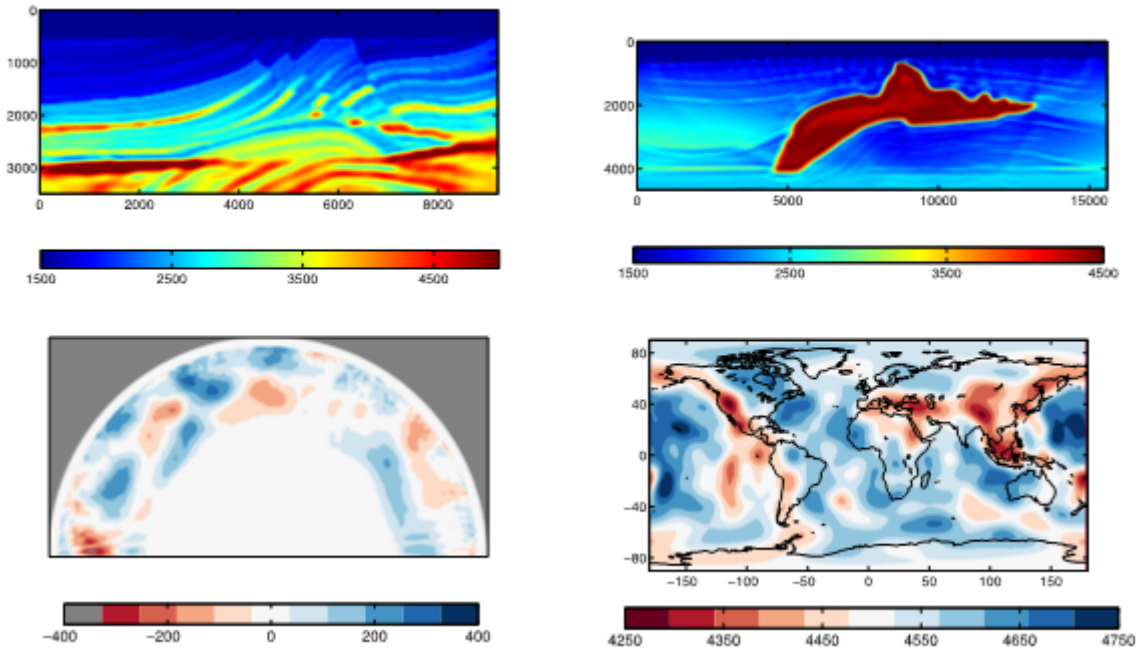

***Top row**: Seismic exploration test cases used to compare optimization algorithms. Each panel represents a vertical cross section through the shallow subsurface. Compressional wave speed is plotted. **Bottom row**: Global tomography test cases. The right panel represents a radial section through the Earth, and the left panel represents a constant depth slice. Compressional wave speed variations are plotted on the left, and 40 s Rayleigh phase velocity is plotted on the right.*

CIG Code(s): SPECFEM2D, SPECFEM3D, SPECFEM3D_GLOBE

References: Ryan Modrak and Jeroen Tromp, Nonlinear optimization algorithms for large-scale seismic waveform inversion, *Geophysical Journal International*, *in prep.*

High-resolution seismic array imaging based on a SEM-FK hybrid method

Ping Tong[1], Wu Chen[2], Dimitri Komatitsch[3], Piero Basin[1], and Qinya Liu[1]

[1]Department of Physics, University of Toronto, [2]Institute of Oceanography, National Taiwan University, [3]LMA, CNRS UPR 7051, Aix-Marseille University

We demonstrate the feasibility of high-resolution seismic array imaging based on teleseismic recordings using full numerical wave simulations. We develop a hybrid method that interfaces a frequency–wavenumber (FK) calculation with a spectral-element (SEM) numerical solver to calculate synthetic responses of local heterogeneous media to plane-wave incidence.This hybrid method accurately deals with local heterogeneities and discontinuity undulations, and provides an efficient tool for the forward modelling of teleseismic coda waves. We compute sensitivity kernels for teleseismic coda waves based on adjoint techniques. These sensitivity kernels provide the basis for mapping variations in subsurface discontinuities, density and velocity structures through non-linear conjugate-gradient methods. Various synthetic imaging experiments, including discontinuity

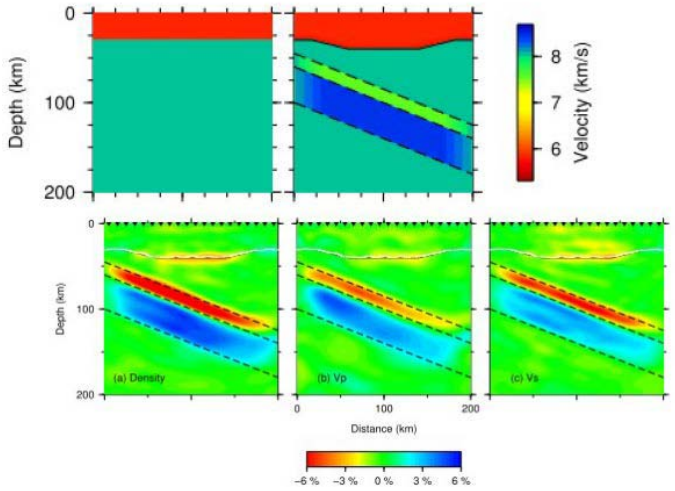

Top two panels: the initial 1D model and synthetic `true' 3D model. Bottom three panels: the recovered density, velocity and Moho variations based on the main P phase and converted/scattered waves.

characterization and volumetric structural inversion for the crust or subduction zones, show that using preconditioners based upon the scaled product of sensitivity kernels for different phases, combining finite-frequency traveltime and waveform inversion, and/or adopting hierarchical inversions from long- to short-period waveforms can reduce the nonlinearity of the seismic inverse problem and speed up its convergence. These encouraging results demonstrate the promising future of teleseismic coda wave imaging based on the SEM-FK hybrid method and adjoint techniques beneath dense seismic array.

CIG Code(s): SPECFEM2D

References:

High-resolution seismic array imaging based on a SEM-FK hybrid method, P. Tong, C. W. Chen, D. Komatitsch, P. Basini and Q. Liu, GJI, 197, 369-395 (2014).

Full-waveform-difference adjoint tomography based on a wavelet multiscale analysis

Yanhua O. Yuan and Frederik J. Simons, Princeton University
Ebru Bozdag, University of Nice Sophia Antipolis

Convergence and stability of full-waveform-difference adjoint schemes are greatly improved when data and synthetics are progressively presented to the algorithms in a constructive multiscale approximation using a (bi)orthogonal wavelet transform. Wavelets provide the nonredundant spectral decomposition that paves the way for the inversion to proceed successively from long-wavelength fitting to detailed exploration of the phases in the seismogram. We have applied the multi-scale approach successfully to body waves generated in a standard model from the exploration industry: a modified two-dimensional elastic Marmousi model. With this model we explored the optimal choice of wavelet family, number of vanishing moments and decomposition depth.

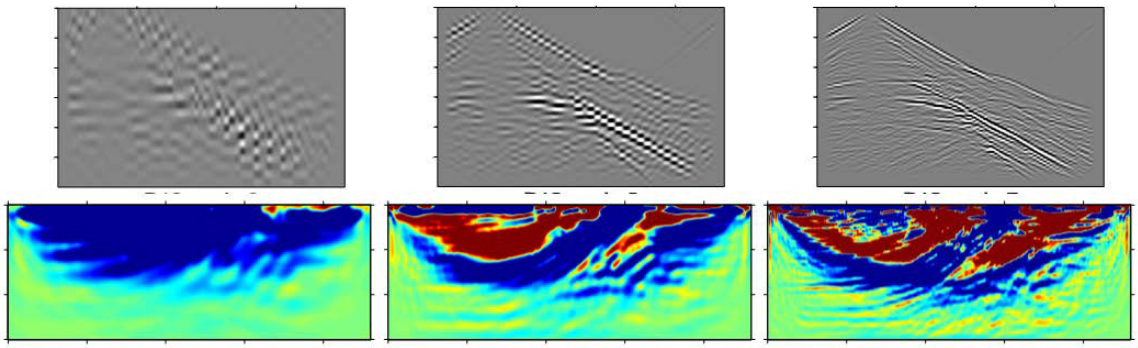

Top: Wavelet-subspace representations of shot gathers from coarse to fine scales. Bottom: Corresponding waveform-adjoint kernels showing increased complexity.

The incorporation of surface waves is rife with cycle-skipping problems compared to the inversions considering body waves only. We implemented an envelope-based objective function probed via a multiscale wavelet analysis to measure the distance between predicted and target surface-wave waveforms in a synthetic model of heterogeneous near surface structure. An elastic shallow model with 100~m in depth is used to test the surface-wave inversion scheme. We also analyzed the sensitivities of surface waves and body waves in full waveform inversions, as well as the effects of incorrect density information on elastic parameter inversions. Based on those numerical experiments, we ultimately formalized a flexible scheme to consider both body and surface waves in adjoint tomography. While our early examples are constructed from exploration style settings, our procedure will be very valuable for the study of global network data.

CIG Code(s): SPECFEM2D

Acknowledgements: U.S. National Science Foundation

References:

Yuan, Y. O., and F. J. Simons, Multiscale adjoint waveform-difference tomography using wavelets, Geophysics, 79(3), WA79-WA95, doi: 10.1190/GEO2013-0383.1, 2014.

Yuan, Y. O., F. J. Simons and Ebru Bozdag, Multiscale adjoint waveform tomography for surface and body waves, Geophysics, 2015 (accepted).

A 3D spectral-element and frequency-wavenumber (SEM-FK) hybrid method for high-resolution seismic array imaging

Ping Tong[1], Dimitri Komatitsch[2], Tai-Lin Tseng[3], Shu-Huei Hung[3], Chin-Wu Chen[4], Piero Basini[1], and Qinya Liu[1]; [1]Department of Physics, University of Toronto, [2]LMA, CNRS UPR 7051, Aix-Marseille University, [3]Department of Geosciences, National Taiwan University, [4]Institute of Oceanography, National Taiwan University

Teleseismic array imaging based on converted and scattered waves is one of the essential tools for investigating the crustal and upper mantle structures, and has contributed significantly to our understanding of tectonic evolution and internal geodynamic processes at regional scales. To model the scattered/converted waves of teleseismic body waves beneath seismic arrays, we present an innovative 3D hybrid method that interfaces the spectral-element methods (SEM) with the frequency-wavenumber (FK) technique. The SEM is capable of dealing with complex structural heterogeneities, surface topography and undulated interfaces with high accuracy, while the FK method supplies the boundary values for 1D layered background models.

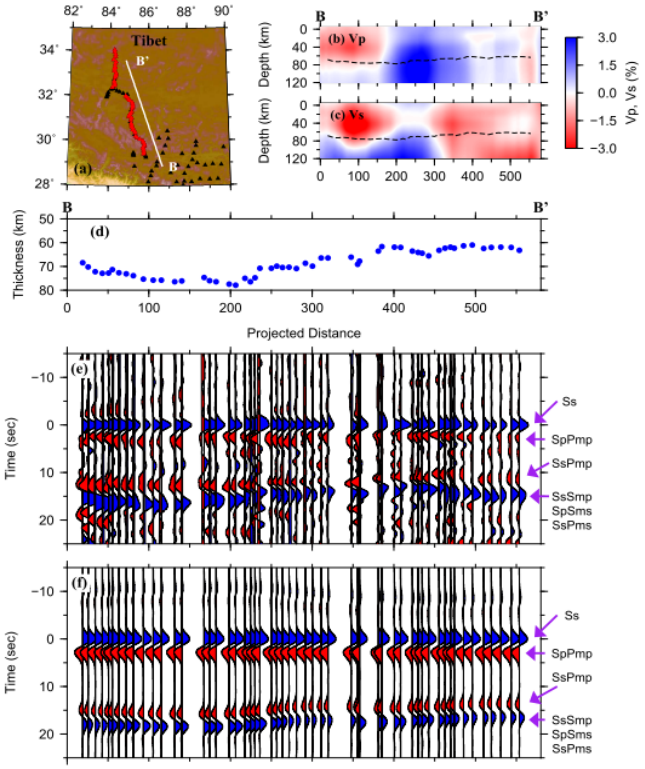

(a-d) Moho profile and 3D velocity variations along BB' on the central Tibet map. (e) Observed S arrival and its converted phases. (f) Synthetic S arrival and converted waves modelled based on 3D SEM-FK techniques.

Synthetic examples for structural models of the central Tibet crust (see figure) show that this hybrid method is capable of accurately capturing interactions between incident S plane waves and local heterogeneities. This hybrid method provides an important tool for the receiver-function and scattering-imaging community to verify and further improve their techniques. These numerical examples also show the promising future of the 3D SEM-FK hybrid method in high-resolution regional seismic imaging based on waveform inversions of converted and scattered waves recorded by seismic array.

CIG Code(s): SPECFEM3D

References:

A 3-D spectral-element and frequency-wave number hybrid method for high-resolution seismic array imaging, Tong, P., D. Komatitsch, T.-L. Tseng, S.-H. Hung, C.-W. Chen, P. Basini, and Q. Liu, Geophys. Res. Lett., 41, 7025–7034 (2014).

Dynamic earthquake rupture and the 2011 M9 Tohoku earthquake

P. Galvez(1), J.-P. Ampuero(2), L.A. Dalguer(3), S.N. Somala(2) and T. Nissen-Meyer. (1)Swiss Federal Institute of Technology, (2) California Institute of Technology. (3) swissnuclear. (4)University of Oxford.

An important goal of computational seismology is to simulate dynamic earthquake rupture and strong ground motion in realistic models that include crustal heterogeneities, non-linear rheologies and complex fault geometries. Increasing computational power is allowing scientists to resolve the small-scale processes through the use of numerical models at high resolution and large scales. Towards this goal, Galvez, et al. (2014) incorporate dynamic rupture modeling capabilities in a spectral element solver on unstructured meshes, the 3-D open source code SPECFEM3D, and employ state-of-the-art software (CUBIT) for the generation of unstructured meshes of hexahedral elements. These tools provide high flexibility in representing fault systems with complex geometries, including faults with branches and non-planar faults.

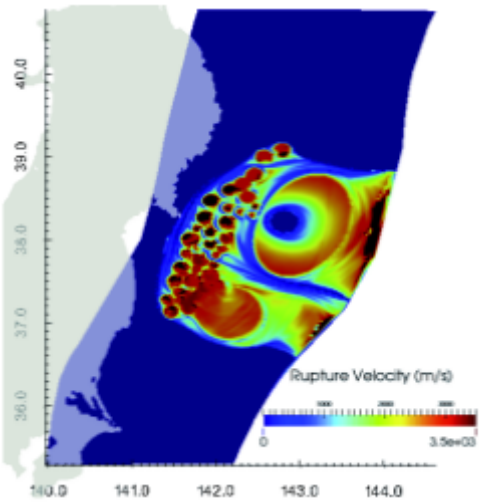

Distribution of rupture velocity in a dynamic rupture model of the Tohoku earthquake. supershear rupture speeds emerges at the rupture near the trench.

The rupture history produced by this model reproduces multiple rupture fronts. The up-dip front gradually accelerates and develops super-shear rupture speeds close to the trench, whereas the down-dip front propagates slowly below the hypocenter and migrates more rapidly towards the South. The team is now developing a refined dynamic rupture model that matches quantitatively the seismological and geodetic observations of the Tohoku earthquake. Overall, this tool offers a great potential to simulate more realistic earthquakes in complex faults systems.

CIG Code(s): SPECFEM3D

References

P. Galvez, J.P. Ampuero, L. A. Dalguer, S. N. Somala, T. Nissen-Meyer (2014). Dynamic earthquake rupture modelled with an unstructured 3-D spectral element method applied to the 2011 M9 Tohoku earthquake. Geophysical Journal International, 198, 1222-1240, doi: 10.1093/gji/ggu203.

Seismic imaging for TTI based on adjoint methods

Herurisa Rusmanugroho, Ryan Modrak and Jeroen Tromp, Princeton University

We propose new concepts of seismic imaging for Tilted Transverse Isotropy (TTI), i.e., a transversely isotropic model with a symmetry axis following the nature of sedimentation and perpendicular to the bedding plane. For the salt model shown in the figure below (upper panel), we create synthetic seismograms as TTI data. If we image the data using an incorrect isotropic assumption, we obtain a poor image (lower-left panel). However, when we image the data using the correct TTI assumption, we obtain a higher-quality image (lower-right panel).

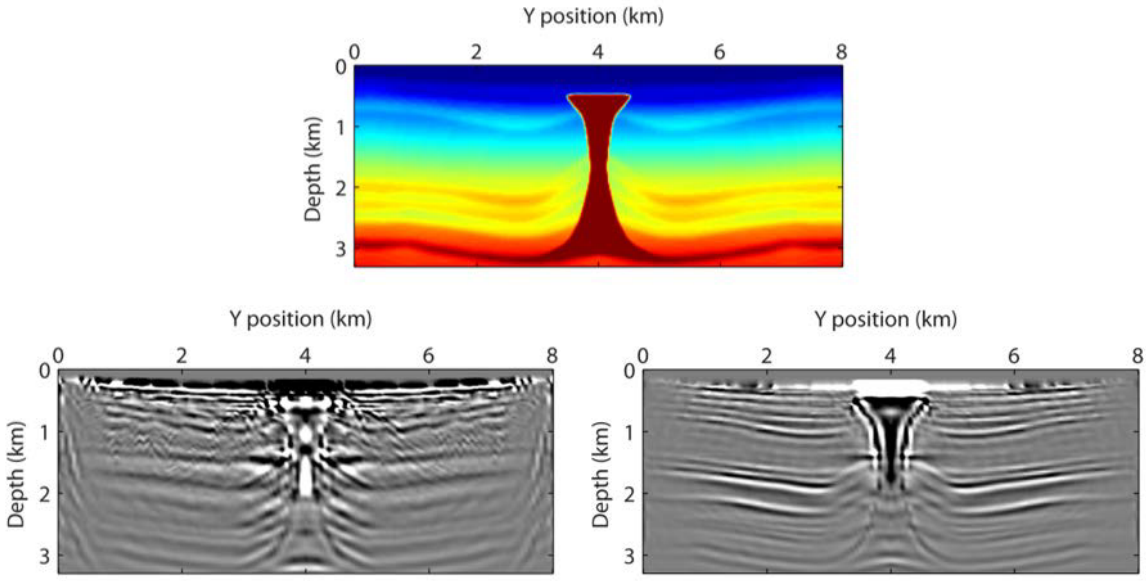

P-wave mode containing a salt structure indicated by the dark red color thrusting the overlying sedimentary layers (upper panel), impedance kernel assuming isotropy (lower left) which images the salt model poorly, and impedance kernel assuming TTI (lower right) which images the model perfectly.

We show that the impedance kernels or migrated images calculated based upon the Thomsen (1986) and Chen & Tromp (2007) parameters are crisp and promising for anisotropic seismic imaging.

CIG Code: SPECFEM3D

Acknowledgements: ConocoPhillips for supporting this research

References

Rusmanugroho, H., R. Modrak and J. Tromp, 2015, Seismic imaging for TTI based on adjoint methods: 85th Annual International Meeting, SEG, Expanded Abstracts, submitted.

Thomsen, L., 1986, Weak elastic anisotropy: Geophysics, 51, 1954–1966.

Chen, M., and T. Tromp, 2007, Theoretical and numerical investigations of global and regional seismic wave propagation in weakly anisotropic earth models: Geophysical Journal International, 168, 1130–1152.

Use of acoustic wave modeling for ocean acoustics and for non-destructive testing of materials

Dimitri Komatitsch and Paul Cristini, Laboratory of Mechanics and Acoustics, CNRS, Marseille, France.

The field of numerical modeling of sound propagation in the ocean has been the subject of increasing interest of the underwater acoustics community for many years. Computing an accurate solution, taking a complex environment into account, is still the subject of active research in ocean acoustics for which the objectives are now to focus on simulations in the time domain for 2D configurations with the prospect of being able to handle 3D configurations in the near future. Nowadays, with the stunning increase in computational power, full wave numerical simulation of complex wave propagation problems in the time domain is becoming possible.

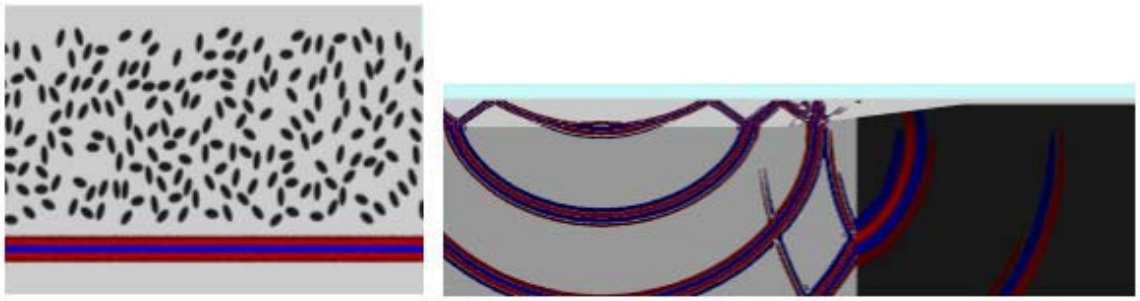

Images of shear wave propagation in a concrete block (left) and acoustic wave propagation in a shallow water fluid-solid model with a viscoelastic ocean bottom (right) computed using the SPECFEM set of codes. These codes allow for the calculation of the wave fields in the time domain in a very accurate fashion. They also make it possible to solve inverse imaging problems for such media.

The spectral-element method (SEM), which is based upon a high-order piecewise polynomial approximation of the weak formulation of the wave equation, has been the subject of many developments in geophysics in the last 20 years from the numerical, physical and computational points of view. We successfully used the SPECFEM set of codes to simulate wave propagation as well as imaging in complex media such as concrete blocks in the context of industrial non-destructive techniques, as well as ocean acoustics.

CIG Codes: SPECFEM3D, SPECFEM2D, SPECFEM3D_GLOBE, and SEISMIC_CPML.

Acknowledgements: French ANR, European Union and Del Duca Foundation for funding, PRACE, GENCI, CINES and Marseille EQUIPEX@MESO for providing CPU hours on large supercomputers.

References

Xie Z., D. Komatitsch, R. Martin and R. Matzen, Improved forward wave propagation and adjoint-based sensitivity kernel calculations using a numerically stable finite-element PML, Geophysical Journal International, vol. 198(3), p. 1714-1747(2014).

Cristini P. and D. Komatitsch, Some illustrative examples of the use of the spectral-element method in ocean acoustics, Journal of the Acoustical Society of America, vol. 131(3), p. EL229-EL235, doi: 10.1121/1.3682459 (2012).

Validation of Western North America Models based on finite-frequency and ray theory imaging methods

Carene S. Larmat[1], Monica Maceira[1], Robert W. Porritt[2,3], David M. Higdon[1], Charlotte A. Rowe[1], and Richard M. Allen[3]

[1]Los Alamos National Laboratory, [2]University of Southern California, [3]UC Berkeley

We validate seismic models by computing synthetic seismograms and quantifying their fit to recorded data. We have tested the effect of imaging methods based on two body-wave models, one built with the FF approach and one with the RT approach. They are part of the DNA09 series, built with the same dataset, processing and reference model.

For 13 seismic events, we computed synthetic seismograms using the SPECFEM3D package and HPC resources at LANL. On average, the delay times of S-waves produced by the FF model are 0.07 s closer to the actual time delays for SV and 0.03 s closer for SH. A simple paired t-test (*Box et al.*, 1978) can be used to quantify the significance of this measured difference. The difference is significant for the SV arrival times (p=0.001) and not for the SH arrival times (p=0.2). Further analysis is published in (Maceira et al., 2015).

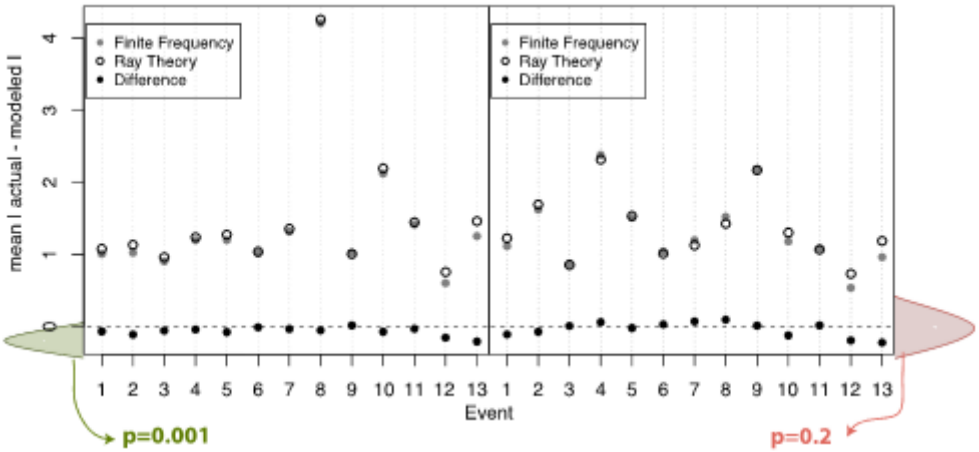

For each station measurement, the misfit between observed and modeled delay times – with respect to iasp91 - is summarized by the mean of the absolute deviations. The differences resulting from each pair of models for the13 events are given by the black dots. The difference is statistically significant, favoring smaller absolute SV residuals for the FF model (schematically represented by the narrower green distribution shifted away from zero). There is no significant difference in mean absolute residuals for the SH delay times (wider and more zero-centered red distribution).

CIG Code(s): SPECFEM3D

Acknowledgements: The authors are grateful to IRIS and LANL Institutional Computing.

References

Box, G. E., W.G. Hunter, and J.S. Hunter (1978), Statistics for experimenters: an introduction to design, data analysis, and model building, Wiley Series in Probability and Statistics.

Maceira, M., C. Larmat, R. W. Porritt, D. M. Higdon, C. A. Rowe, and R. M. Allen (2015), On the validation of seismic imaging methods: Finite frequency or ray theory? *Geophys. Res. Lett.*, doi:10.1002/2014GL062571

The Effect of Topography on the Seismic Wavefield

Ulrika Miller and Carl Tape, University of Alaska Fairbanks

Recent studies using numerical simulations in 3D models have shown how topography can influence the seismic wavefield. These effects are strongest at higher frequencies, but they are also quantifiable at lower frequencies, such as those used within simulation-based tomographic inversions. Here we perform a series of seismic wavefield simulations in 3D structural models in order to quantify the effect of topography on seismic waveforms. Our procedure involves three components: (1) constructing a finite-element, unstructured hexahedral mesh, (2) performing seismic wavefield simulations, and (3) quantifying differences between seismograms. We consider three different structural models: homogeneous, layered, and realistic 3D variations. For each structural model we produce a mesh with and without topography. For each of these meshes we produce a finer version in order to demonstrate the minimum resolvable period for the coarser meshes. The target regions is southern California which exhibit large topographic variations and also have abundant seismic stations that allow for comparisons with recorded data. We selected 137 events ranging from Mw 3.4 to 5 in addition to our initial Mw 7.6 point source to have a station and source specific analysis. Our simulations shows that the topography has the strongest effects on surface waves, whereby a phase shift of the main arrival occurs due to the different thickness of the uppermost layer (which includes the topography or not). Scattered waves are visible in the coda due to surface wave reflections that occur off the direct source-station path. Our analysis emphasizes seismograms with periods 1 s, with the motivation to understand the topographic signatures that may influence measurements used within adjoint-based tomographic inversions with earthquake data.

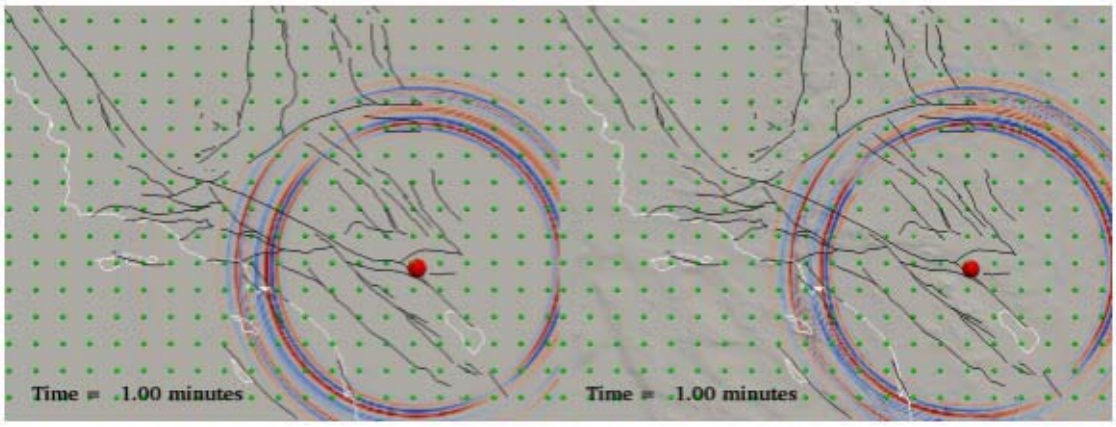

Snapshots from seismic wavefield simulations for a model without topography (left) and with topography (right). The differences tend to be most pronounced in the coda of the surface wave and in the direction of nodal surface wave radiation (here, to the northwest).

CIG Code(s): GEOCUBIT, SPECFEM3D

References

Cahayani, U. and C. Tape, 2014, The effect of topography on the seismic wavefield, Abstract S41E-05 presented at 2014 Fall Meeting, AGU, San Francisco, Calif., 15-19 Dec.

Towards Adjoint Tomography of 3D Structure of the Juan de Fuca Plate and Cascadia Trench

Youyi Ruan, Department of Geosciences, Princeton University
Samuel Bell and Donald Forsyth, Department of Geological Sciences, Brown University

Imaging a high-resolution seismic model of Juan de Fuca Plate and Cascadia subduction zone in a historically seismogenic zone is essential to facilitate the assessment of tsunami and seismic hazards and better understand subducting processes of the Juan de Fuca plate. Over a four-year period (2011-2015), the ambitious Cascadia Initiative repeatedly deploy 60 ocean-bottom seismometers to cover all of the Juan de Fuca plate and operate many land stations throughout the period. With the availability of seismic data from the first three year deployment, we employ a two-step inversion procedure for a regional 3D model of crust and upper mantle. We first constructed a reference 3D model based on array analysis of teleseismic data, and then will apply an adjoint tomography technique to improve the reference 3D model iteratively.

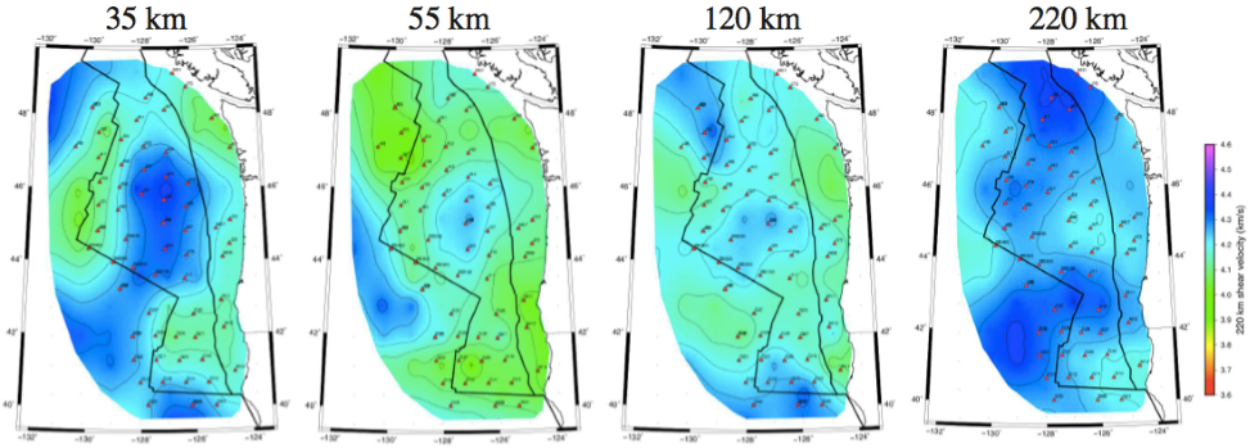

Images of the shear wavespeed tomography model using teleseismic Rayleigh waves at depth of 35 km, 55 km, 120 km and 220 km (Bell et al, 2014).

CIG Code(s): SPECFEM3D, SPECFEM2D

Acknowledgements: XSEDE for providing CPU hours on Texas Advanced Computing Center's supercomputers, Cascadia Initiative and OBSIP for data collection and archiving.

References

Bell, S., Y. Ruan and D. W. Forsyth, Rayleigh Wave Tomography of Noise-Removed Cascadia Initiative Data. *American Geophysical Union, Fall Meeting 2014*, San Francisco, CA.

Ruan, Y., and D. W. Forsyth, Towards Adjoint Tomography of 3-D Structure of the Juan de Fuca Plate and Cascadia Trench. *American Geophysical Union, Fall Meeting 2013*, San Francisco, CA.

Numerical Resolution of Seismic Wavefield Simulations in Southern California

Carl Tape (University of Alaska Fairbanks) and Emanuele Casarotti (INGV Rome)

Seismic wavefield simulations can provide accurate solutions to the wave equation, even for three-dimensional seismic velocity models with topography, basin structures, anisotropy, attenuation, and other complexities. But how accurate are these numerical solutions? In many cases the effect of numerical dispersion on the synthetic seismograms looks quite similar to the effects of structural complexities. Therefore it is important to know the numerical resolution of the synthetic seismograms, that is, the minimum period that provides a quantifiably numerically accurate solution to the wave equation. Numerical resolution can be discussed in terms of a combined mesh and velocity model, or in terms of an individual source-station path within the same mesh and velocity model. Here we discuss two approaches for quantifying the numerical resolution. In the first approach we empirically estimate the minimum resolvable period of each element within the finite element mesh (see figure). In the second approach we choose a set of earthquakes to be used within a tomographic inversion. For each earthquake we compute one simulation using a fine discretization of gridpoints on the finite-element mesh and another simulation using a coarse discretization. We filter both sets of seismograms over a range of periods and then quantify the waveform differences. The minimum resolvable period (or numerical resolution) is identified by the minimum period for which the synthetic seismogram from the coarse-mesh and fine-mesh simulations is quantifiably the same. This calculation provides a path-specific minimum resolvable period that can be used to guide the choice of measurement filtering for a tomographic inversion.

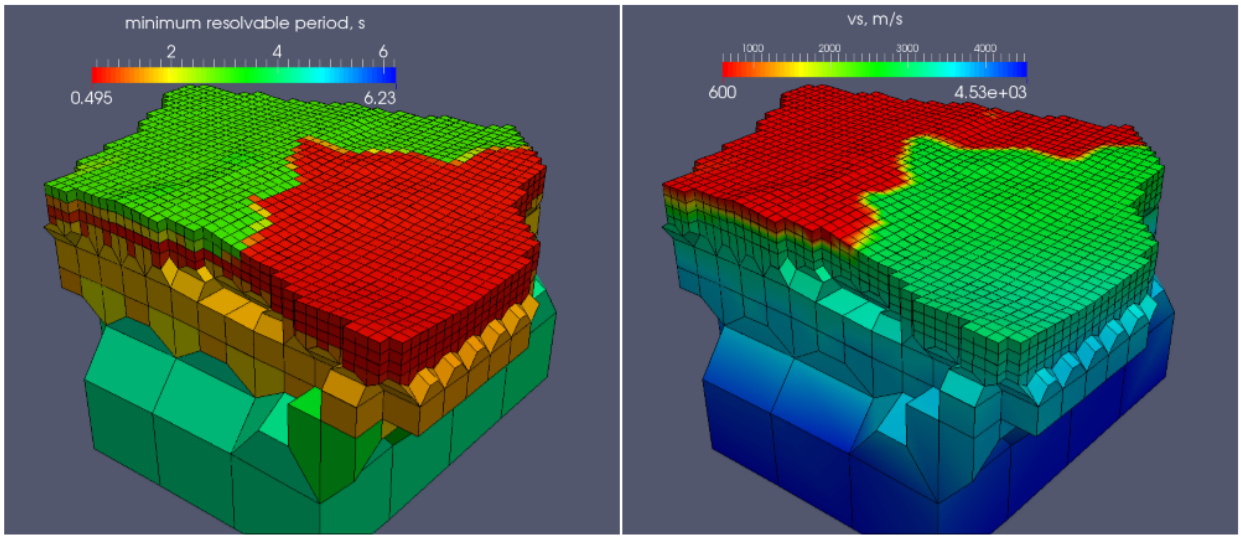

A single partition of the finite-element mesh showing the empirically estimated minimum resolvable period for each element (left), which is based on the geometry of each element and the minimum wavespeed within each element (right).

CIG Code(s): GEOCUBIT, SPECFEM3D

References

Tape, C., and E. Casasrotti, 2014, The effect of topography on the seismic wavefield, Abstract S42A-08 presented at 2014 Fall Meeting, AGU, San Francisco, Calif., 15-19 Dec.

Seismic wavefield simulations of earthquakes within a complex crustal model for Alaska

Carl Tape and Vipul Silwal, University of Alaska Fairbanks

We explore the effects of two major sedimentary basins (Cook Inlet and Nenana) on the seismic wavefield in Alaska, in preparation for an iterative tomographic inversion using spectral-element and adjoint methods. Our 3D reference seismic velocity model contains three geometrical interfaces: the Moho surface, the basement surface of the sedimentary basins, and the topographic surface. The crustal and upper mantle tomographic model is from Eberhart-Phillips et al. (2006), but modified by removing the uppermost slow layer and then embedding models for the two major sedimentary basins. Synthetic seismograms are computed using the spectral-element method. We quantify the accuracy of the initial 3D reference model by comparing 3D synthetics with observed data for several earthquakes originating in the crust and underlying subducting slab. We explore the effect of complex crustal structure on the seismic wavefield of the 1964 Mw 9 earthquake source model of Ichinose et al. (2007), which was obtained using geodetic data, tsunami arrival times, and teleseismic P waves recorded from the earthquake. The relatively large simulation region can be used to test different scenario megathrust earthquakes as well as different models of the 1964 earthquake.

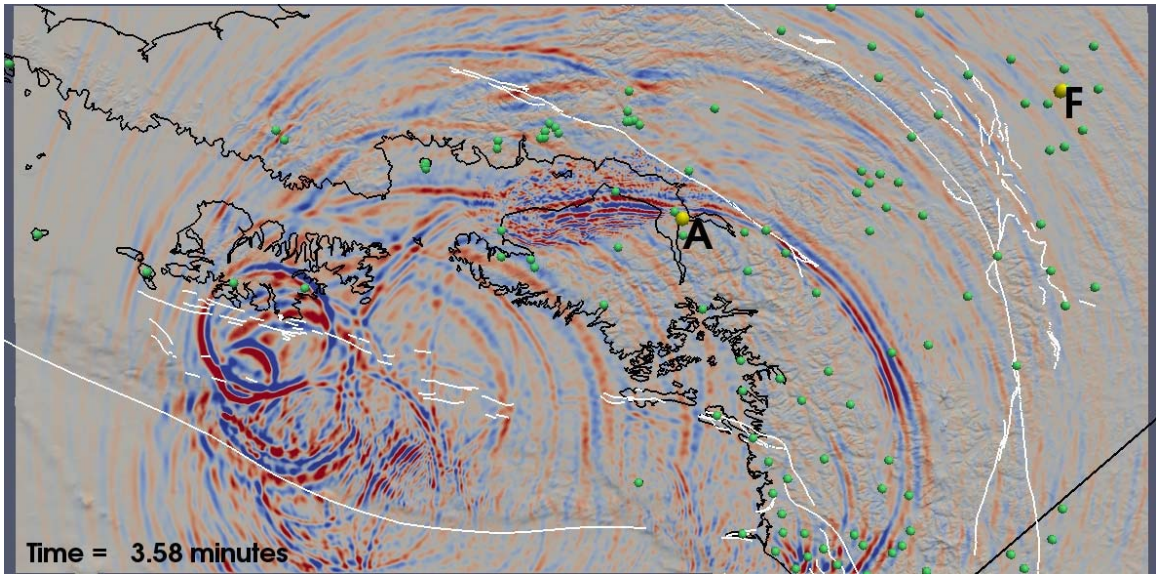

Snapshot from a seismic wavefield simulation of the 1964 M 9.2 Alaska earthquake. A = Anchorage, F = Fairbanks. Strong shaking west of Anchorage is due to the resonance of the Cook Inlet sedimentary basin. At this time (3.58 minutes), the rupture is near the island of Kodiak.

CIG Code(s): GEOCUBIT, SPECFEM3D

References

Tape, C., 2014, "Seismic wavefield simulations of earthquakes within a complex crustal model for Alaska," 2014. Abstract presented at the 2014 SSA Annual Meeting, Anchorage, Alaska, April 30 - May 2.

Tape, C., 2012, "A three-dimensional seismic velocity reference model for Alaska," Abstract S41A-2363 presented at 2012 Fall Meeting, AGU, San Francisco, Calif., 13-17 Dec.

Coupling hydrodynamic and wave propagation modeling for waveform modeling of SPE

Carene S Larmat, David W. Steedman, Esteban Rougier and Chris R. Bradley, Los Alamos National Laboratory

The goal of the Source Physics Experiment (SPE) is to bring empirical and theoretical advances to the problem of detection and identification of underground nuclear explosions. Improving the community's confidence in verification and monitoring is essential and requires understanding of all the processes that affect seismic wave propagation from the hydrodynamic/plastic source region to the elastic/anelastic far field. To completely understand this process, the prompt processes that take place in the near source region must be joined/coupled to the ones taking place later in time due to wave propagation in complex 3D geologic environments. In recent years, significant progress has been made in the numerical modeling arena, and the capabilities are now mature enough to address multi-physics modeling comprising the coupling of different numerical tools. In this paper, we report on results of first-principles simulations coupling hydrodynamic simulation codes (Abaqus and CASH), with a 3D full waveform propagation code, SPECFEM3D. Abaqus and CASH model the shocked, hydrodynamic region via equations of state for the explosive, borehole stemming and jointed/weathered granite. SPECFEM3D is based on the spectral element method that is a direct numerical method for full waveform modeling with mathematical accuracy (e.g. Komatitsch, 1998, 2002) due to its use of the weak formulation of the wave equation and of high-order polynomial functions. We will present waveforms modeled for the three SPE tests conducted so far with yields of 100, 1000, and ~900kg.

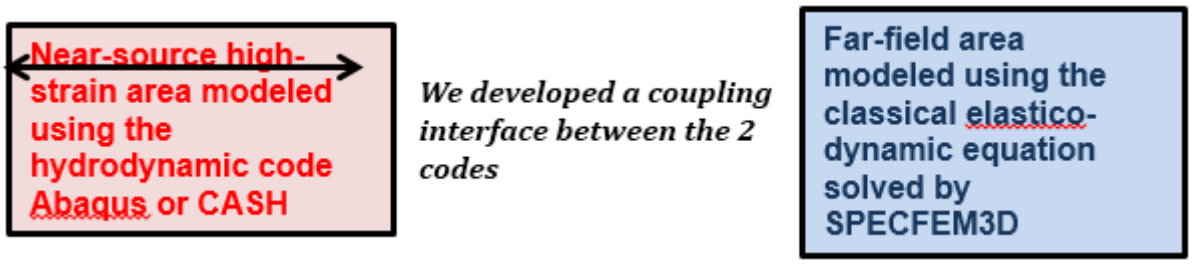

CIG Code(s): SPECFEM3D Cartesian

Acknowledgements: The authors wish to express their gratitude to the National Nuclear Security Administration, Defense Nuclear Nonproliferation Research and Development (DNN R&D), and the SPE working group, a multi-institutional and interdisciplinary group of scientists and engineers. This work was done by Los Alamos National Laboratory under award number DE-AC52-06NA25946.
LA-URs: LA-UR-13-22844 & LA-UR-14-23017

References

Komatitsch, D., and J.-P. VILOTTE (1998), The spectral element method: An efficient tool to simulate the seismic response of 2D and 3D geological structures, *Bull. seism. Soc. Am.*, *88*(2), 368–392.

Komatitsch, D (2002), The Spectral-Element Method, Beowulf Computing, and Global Seismology, Science, 298 (5599) DOI: 10.1126/science.1076024

Global Adjoint Tomography

Ebru Bozdag[1], Matthieu Lefebvre[2], Wenjie Lei[2], Daniel Peter[3], James Smith[2], Dimitri Komatitsch[4] and Jeroen Tromp[2].

[1]University of Nice Sophia Antipolis, [2]Princeton University, [3]ETH Zurich, [4]University of Aix-Marseille

Our aim is to take adjoint tomography further to image the entire planet which is one of the extreme cases in seismology due to its intense computational requirements and vast amount of high-quality seismic data that can potentially be assimilated in inversions. We have performed 12 iterations with low resolution (T > 27 s) simulations and continue higher-resolution (T > 17 s) global inversions with 253 earthquakes for a transversely isotropic crust and mantle model on the Oak Ridge National Laboratory's Cray XK7 "Titan" system. We use both minor- and major-arc body and surface waves running 180 min-long simulations. Our initial results after 12 iterations already indicate several prominent features such as enhanced slab (e.g., Hellenic, Japan, Bismarck, Sandwich), plume/hotspot (e.g., the Pacific superplume, Caroline, Yellowstone, Hawaii) images, etc. While keeping track of the progress and illumination of features in our models with a limited data set, we work towards going down to 9 s in simulations to incorporate high-frequency body waves and assimilating all available data in inversions from all seismic networks and earthquakes in the global CMT catalogue within the magnitude range 5.5 ≤ Mw ≤ 7.0.

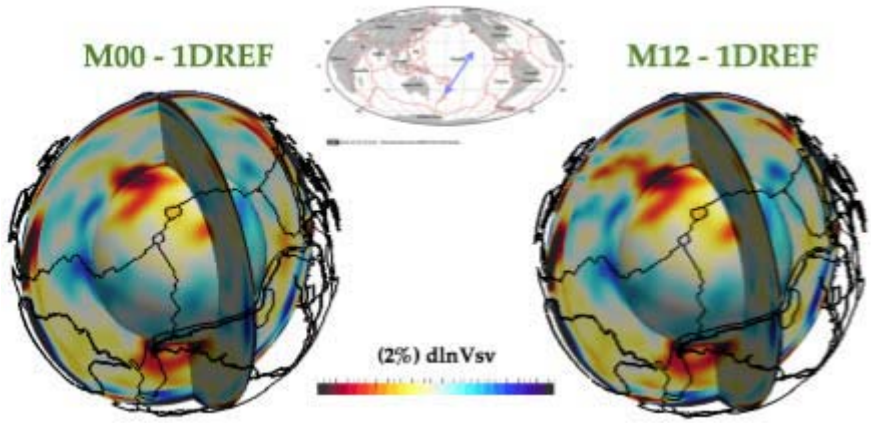

Vertical cross-sections across Pacific super plume region showing S-wave perturbations for initial mantle model S362ANI by Kustowski et al. (2008) (M00, left) and 12th iteration model M12 (right) with respect to 1D model STW105. The map at the top shows the direction of the cross section and map views indicate the core-mantle boundary.

CIG Code(s): SPECFEM3D_GLOBE

References

Bozdag, E., M. Lefebvre, W. Lei, D. Peter, J. Smith, D. Komatitsch and J. Tromp, Global Adjoint Tomography: Combining big data with HPC simulations, 2014 AGU Fall Meeting, December 15-19, San Francisco, CA, USA.

Bozdag, E., M. Lefebvre, W. Lei, D. Peter, J. Smith, D. Komatitsch and J. Tromp, Global Adjoint Tomography, In preparation.

Efficient numerical solution of global dynamic and quasistatic problems using a spectral-infinite-element method

Hom Nath Gharti and Jeroen Tromp, Princeton University, USA

The complete set of governing equations for global dynamic and quasistatic problems --- such as wave propagation, post-seismic relaxation, post-glacial rebound, and tides --- involves a coupling between the conservation laws of continuum mechanics and Poisson/Laplace's equation. For dynamic problems, it is possible to decouple Poisson's equation using an explicit time marching scheme so that it can be solved independently. For quasistatic problems, inertia is neglected, requiring an implicit time marching scheme. In the latter case, Poisson's equation cannot be decoupled. Although an explicit time scheme with an independent Poisson's solver is generally fast, such an approach is limited by conditional stability, such that a very large number of time steps is often necessary. On the other hand, an implicit time scheme coupled with Poisson's equation is generally slow but unconditionally stable. In both cases, the unbounded and large-scale nature of the problem poses numerical challenges, particularly for 3D Earth models. Most of the existing methods use spherical harmonics to solve the unbounded Poisson/Laplace's equation. Such methods are often limited to spherically-symmetric models or have to rely on iterative procedures.

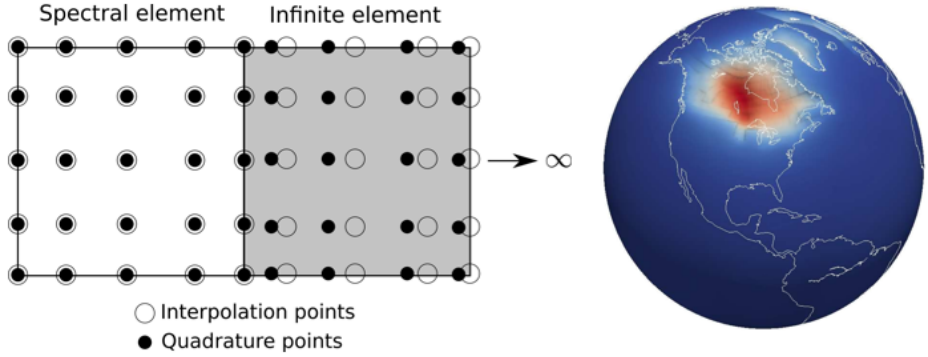

(Left) Coupling between spectral and infinite elements. (Right) Typical response under glacial loading.

In view of these challenges, we develop a parallel software package based on the spectral-element method combined with a mapped infinite-element approach. In the infinite element approach, a so-called infinite-element layer is used to mimic all of outer space. Spectral and infinite elements share identical quadrature points on infinite-element boundaries, thereby providing a natural coupling of the infinite-element method with the spectral-element method. We use a generalized Maxwell rheology for viscoelastic deformation and accommodate topography and ellipticity. Both explicit and implicit time schemes are implemented in order to address a range of problems, including long-period seismology, glacial rebound, tidal loading, etc.

CIG Code: SPECFEM3D_GLOBE

Acknowledgments: The Princeton Institute for Computational Science and Engineering (PICSciE), USA.

References

H. N. Gharti, J. Austermann, D. Komatitsch, H. Lau, J. X. Mitrovica, P. Peter, J. Tromp, Z. Xie, and S. Zampini. Ecient numerical solution of global dynamic and quasistatic problems using a spectral-element method coupled with an infinite-element approach. In AGU Fall Meeting Abstracts , volume 1, 2013.

High-Performance I/O for Large Scale Seismic Imaging Computations

Matthieu Lefebvre, Princeton University, Princeton NJ, USA.

Knowledge about Earth's interior comes mainly from seismic observations and measurements. Seismic tomography is the most powerful technique for determining 3D images of the Earth —usually in terms of wavespeeds, density, or attenuation— using seismic waves generated by earthquakes or man-made sources recorded by a set of receivers. Advances in the theory of wave propagation and 3D numerical solvers together with dramatic increases in the amount and quality of seismic data and rapid developments in high-performance computing offer new opportunities to improve our understanding of the physics and chemistry of Earth's interior. Adjoint methods provide an efficient way of incorporating 3D numerical wave simulations in seismic imaging, and have been successfully applied for regional- and continental-scale problems and —to some extent— in exploration seismology. However, it has so far remained a challenge on the global scale and in 3D exploration, mainly due to computational limitations.

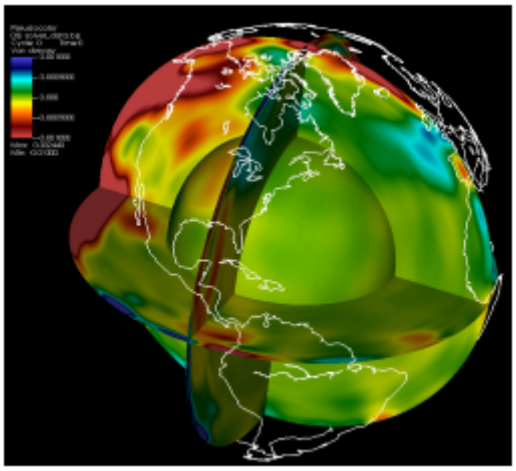

Large scale visualization of shear wave speed perturbations during one iteration of a global inversion. Data were produced using SPECFEM3D_GLOBE, taking advantage of ORNL's ADIOS library to produce files suitable for parallel visualization in VisIt.

Image courtesy of David Pugmire, ORNL.

We accommodate the ADIOS libraries in our numerical solvers to reduce the impact of accessing files on disk during simulations (i.e., meshes, kernels, models, etc.) and also during other processing steps. We adjust post-processing tools (i.e., summing, pre-conditioning and smoothing gradients, model updates, etc.) accordingly. Moreover, parallel visualization tools, such as VisIt, take advantage of metadata included in our ADIOS outputs to extract features and display massive datasets.

CIG Code(s): SPECFEM3D_GLOBE, SPECFEM3D

Acknowledgements: Oak Ridge National Laboratory (ORNL)

References

M. Lefebvre, E. Bozdag, H. Calandra, J. Hill, W. Lei, D. Peter, N. Podhorszki, D. Pugmire, H. Rusmanugroho, J. Smith, and J. Tromp. A data centric view of large-scale seismic imaging workflows. In *4th SC Workshop on Petascale Data Analytics*, 2014

Global structure of the crust and upper mantle based on adjoint tomography

Wenjie Lei, Youyi Ruan, Ebru Bozdag, Matthieu Lefebvre, James Smith, Jeroen Tromp, Princeton University

With rapid developments in High Performance Computing (HPC) and the availability of more advanced numerical methods [e.g., the spectral-element method; Komatitsch and Tromp, 1999], we are now able to simulate the seismic wave propagation in the 3D global earth models. Currently available 3D models, e.g., S362ANI, provide good seismograms at long periods, but discrepancies exist at shorter periods. The remaining difference motivates the construction of higher resolution global models at shorter periods.

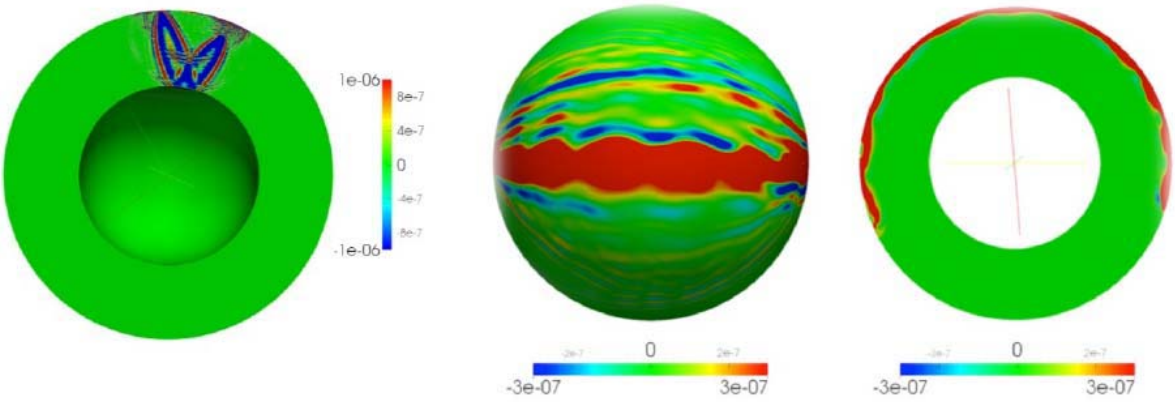

Images of ScS phase kernel (left) and major---arc surface wave kernels (middle and right). The ScS kernel provides resolution in vertical direction while the surface wave kernels are only sensitive to the shallow structure.

Our research is focused on imaging the 3D structure of the earth using the adjoint state method. This method—an iterative optimization approach– has been employed successfully on regional scales, e.g., Europe [Zhu and Tromp, 2013]. The inversion generally consists of three phases:
a) Elastic structure: phase information used to resolve elastic properties of the earth; b) Anelastic structure: combination of phase and amplitude information to resolve anelastic structure; and c) Anisotropy: radial and azimuthal anisotropy. Also, source complexity should be considered in the full 3D inversion. Finally, the seismic inversion results, combined with geodynamics and mineralogy, can provide a better understanding of the interior of the earth.

CIG Codes: SPECFEM3D_GLOBE, FLEXWIN

Acknowledgements: The Princeton Institute for Computational Science and Engineering (PICSciE) and Oak Ridge National Lab for providing CPU hours on supercomputers

References

Komatitsch, D. and Tromp, J. (1999), Introduction to the spectral---element method for 3---D seismic wave propagation, Geophys. J. Int., (139)805---822

Zhu H. and Tromp J. (2013), Mapping Tectonic Deformation in the Crust and Upper Mantle
Beneath Europe and the North Atlantic Ocean, Science, (341)871---875

Towards a comprehensive seismic earth model across the scales

Michael Afanasiev, Andreas Fichtner, Daniel Peter, Laura Ermert, Korbinian Sager, Saulé Zukauskaité, ETH Zürich

We present the current state of the 'Comprehensive Seismic Earth Model' (CSEM), a solver-independent multi-scale model of the global distribution of density and visco-elastic parameters. The overall goal of this project is to produce a model that represents the Earth on all seismically accessible scales; which contains high resolution sub-models where data and computational concerns allow, and which presents a low wavenumber Earth in regions yet to be probed in detail. To accomplish this, we have designed the model to be independent of any particular forward solver. This allows the usage of a wide variety of forward and inverse techniques, each of which may contribute updates within their respective regimes of validity.

To support future multiscale inversions, we report on methodological developments surrounding the project, including specific interfaces with forward solvers and a suite of tools for processing gradient-based model updates. Advances in forward modelling codes, such as the porting of the spectral element solver SPECFEM3D_GLOBE to heterogeneous computing clusters, allows for the efficient and fully numerical calculation of sensitivity kernels on the global scale. Taking advantage of these developments, we present a global-scale transversely isotropic mantle-and-crust update to the CSEM, with a misfit criterion based on waveform phase differences, and iterative nonlinear model perturbations found via adjoint techniques. Additionally, regional scale updates from both travel time and waveform tomography are presented and discussed.

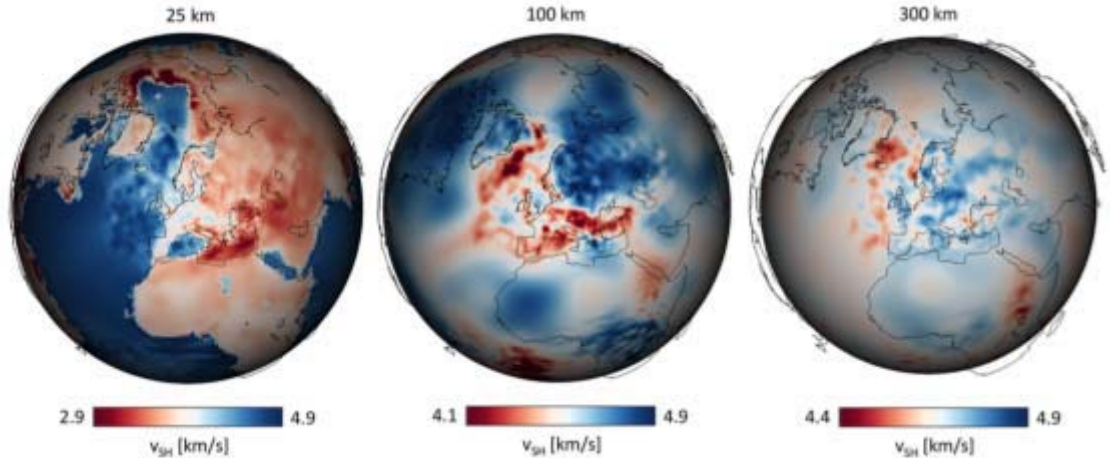

Images of SH velocity at various depth, taken from the Comprehensive Seismic Earth Model. Notice the detailed structure within Europe (a high-resolution sub region).

CIG Code(s): SPECFEM3D_GLOBE

References

Michael Afanasiev, Andreas Fichtner, Daniel Peter, Laura Ermert, Korbinian Sager, Saulé Zukauskaité, "Towards a comprehensive Earth model across the scales" Abstract S32A-03 presented at 2014 Fall Meeting, AGU, San Francisco, Calif., 15-19 Dec.

Short-Period, anelastic and anisotropic, waveform-based 3D Middle East model

Brian Savage[1] and Chistina Mornecy[2] and Jeroen Tromp[3], and Arthur Rodgers[2], [1]University of Rhode Island, [2]Lawrence Livermore National Laboratory, and [3]Princeton University,

Utilization of the full, seismic-waveform based techniques for discrimination purposes is currently effective and efficient for large magnitude, > M 4.5, well-recorded events. However, a need to reduce the magnitude threshold requires predictive capabilities at shorter periods, <~10 seconds, if waveform based techniques are to be used in routine event evaluations. Recent efforts using adjoint tomography (Komatitsch et al., 2002; Tromp et al., 2005) to improve the seismic waveform, prediction capabilities of existing models have proven successful by reducing an acceptable period for prediction to 15 - 20 seconds.

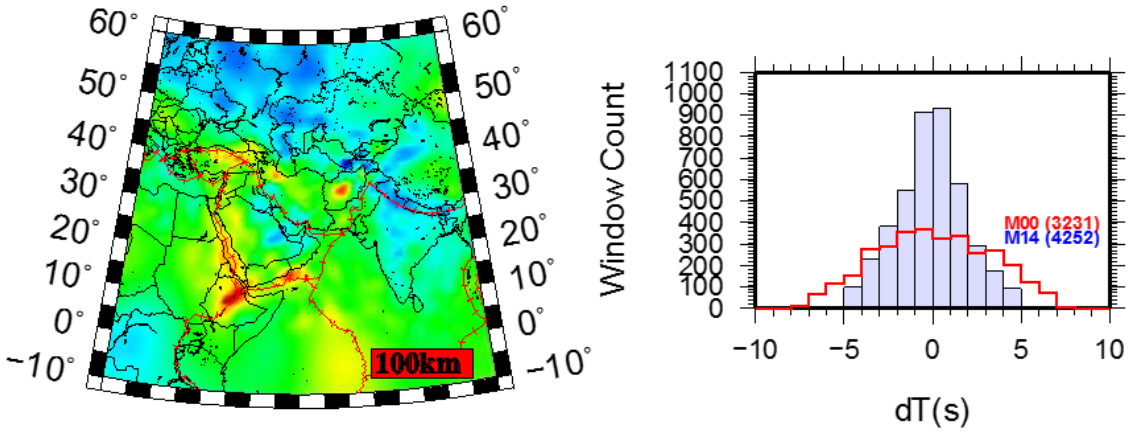

Images of the relative shear wave speed at 100 km (left), and the improvement to the model as measured by time shifts between data and synthetics after 14 iteration (right).

However, as the minimum period continues to drop, effects of attenuation and anisotropy will become more significant and require quantification. As such, current generation models lack both heterogeneous anelastic attenuation and a more robust treatment of anisotropy. We are pushing the predictive capabilities of the current 3D Middle East wave speed model to shorter periods. In doing so, 3D anleastic attenuation and anisotropic models will be incorporated into a seamless seismic Earth model of the Middle East region. Anelastic attenuation will be embedded along side a 3D wave speed model and the anisotropic component will be parameterized as transverse isotropy with a variably oriented symmetry axis.

CIG Code(s): SPECFEM3D_GLOBE

Acknowledgements (optional): Contributors to SPECFEM and Adjoint codebases

References

Komatitsch, D., J. Ritsema, and J. Tromp, The Spectral-Element method, Beowulf computing, and global seismology, Science, 298, 1737–1742, 2002.

Tromp, J., C. Tape, and Q. Liu, Seismic tomography, adjoint methods, time reversal and banana-doughnut kernels, Geophysical Journal International, 160(1), 195– 216, doi:10.1111/j.1365-246X.2004.02453.x, 2005.

An Adaptable Seismic Data Format Suitable for Large Seismic Inversions Including Global Adjoint Tomography

James Smith, Wenjie Lei, and Jeroen Tromp, Princeton University. Lion Krischer, Ludwig Maximilian University of Munich

Increases in the amounts of seismic data as well as computational power enable us to tackle larger and more complex problems. This comes with a slew of new problems, two of which are the need for a more efficient use of available resources and a sensible organization and storage of the data.

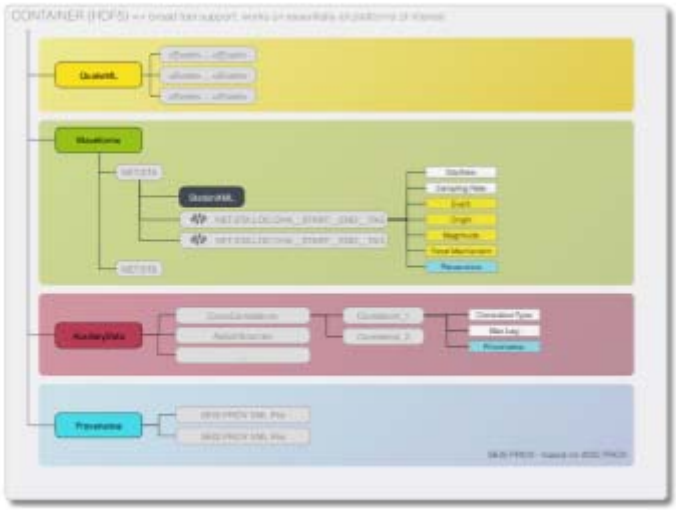

The ASDF container stores an arbitrary number of waveforms per station using the SEED standard, Auxiliaries can store future measurements for exchange, and Provenance allows for reproducibility.

The Adaptable Seismic Data Format (ASDF) stores all information associated with an event in a single file. Existing standards FDSN StationXML and QuakeML along with waveform and auxiliary data are incorporated into a common container based on the HDF5 standard. Provenance information is stored as an extension of W3C PROV, assisting with the general problem of reproducibility. Furthermore, intermediate products like adjoint sources, cross correlations, and receiver functions can be described and exchanged with others. ASDF is integrated into the preprocessing workflow for global adjoint tomography that utilizes the CIG software SPECFEM3D_GLOBE to simulate wave propagation and the CIG FLEXWIN package to select windows where measurements will be made. The license is open and the community can contribute to the evolving wiki and standard. ASDF will be implemented in other CIG wave solvers and tools as applications that demand a new seismic data format are implemented.

CIG Code(s): SPECFEM3D_GLOBE, FLEXWIN

References

Krischer, L., Smith, J., Spinusso, A., Tromp, J. A Self-Describing Data Format for Seismology Suitable for Large-Scale Workflows Including Data Provenance

Tromp J., Schenk O. *Global Seismic Tomography based on Spectral-Element and Adjoint Methods* 2012: INCITE Proposal. 1-15

The Effects of 3D Heterogeneity on Regional Moment Tensor Source-Type Discrimination

Andrea Chiang[1], Douglas S. Dreger[1], Arben Pitarka[2], Sean R. Ford[2]
[1]University of California, Berkeley
[2]Lawrence Livermore National Laboratory

Waveform inversion to determine the seismic moment tensor can be used to discriminate different types of seismic sources. However, the 1D velocity model assumption to compute Green's function is the greatest source of error in the moment tensor solution and has not been thoroughly investigated for source-type discrimination. We determine the effects of a 1D velocity model assumption through synthetic studies, and the application to Western US events where we have 1D moment tensor solutions for various sources. In the synthetic study we produce waveforms with the effects of 3D velocity heterogeneity using the finite-difference code SW4, and the effects of the 1D velocity model assumption can then be interpreted via the difference between input and inverted solutions. We will also compute 3D Green's functions through finite-difference and reciprocity for moment tensor inversion and compare the results to the moment tensor solutions obtained from 1D models.

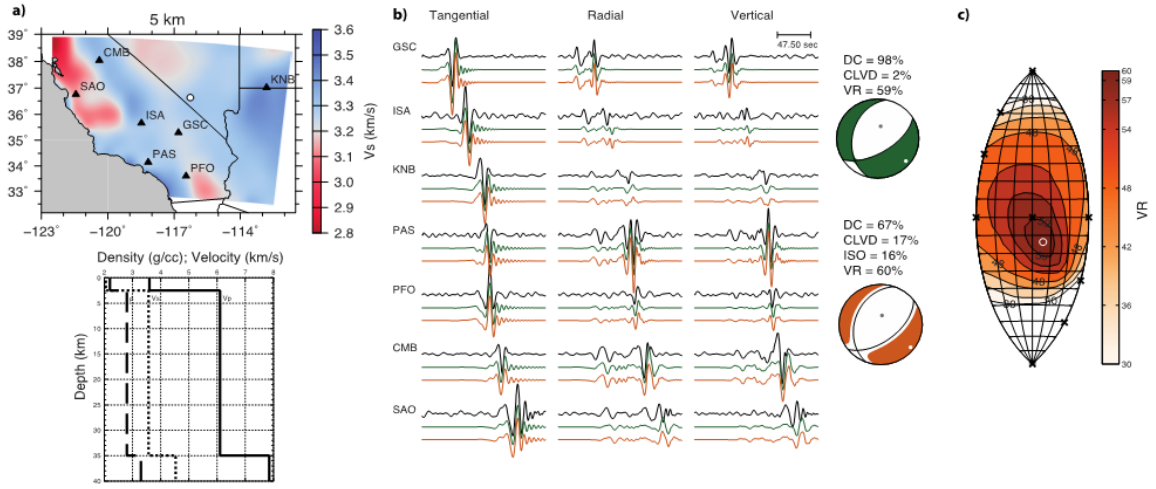

a) Surface wave tomography from Moschetti et al. (2010) used to generate waveform data, event and station locations are shown as white circle and black triangles, respectively. 1D model from Song et al. (1996). b) Deviatoric (green) and full (brown) moment tensor inversions from inverting 3D waveform data using 1D Green's functions at 10-50 seconds. c) Network Sensitivity Solution for the same event, full moment tensor solution plotted as a white circle.

CIG Code(s): SW4 (Seismic Waves, 4th order)

References

Mochetti, M. P., M. H. Ritzwoller, F.-C. Lin and Y. Yang. Crustal Shear Wave Velocity Structure of the Western United States Inferred from Ambient Seismic Noise and Earthquake Data, J. Geophys. Res., 115 (2010), B10306.

Petersson, N. A. and B. Sjogreen. Super-Grid Modeling of the Elastic Wave Equation in Semi-Bounded Domains, Commun. Comput. Phys., 16 (2014), pp. 913-955.

Song, X. J., D. V. Helmberger and L. Zhao. Broad-Band Modeling of Regional Seismograms: The Basin and Range Crustal Structure, Geophys. J. Int., 125 (1996), pp. 15-29.

Brittle Solvers: Lessons and insights into effective solvers for visco-plasticity in geodynamics

Marc Spiegelman, Columbia University/LDEO, Dave May, ETH/Zurich, and Cian Wilson LDEO

Plasticity/fracture and rock failure are essential ingredients in geodynamic models as terrestrial rocks do not possess an infinite yield strength. Numerous physical mechanisms, which limit the strength of rocks, have been proposed, including low temperature plasticity and brittle fracture. Whilst the ductile and creep behavior of rocks at depth is largely accepted, the precise description of the constitutive behavior associated with the brittle failure, or shear localization, is more controversial. Nevertheless, there are, in reality, only a few macroscopic constitutive laws for visco-plasticity that are regularly used in geodynamics models, all of which can be cast as simple effective viscosities which act as stress limiters with different choices for yield surfaces, the most common choices being von Mises (constant yield stress) or Drucker-Prager (pressure dependent yield-stress) models. The choice of plasticity model, however, can have significant consequences for the degree of non-linearity in a problem and the choice and efficiency of non-linear solvers.

Using TerraFERMA and pTatin, we explore a series of simplified 2 and 3-D model problems, similar to many in the literature, to elucidate several issues associated with obtaining accurate description and solution of visco-plastic problems. In particular, we demonstrate that:

- Picard/Successive substitution schemes for solution of the non-linear problems can often stall at large values of the non-linear residual, producing spurious solutions. Non- linear solutions should always provide proof of small non-linear residuals.
- Combined Picard/Newton schemes can be effective for a range of plasticity models; however, they can produce serious convergence problems for strongly pressure dependent plasticity models such as Drucker-Prager.
- Drucker-Prager may not be the plasticity model of choice for strong materials as the dynamic pressures produced in these layers can develop pathological behavior leading to stress strengthening rather than stress weakening behavior.
- For any incompressible Stoke's problem, one should evaluate the validity of dynamic pressure fields, particularly if they are being fed back into the rheology.

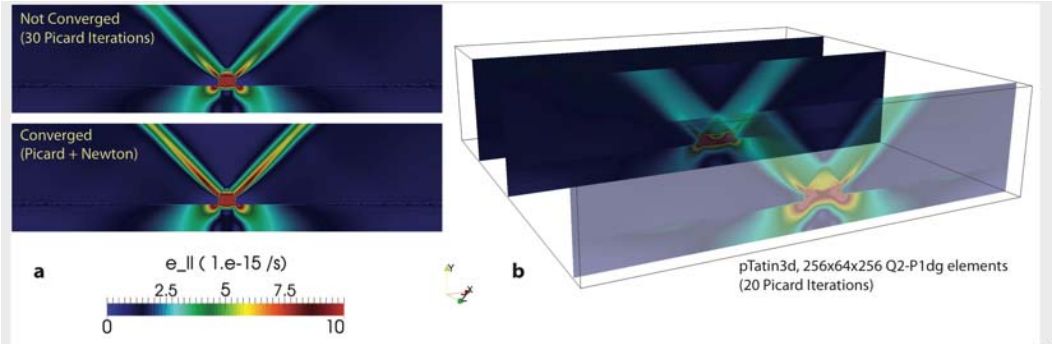

(a) Comparison of strain-rate invariant fields $\dot{\epsilon}_{II}$ between a poorly-converged solution (Picard with $||F||_2 \sim 10^{-2}$) and a well converged solution (Picard+Newton with $||F||_2 \sim 10^{-10}$. Converged calculations have more strongly defined shear-bands with a factor of ~ 2 greater strainrate than poorly converged calculations. **(b)** Strain-rate field for the comparable 3-D problem, that has the notch extending only half-way across the domain. Figure shows results after 20 Picard iterations.

Codes: TerraFERMA

References:

Spiegelman, M, D. May and CR Wilson, Brittle Solvers: Lessons and insights into effective solvers for visco-plasticity in geodynamics, AGU Fall meeting 2014.

TerraFERMA: The Transparent Finite Element Rapid Model Assembler

Cian Wilson, Marc Spiegelman, Columbia University/LDEO

Coupled multi-physics problems in Earth Sciences, such as the interactions of fluids and magmas with the convecting mantle or reactive fluid flow in brittle media are important but computationally challenging. Key challenges include the need to explore a wide range of constitutive relations and coupled conservation equations where small changes in model assumptions can often lead to dramatic changes in physical behavior. To make progress on these problems requires software that provides individual users with significant flexibility in both problem description and solution strategies. As importantly, multi-physics software should also make the users choices transparent, so results can be reproduced, verified and modified in a manner such that the best ideas in computation and earth science can be more easily shared and reused.

With these design issues in mind, we have developed a new software infrastructure *TerraFERMA* (TF) for the rapid and reproducible description and solution of coupled multi-physics problems. TF leverages three advanced open-source libraries for scientific computation. FEniCS provides hig- level problem description. PETSc provides composable solvers for coupled multi-physics problems and SPuD, which provides a science neutral options handling system. TF integrates these libraries into an easier to use interface that organizes all scientific and computational choices into a single options file, from which a custom compiled application is generated and run. Because all models share the same infrastructure, they become more reusable and reproducible. TF is open source and available as a developers release git repository at bitbucket.org/tferma/tferma

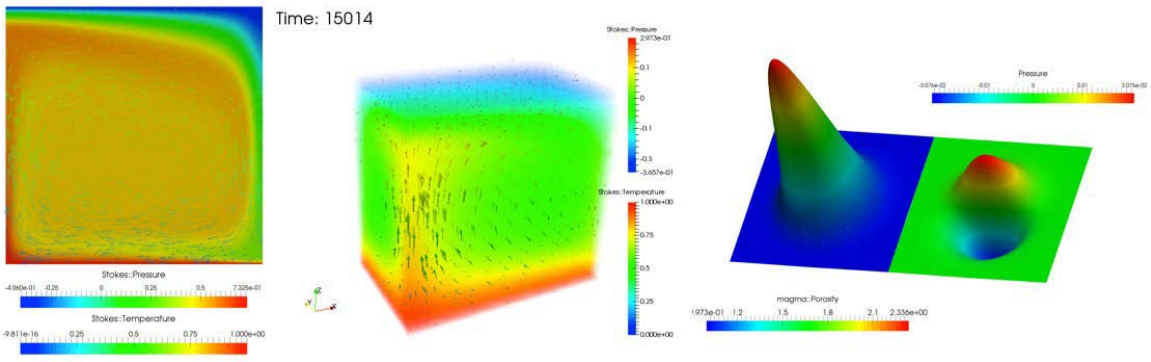

Three of the ~50 benchmark problems validated in TF (a) 2-D Temperature-dependent convection (Blankenbach, 2a, doi:10.1111/j.1365-246X.1989.tb05511.x) (b) 3-D thermal convection (Busse, 1a, 1994; doi:10.1080/03091929408203646) Non-linear magmatic solitary waves (Simpson and Spiegelman, 2011; doi:10.1007/s10915-011-9461-y)

Codes: TerraFERMA (donation pending)

References

Wilson, C.R., Marc Spiegelman, 2013. Software: TerraFERMA v0.1a --- The Transparent Finite Element Rapid Model Assembler, open-source repository: bitbucket.org:/tferma/tferma.

Spiegelman, M., Wilson, C.R., 2014. TerraFERMA: A cookbook tutorial.

Advanced fluid flow modeling in subduction zones using *TerraFERMA*: The role of solid rheology and compaction pressure

Cian Wilson, Marc Spiegelman, Columbia Unversity/LDEO
Peter van Keken, U. Michigan, Brad Hacker UC Santa Barbara.

Arc volcanoes tend to occur at locations where the slab is at approximately 100 km depth but most models of fluid production from the downgoing slab suggest fluids are released over a wide range of depths. Reconciling the models with the observations suggests that focusing of slab-produced fluids is necessary if flux-melting is a primary mechanism for the production of arc magmas. Wilson (2014, EPSL doi:10.1016/j.epsl.2014.05.052) uses our multi-physics software *TerraFERMA* to investigate one possible mechanism for inducing focusing of fluid flow toward the sub-arc mantle, the role of compaction pressure gradients in modifying fluid flow. These gradients are produced by variations in fluid flux interacting with the permeability and viscosity structure of the solid mantle. When these gradients are neglected, high-permeability systems are dominated by buoyancy and fluid flow is primarily vertical. However, when included, compaction pressure terms have three principal effects: (i) enhancement of upslope flow within high-permeability layers in the slab produced by local dehydration reactions, (ii) deflection of fluids along the sloping rheologically strengthening region in the upper thermal boundary layer, and (iii) production of non-linear porosity waves that locally modulate the flow of fluids and can allow significant transient accumulation of fluids. We demonstrate significant localization of fluid flux toward the sub-arc region due to the permeability and solid viscosity structure. We also estimate the amount of melting expected among the different models and show that models with compaction pressure could produce ~10% flux melting, whereas distributed fluid flow produces <1% in most cases.

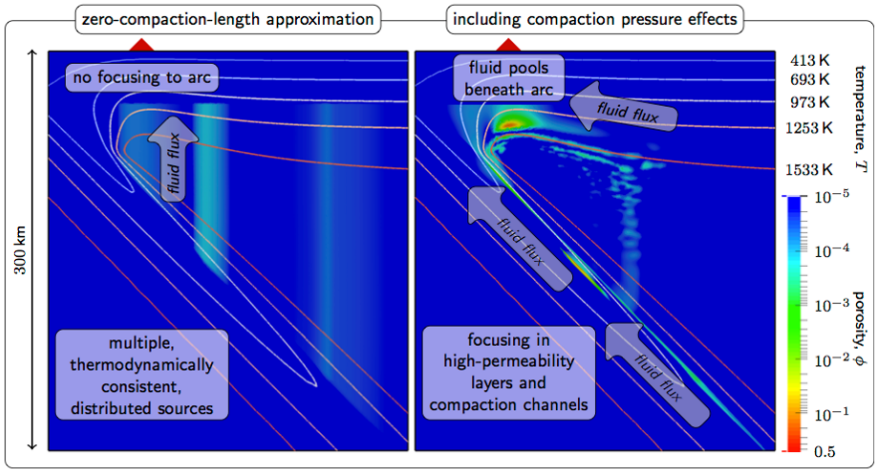

Example TerraFERMA calculations from Wilson et al. (2014, doi:10.1016/j.epsl.2014.05.052) showing the flow of fluid and solid in an idealized subduction zone. Figure on the left has only buoyancy driven flow of fluid. Figure on the right includes compaction pressure gradients due to interaction of fluid flux with the rheological structure induced by Temperature dependent viscosity. These compaction pressure gradients drive various focusing methods to transport fluid towards the wedge corner.

Codes: TerraFERMA

Simulating Gravity Changes and InSAR interferograms in Topologically Realistic Driven Fault Networks

Kasey W. Schultz, Michael K. Sachs, Eric M. Heien, John B. Rundle, and Don L. Turcotte, University of California, Davis, and Andrea Donnellan NASA Jet Propulsion Laboratory

Currently GPS and InSAR measurements are used to monitor deformation produced by slip on earthquake faults. It has been suggested that another method to accomplish many of the same objectives would be through satellite-based gravity measurements. The GRACE mission has shown that it is possible to make detailed gravity measurements from space for climate dynamics and other purposes. We used Virtual Quake simulated earthquake catalogs and custom implementations of the gravity Green's functions given in Okubo (1992) and of the displacement Green's functions given in Okada (1995) to compute co-seismic gravity changes and displacements for simulated faulting in an elastic half-space.

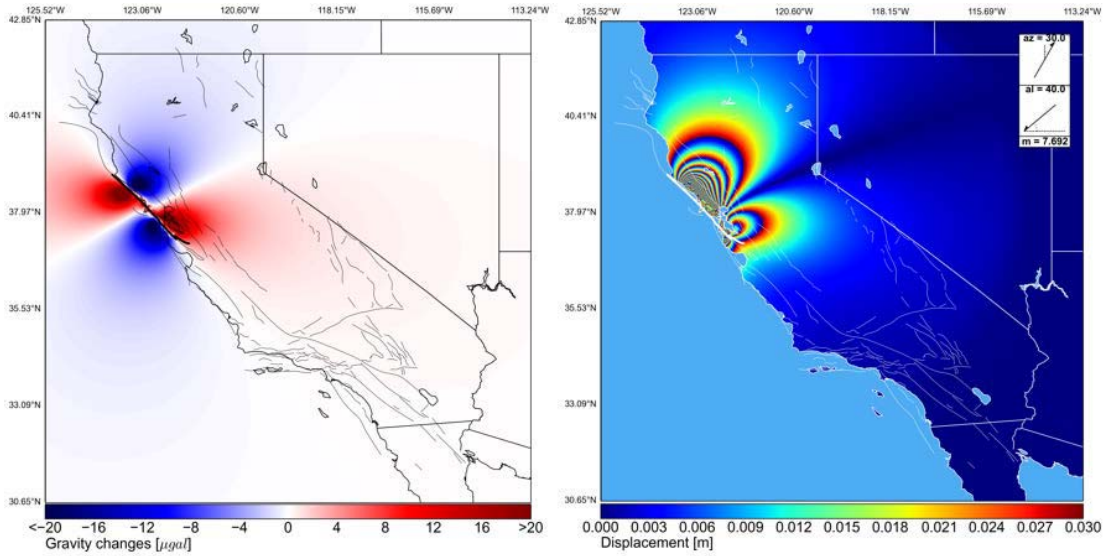

Co-seimic gravity changes (left) and InSAR interferogram (right) for a synthetic magnitude 7.69 earthquake on the San Andreas fault, simulated by Virtual Quake.

We produce ensembles of these gravity and InSAR patterns and find that dedicated gravity missions at the current spatial and temporal resolution (e.g. GRACE) are not well suited for California's predominantly strike-slip fault system. Strike-slip faults produce gravity change patterns with positive and negative poles within the spatial resolution limit of current satellite gravimetry, a few hundred kilometers.

CIG Code(s): Virtual Quake

Acknowledgements: NASA NESSF fellowship number NNX11AL92H

References

K.W. Schultz, M.K. Sachs, E.M. Heien, J.B. Rundle, D.L. Turcotte, and Andrea Donnellan, Simulating Gravity Changes in Topologically Realistic Driven Earthquake Fault Systems: First Results, Pure and Applied Geophysics, doi: 10.1007/s00024-014-0926-4, in press 2015

M. K. Sachs, E. M. Heien, D. L. Turcotte, M. B. Yikilmaz, J. B. Rundle, and L. Kellogg. Virtual California Earthquake Simulator. Seismological Research Letters, 83(6):973–978, 2012.

An Earthquake Model for Studying Interaction of Faults and Earthquake Simulations in Taiwan

Yi-Hsuan Wu and Chein-Chih Chen, National Central University
Eric M. Heien and John B. Rundle, University of California Davis

In recent decades, earthquake simulation considering the interaction of faults has become an necessary tool to develop earthquake forecasting method or understand the earthquake physics. However, the earthquake simulation in Taiwan is absent. The complex fault system of Taiwan makes an earthquake simulation based on the fault system difficult. We implement Virtual Quake (VQ) to build an earthquake model based on Taiwan faults. Virtual Quake is a boundary element code that performs simulations of fault systems based on stress interactions between fault elements to understand long term statistical behavior. It performs these simulations using a model of faults embedded in a homogeneous elastic half space with arbitrary dips and rakes. The code performs calculation assuming linear stress increase in the long term based on element-element interaction calculations governed by Okada's implementation of Green's functions. During the rupture (earthquake) phase elements may fail and release stress based on a combination of static and dynamic stress thresholds. The behavior of the system is determined by interactions between elements from the Green's function and the stress release from elements during events. As shown in the figure, we use the mesher in VQ to mesh the fault into segments and construct a Taiwan fault model. Based on the Taiwan fault model, VQ yield a simulated earthquake data. The recurrence time obtained from the simulated data and confirmed with geology data is important to Probabilistic Seismic Hazard Analysis and the seismic pattern before large event is helpful on detecting seismic precursors.

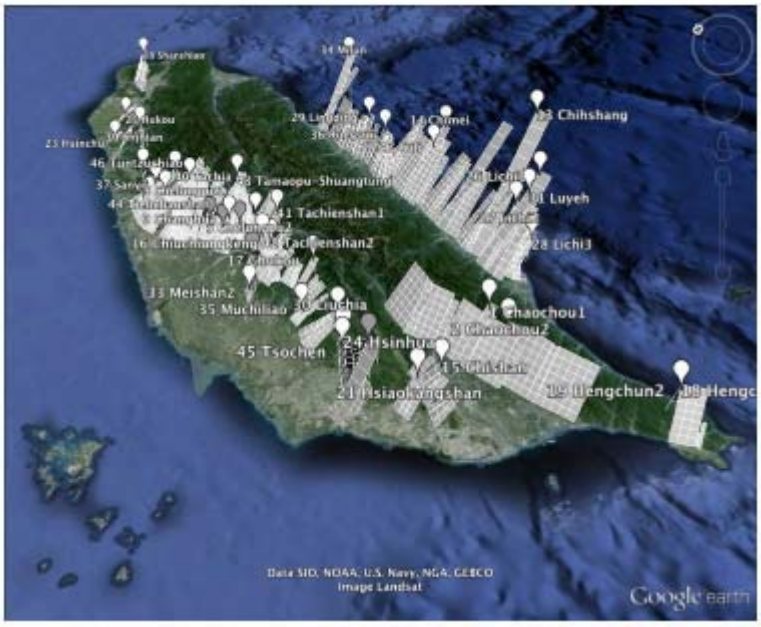

Map of Taiwan fault model.

CIG Code(s): Virtual Quake

The Virtual Quake earthquake simulator: A simulation based forecast of the El Mayor-Cucapah region and evidence of earthquake predictability

M.R. Yoder[1], K.W. Schultz[1], E.M. Heien[2], J.B. Rundle[123], D.L. Turcotte[2], J.W. Parker[4], A. Donnellan[4]

[1] Dept. of Physics, University of California Davis
[2] Dept. of Earth and Planetary Sciences, University of California Davis
[3] Santa Fe Institute
[4] NASA Jet Propulsion Laboratory

Two significant challenges to earthquake forecasting and earthquake predictability science are 1) contemporary seismographic catalogs are short compared to recurrence intervals of large earthquakes (insufficient data), and 2) sequences of events from multiple rupture sources are difficult to separate from one another (data partitioning). We address these problems using the Virtual Quake (VQ) earthquake simulator. We present a framework for simulation based earthquake forecasting, and we show that, though the system as a whole behaves quite randomly, the recurrence of large *m>7* events may exhibit predictability on specific fault segments. We discuss these aspects of VQ specifically with respect to faults in the Salton Basin and near the El Mayor-Cucapah region in southern California USA and northern Baja California Norte, Mexico.

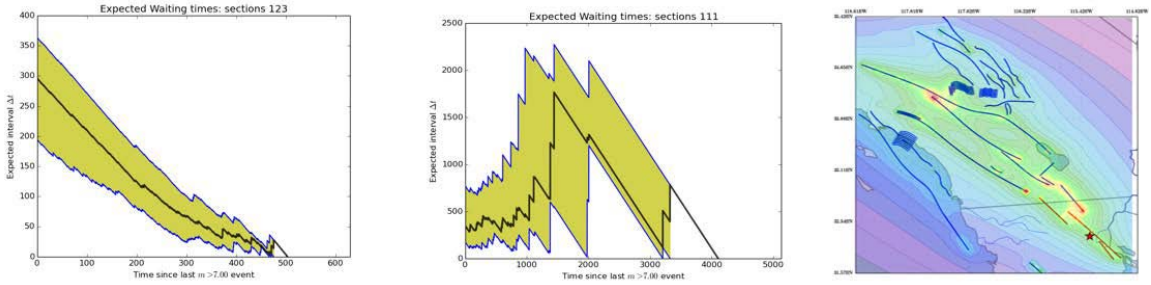

Left and center – Expected waiting times between m>7 earthquakes on two fault segments in the (simulated) El Mayor-Cucapah region. Note that for the center figure, the shortest recurrence interval is expected immediately following a large m>7 event. Right: Map of simulated seismicity rates based on a 10,000 year of a simulation. Off-fault seismicity is generated using an ETAS type aftershock formulation (Yoder et al. 2014).

CIG Code: Virtual Quake

Acknowledgements: This research supported by NASA grant NNX08AF69G and JPL Subcontract 1291967.

References

M.R. Yoder, J.B. Rundle, and M.T. Glasscoe, Near-field ETAS constraints and applications to seismic hazard assessment (2014), doi: 10.1007/s00024-014-0785-z

B. Education and Outreach

B.1 Workshops and Tutorials 2010-2015

Workshop	Date/Location	Other Sponsors	Early Career/ Total
GLADE Workshop	July 26-29, 2010 San Diego, California	Scripps Institute of Oceanography	29/95
Pylith and GALE Tutorials at EarthScope	May 17, 2011 Austin, Texas		10/17
Crustal Deformation Modeling Tutorial	June 20–24, 2011 (Virtual)		68/76
GALE/Underworld Tutorial at GSA	10/8/2011 Minneapolis, Minnesota	GSA	25/47
Crustal Deformation Modeling Workshop	June 18–22, 2012 Golden, CO	SCEC NASA	39/63
Mantle Convection and Lithospheric Dynamics Workshop	August 2, 2012 Davis, California		67/79
Geodynamo Developer Meeting	October 8-10, 2012 Boulder, Colorado		10/21
EarthCube Modeling Workshop for the Geosciences	April 22-23, 2013 Boulder, CO	CUAHSI CSDMS	19/31
Crustal Deformation Modeling Tutorial	June 24-28, 2013 (Virtual)		62/77
CIG/QUEST/IRIS Joint Workshop on Seismic Imaging of Structure and Source	July 14–17, 2013 Fairbanks, Alaska	QUEST IRIS	57/91
Implementing Solvers in CitcomCU and CitcomS	September 16-17, 2013 Davis, California		17
EarthScope Institute for Lithospheric Modeling Workshop	February 3–4, 2014 Tempe, Arizona	EarthScope	18/45
Joint CIG-CGU Mantle and Lithospheric Dynamics Workshop	May 4–7, 2014 Banff, Alberta Canada	CGU	18/45
ASPECT Hackathon	May 14–23, 2014 College Station, Texas	Texas A&M	13/14

B.1 Workshops and Tutorials 2010-2015 (continued)

Workshop	Date/Location	Other Sponsors	Early Career/ Total
Crustal Deformation Modeling Workshop	June 23–27, 2014 Stanford, California	SCEC	31/80
CIG Tutorials at CIDER	July 7–9, & 16, 2014 Santa Barbara, California	CIDER	41/81
ELSI Summer School	August 2–3, 2014 Tokyo, Japan	ELSI	21
Geodynamo Benchmarking Workshop	February 5-6, 2015 Boulder, Colorado		5/33
ASPECT Hackathon	May 19-30, 2015 Bodega, CA	UC Davis Bodega Marine Laboratory	19/24

B.2 Webinars

2012-13

October 11: Wolfgang Bangerth, PhDTexas A&M. *Using Existing Libraries to Improve and Solve Computational Problems*

November 15: Timo Heister, Ph.D, Texas A&M. *Modern Numerical Methods for Modeling Convection in the Earth´s Mantle*

January 10: Jed Brown, Ph.D., Argonne National Laboratory. *High Performance Implicit Solvers for Geodynamics*

March 21: Sylvain Barbot, PhD, Earth Observatory of Singapore. *Using Relax to probe the rheology of the lithosphere*

April 11: Sarah Minson, Ph.D, USGS. *Bayesian Earthquake Modeling*

May 16: Nick Featherstone, Ph.D., University of Colorado Boulder. *Stellar Scalable Pseudospectral Methods and the Geodynamo*

2013-2014

October 10: Scott King, PhD, VT. *The World Is Not Enough: Mantle Dynamics from a Planetary Perspective*

November 14: Giorgio Spada, PhD, Universita di Urbino. *Using SELEN to Solve the Sea Level Equation*

January 9: Oliver Kreylos, Ph.D., UC Davis. *Interactive Visualization for Scientific Data Analysis*

February 13: Hank Childs, Professor, University of Oregon. *Exascale Visualization: Why Things Will Change For You*

March 13: MacKenzie Smith, University Librarian, UC Davis. *Software and the Scholarly Record*

April 10: ASPECT Team. *ASPECT: Science Highlights*.

May 15: Jon Aurnou, Professor, UCLA. *CIG's Community Dynamo Code Development Project*

2014-2015

October 9: Anna Kelbert, Ph.D., Oregon State University. *Earth System Bridge: NSF's Earth-Cube entry point for solid Earth geosciences*

November 13: Jed Brown, Ph.D., Argonne National Lab. *Software Design and packaging for extensibility, provenance, and sharing*

January 15: Professor Louise Kellogg & Pierre Arrial, Ph.D., UC Davis. *Influence of numerical discretization on preferred thermal convection patterns in a 3D spherical shell*

February 12: Eric Heien, Ph.D., & Hiro Matsui, Ph.D, UC Davis. *Accuracy and Performance Benchmarks for Geodynamo Simulation*

March 12: Cedric Thieulot, Ph.D.; Anne Glerum, and Menno Fraters, University of Utrecht. *ASPECT: from benchmarking to 3D subduction applications*

April 9: Professor Lucy Flesch, Purdue University. *Work flows and 3D geodynamic simulations of the India-Eurasia collision zone*

May 14: Arben Pitarka, Ph.D., Stanley Ruppert, Ph.D., & Douglas Dodge, Ph.D., Lawrence Livermore National Lab. *Ground motion simulation, seismic imaging, large-scale time series processing, and Big Data technology for solving earth science problems*

C. Software

C.1 Software Best Practices

Summary

The CIG community has put forth the following standards for software best practices for its codes:

I. ***Minimum Best Practices.*** Required for all codes hosted, developed and distributed by CIG.

II. ***Standard Best Practices.*** Should be met by all codes developed by the CIG community. Codes which are deficient should have a plan of active development to achieve this level.

III. ***Target Best Practices.*** Should be a part of the development plan for all codes under active development by CIG.

Software Best Practices

I. Minimum Best Practices

Practices that all codes must follow in order to be accepted by the CIG community.

1. Licensing
    a. Open source license: GPL, MIT and BSD recommended
2. Version control
    a. Use of version control to manage code changes: git recommended
3. Coding
    a. Portability
        i. Code builds on Unix----like machines e.g. Linux and Darwin with free tools (compilers)
        ii. Well designed, portable build system: cmake, make, configure----*unix only* and setup.py
4. Configuration and Build – *none specified*
5. Testing
    a. Code includes tests to verify that it runs properly.
    b. Established benchmarks for accuracy and performance, if available.
6. User Workflow – *none specified*
7. Documentation
    a. Instructions for build and installation
    b. Description of physics implemented
    c. Illustration of how to use the code to solve scientific problems
    d. Sample, editable input files: example runs and cookbooks
    e. Documentation (glossary) of all I/O parameters including units or, if dimensionless, specify what scaling was used.
    f. Citable publication

II. Standard Best Practices

Practices that should be used by all codes developed within the CIG community. Codes not meeting all standards should be actively working to eliminate deficiencies.

1. Licensing ---- *no additional requirements*
2. Version control
    a. Differentiation between maintenance (bug fixes) and new development.
    b. Source tree limited to files necessary to build software and documentation and run small verification tests
3. Coding
    a. User----friendly specification of parameters (e.g. graphical user interfaces, human readable parameter files, etc.) outside of source code/specified at run time
    b. Use of standard file formats for input and output
    c. Development plan, updated yearly, with prioritization of new features and estimated timetable for their implementation
    d. Comments in code describing:
        i. Algorithms with appropriate references
        ii. Purpose of functions, objects, etc. and descriptions of arguments (inputs / outputs), groups of objects, and tutorials
    e. Modular design
        i. Balance use of external libraries (e.g. PETSc) to maximize reuse while minimizing dependencies and maintenance
        ii. Allow users to extend code, new features or alternative implementations, without destroying original functionality or modifying main branch
    f. Error trapping
        i. Informative error messages allowing the user to debug and correct
        ii. User errors should never result in a crash
        iii. Consistency checking to catch internal errors. See above. Internal errors are generally bugs or unintended uses.
    g. Scalable
        i. Use of distributed/parallel data structures
        ii. Messages used to transfer information (e.g. MPI) instead of using the file system
4. Configuration and Build
    a. Automation and portability of configuration and building
    b. Output all configuration and build options during runtime e.g. commit id, compiler options, checksum, etc.

5. Testing
    a. Code includes tests that verify (pass/fail) that it is "running properly".
6. User Workflow
    a. No rebuild required to run a different simulation (change input parameters)
    b. User specified directories and filenames for input and output
    c. Use of standard binary file formats (e.g., NetCDF, HDF5)
7. Documentation
    a. Developer documentation. Description of how to extend code in anticipated ways.
    b. User documentation
    c. Workflow examples for research applications

III. Target Best Practices

Desirable practices that developers should consider in defining long----term development priorities for codes developed within the CIG community. These go beyond the "Standard Best Practices" are important for long----term projects.

1. Licensing *no additional requirements*
2. Version Control
    a. New features added in separate branches
    b. Stable development (master) branches for rapid release of new features
3. Coding
    a. Functionality implement as a library rather than an application:
        i. Leverage alternative implementations via plugins
        ii. Extend library features in applications without modifying original code
        iii. Construct higher level applications using libraries as building blocks
    b. Output of provenance information (parameters used)
    c. Scalability
        i. Parallel access to inputs and outputs (e.g. HDF5)
    d. Checkpointing
4. Configuration and Build
    a. Ability to select compilers, optimization, additional build flags during configuration without modifying files under version control
    b. Permits multiple builds using the same source tree
    c. Permits code installation at central location

5. Testing
    a. Unit testing for code verification at a fine grain level
        b. Method of Manufactured Solutions for code verification at a coarse grain level
6. User Work Flow
    a. Specify requirements necessary to document workflow for reproducibility
7. Documentation
    a. Reproducibility
        i. Includes separate citation to code and or landing page.
        ii. Discoverable archive of previous release(s).
    b. Usage recommendations for implemented code features
    c. FAQs / knowled

C.2 The Repository

The CIG software repository on github (https://github.com/geodynamics) hosts the 31 geodynamics modeling packages developed, maintained, or archived by CIG. Six of these packages were donated (NEW) in the past five years. Statistics given are as reported by git. However, as some contributions or releases did not flow through git or its predecessor SVN, some statistics maybe under reported. For example, ASPECT as had 6 major releases beginning with v0.1 and closer to 30 contributors some of whom sent patches directly to the lead developers.

The Primary Developers for each code may reflect the original code developers and/or the current core development team.

Status indicates the software support category assigned. Software in CIG's open source library are assigned one of the following support categories:

Developed. Actively adding features to support improved science or performance by CIG (D_CIG) or by community contributors (D_CONTRIB).
Supported. Actively supported, maintained and upgraded by CIG (S_CIG) or by community contributors (S_CONTRIB).
Archive. No development activity; not supported. No commitment to updates. (A)

Developed Codes have been validated, passed benchmarks established by the appropriate community, and are leading edge codes in geodynamics. Developed codes may either be donated or developed by CIG Staff or the community. These codes are under active development or enhancements and often are actively supported by CIG through maintenance, technical assistance, training and documentation.

Supported Codes are mature codes that meet community standards but are no longer undergoing active development. Codes have been benchmarked and documented with examples and references such that they remain useful research tools. Supported codes include codes donated to CIG from members of our community. Minor changes such as bug fixes and binary upgrades are supported.

Archived Codes. Bug reports can be submitted via github but no resources are available for its development, maintenance, or support.

SHORT TERM CRUSTAL DYNAMICS

PyLith

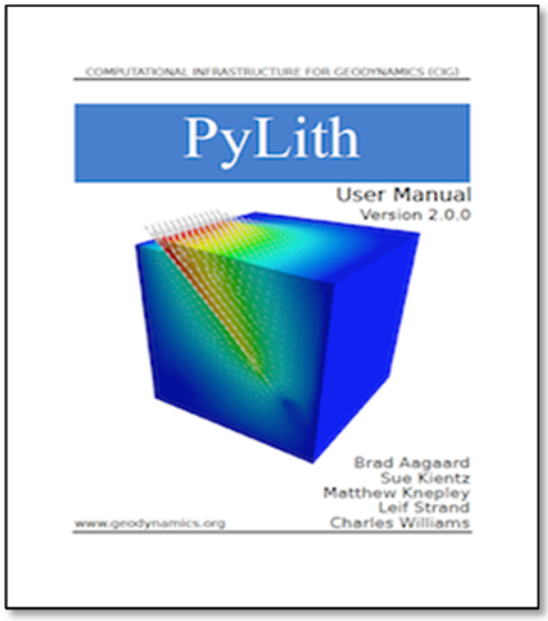

Description:
PyLith is a finite-element code for dynamic and quasistatic simulations of crustal deformation, primarily earthquakes and volcanoes.

Primary Developers:
Brad Aagaard, USGS; Matt Knepley, U. Chicago; Charles Williams, GNS Science

Status: D_CIG
Created: April 2004
Last Release: 2.1.0, 2015-02-19
# of Releases: 30
# of Commits: 5,634
# of Contributors: 4

RELAX *NEW

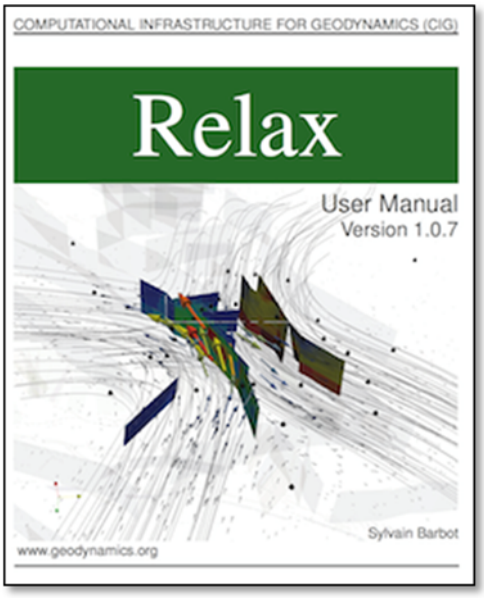

Description:
Relax implements a semi-analytic Fourier-domain solver and equivalent body forces to compute quasi-static relaxation of stress perturbation to solve problems in earthquake-cycle modeling and loading cycles of lakes and monsoons.

Primary Developers:
Sylvain Barbot, Earth Observatory Singapore

Status: D_CONTRIB
Created: January 2011
Last Release: 1.0.7, 2004-09-30
# of Releases: 9
# of Commits: 369
# of Contributors: 4

Virtual Quake *NEW

Description:

Virtual California is a boundary element code that performs simulations of fault systems based on stress interactions between fault elements to understand long-term statistical behavior.

Primary Developers:

Eric Heien, Kasey Schultz, and Michael Sachs, UC Davis

Status: D_CIG
Created: May 2014
Last Release: 1.1.0, 2014-10-27
# of Releases: 32
# of Commits: 511
# of Contributors: 3

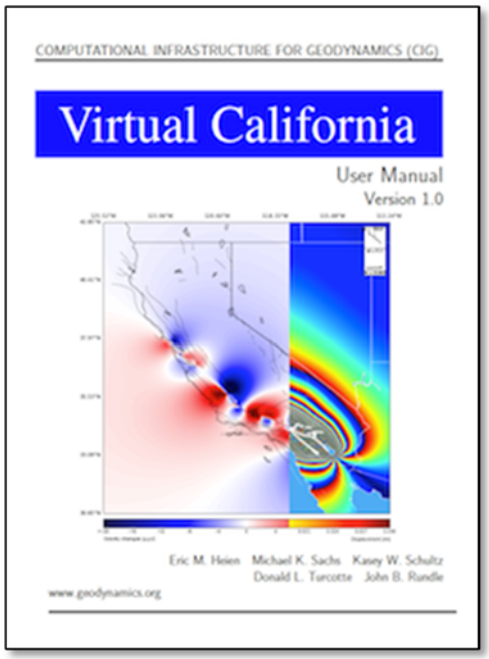

SELEN *NEW

Description:

The open source program SELEN solves numerically the "Sea Level Equation" for a spherical, layered, non-rotating Earth with Maxwell viscoelastic rheology. SELEN can compute vertical and horizontal surface displacements, gravity variations and sea level changes on a global and regional scale.

Primary Developers:

Giorgio Spada, Universita di Urbino; Daniele Melini, Istituto Nazionale di Geofisca e Vulcanologia

Status: S_CONTRIB
Created: January 2013
Last Release: 2.9.11, 2013-09-12
# of Releases: 2
# of Commits: 86
# of Contributors: 3

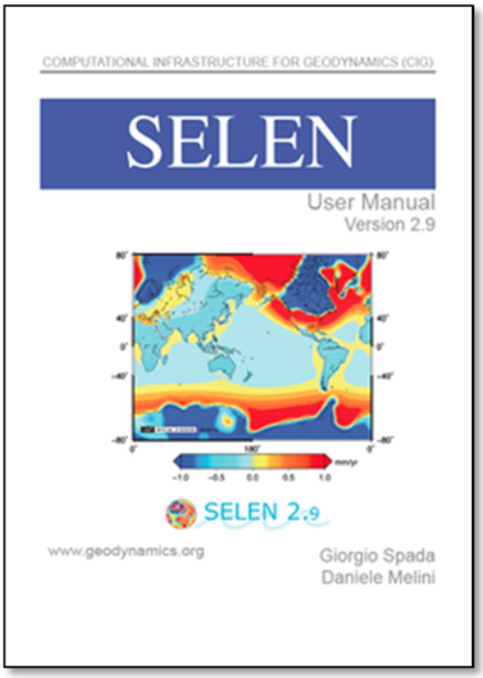

LithoMop
Description:
LithoMop is a finite element code for the solution of the visco-elastic/plastic deformation that was designed for lithospheric modeling problems.
A newer version of LithoMop, called PyLith, has been released by CIG.
Primary Developers: Matt Knepley, U. Chicago; Charles Williams, GNS Science
Status: A
Created: April 2004
Last Release: 0.7.2, 2006-04-12
# of Releases: 1
# of Commits: 1,079
# of Contributors: 3

LONG-TERM TECTONICS

GALE
Description:
Gale is a 2D/3D code for the long-term tectonics community. The code solves problems related to orogenesis, rifting, and subduction.
Primary Developers: Walter Landry, California Institute of Technology
Status: A
Created: March 2007
Last Release: 2.0.1, 2012-08-22
# of Releases: 6
# of Commits: 4,505
# of Contributors: 3

SNAC

Description:

Updated Lagrangian explicit finite difference code for modeling a finitely deforming elasto-visco-plastic solid in 3D. In SNAC, nodal velocities satisfying a weak-form of the momentum balance are obtained as the nodal solution.

Primary Developers: Eun-seo Choi, Michael Gurnis, and Colin Stark, California Institute of Technology

Status: A
Created: September 2008
Last Release: 1.2.0, 2010-04-14
# of Releases: 0
# of Commits: 188
# of Contributors: 2

Plasti

Description:

2D ALE (Arbitrary Lagrangian Eulerian) code. The code originated at Dalhousie University in Canada.

Primary Developers: Sean Willett and Chris Fuller, University of Washington.

Status: A
Created: June 2006
Last Release: 1.0.0, 2006-06-23
# of Releases: 1
# of Commits: 8
# of Contributors: 0

MANTLE CONVECTION

ASPECT
Description:
Finite element parallel code to simulate problems in thermal convection in both 2D and 3D models
Primary Developers: Wolfgang Bangerth, TAMU; Timo Heister, Clemson University
Status: D_CIG
Created: October 2011
Last Release: 1.2, 2015-01-26
# of Releases: 2
# of Commits: 2,944
# of Contributors: 15

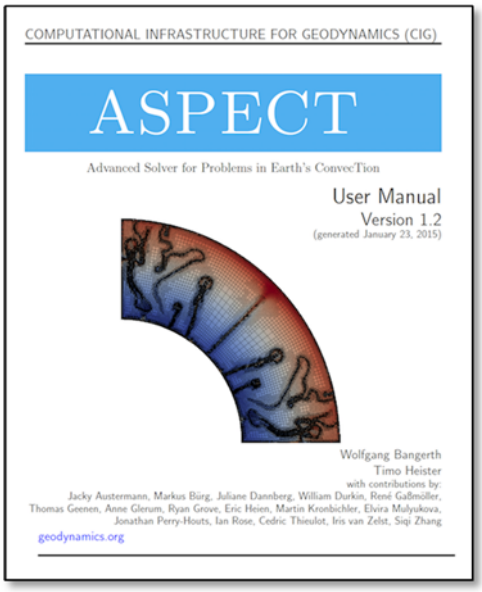

CitcomCU
Description:
CitcomCU is a finite element parallel code capable of modeling thermochemical convection in a three-dimensional domain appropriate for convection within the Earth's mantle.
Primary Developers: Shijie Zhong, University of Colorado, Boulder; and Eh Tan, California Institute of Technology
Status: D_CONTRIB
Created: October 2005
Last Release: 1.0.3, 2009-11-19
# of Releases: 4
# of Commits: 112
# of Contributors: 3

CitcomS

Description:

CitcomS is a finite element code designed to solve compressible thermochemical convection problems relevant to Earth's mantle.

Primary Developers: Eh Tan and Eunseo Choi, California Institute of Technology; Thorsten Becker, USC

Status: D_CONTRIB
Created: March 2003
Last Release: 3.3.1, 2014-11-19
# of Releases: 18
# of Commits: 2,043
# of Contributors: 6

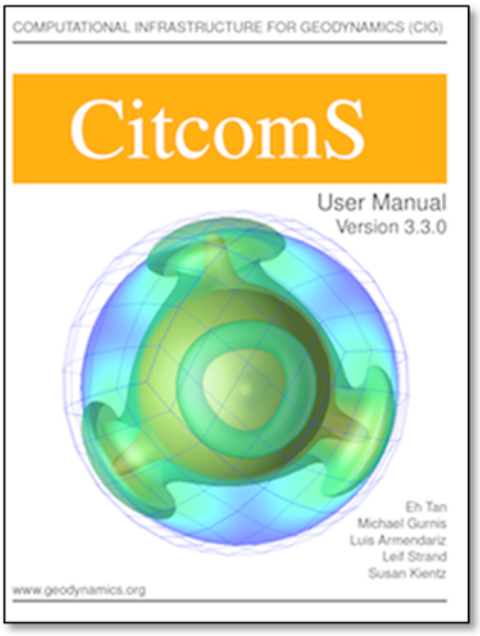

ConMan

Description:

ConMan is a finite element program for the solution of the equations of incompressible, infinite-Prandtl number convection in two dimensions.

Primary Developers: Scott King, VPI; Brad Hager, California Institute of Technology; Arthur Raefsky.

Status: S_CONTRIB
Created: June 2008
Last Release: 2.0.0, 2008-09-07
# of Releases: 18
# of Commits: 1
# of Contributors: 2

HC

Description:

HC is a global mantle circulation solver following based on code by Brad Hager, Richard O'Connell, and Bernhard Steinberger which can compute velocities, tractions, and geoid for simple density distributions and plate velocities.

Primary Developers: Thorsten Becker, USC; and Craig O'Neill

Status: A
Created: April 2006
Last Release: 1.0, 2009-04-15
# of Releases: 1
# of Commits: 133
# of Contributors: 3

Ellipsis3D

Description:

Ellipsis3d is a three-dimensional version of the particle-in-cell finite element code Ellipsis, a solid modeling code for visco-elastoplastic materials. The particle-in-cell method combines the strengths of the Lagrangian and Eulerian formulations of mechanics while bypassing their limitations.

Primary Developers: Richard Albert and Craig O'Neill

Status: A
Created: April 2007
Last Release: 1.0.2, 007-04-18
# of Releases: 3
# of Commits: 29
# of Contributors: 0

SEISMOLOGY

SPECFEM3D Cartesian

Description:

SPECFEM3D Cartesian simulates acoustic (fluid), elastic (solid), coupled acoustic/elastic, poroelastic or seismic wave propagation in any type of conforming mesh of hexahedra (structured or not.) It can, for instance, model seismic waves propagating in sedimentary basins or any other regional geological model following earthquakes. It can also be used for non-destructive testing or for ocean acoustics.

Primary Developers: Dimitri Komatitsch, CNRS/University of Aix-Marseille, France; Daniel Peter, University of Princeton; Elliot Sales de Andrade, University of Toronto; Carl Tape, University of Alaska, Fairbanks.

Status:	D_CIG
Created:	December 2002
Last Release:	*available as pull from github*
# of Releases:	8
# of Commits:	1,990
# of Contributors:	14

SPECFEM3D GLOBE

Description:

SPECFEM3D_GLOBE simulates global and regional (continental-scale) seismic wave propagation. Effects due to lateral variations in compressional-wave speed, shear-wave speed, density, a 3D crustal model, ellipticity, topography and bathymetry, the oceans, rotation, and self-gravitation are all included.

Primary Developers: Dimitri Komatitsch, CNRS/University of Aix-Marseille, France; Daniel Peter, University of Princeton; Elliot Sales de Andrade, University of Toronto; **Status:** D_CIG

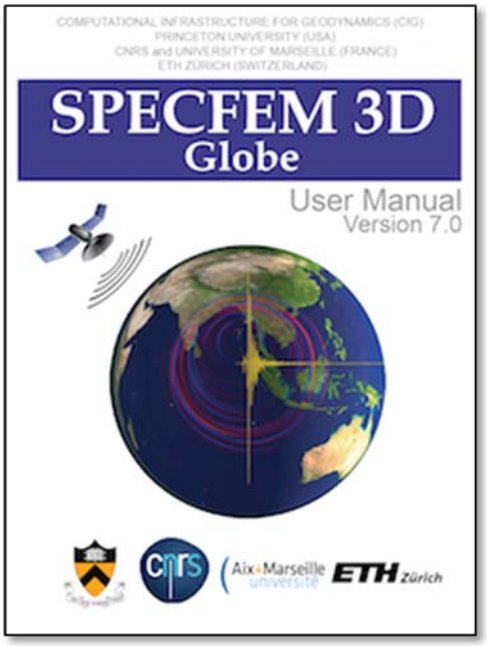

Created: November 2002
Last Release: *available as pull from github*
# of Releases: 24
# of Commits: 2,612
# of Contributors: 18

SPECFEM2D

Description:

SPECFEM2D simulates forward and adjoint seismic wave propagation in two-dimensional acoustic, (an)elastic, poroelastic or coupled acoustic-(an)elastic-poroelastic media, with Convolution PML absorbing conditions.

Primary Developers: Dimitri Komatitsch, CNRS/University of Aix-Marseille, France; Xie Zhinan; Elliot Sales de Andrade, University of Toronto

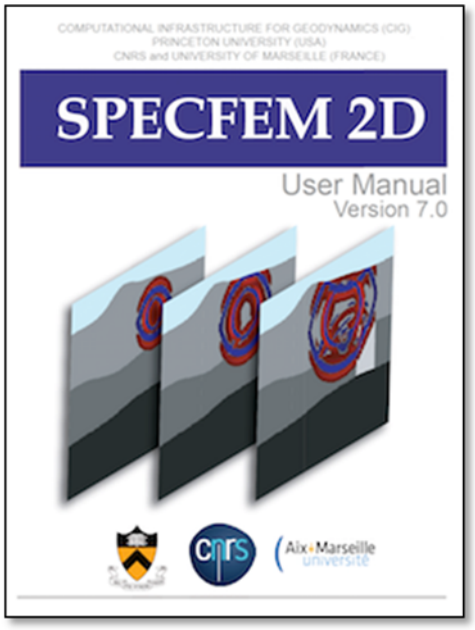

Status: D_CONTRIB
Created: February 2004
Last Release: *available as pull from github*
# of Releases: 0
# of Commits: 1,462
# of Contributors: 11

SPECFEM3D GEOTECH

Description:

SPECFEM3D_GEOTECH is an open-source command-driven software for 3D slope stability analysis and simulation of 3D multistage excavation based on the spectral-element method.

Primary Developers: Dimitri Komatitsch, CNRS/University of Aix-Marseille, France

Status: D_CONTRIB
Created: June 2011
Last Release: 1.1b, 2012-04-23
# of Releases: 0
# of Commits: 16
# of Contributors: 1

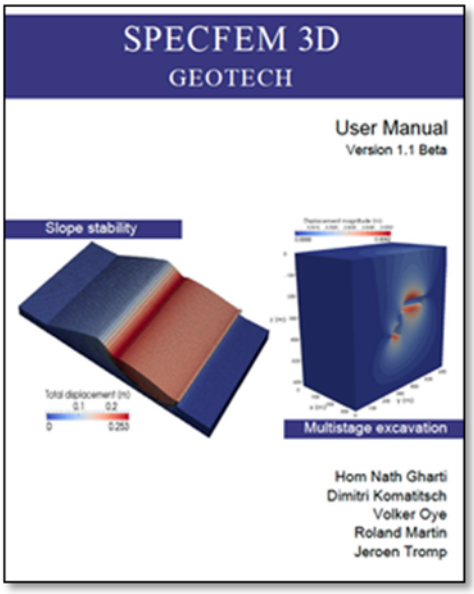

BurnMan *NEW

Description:

BurnMan is an open source mineral physics toolbox written in Python to determine seismic velocities for the lower mantle. BurnMan calculates the isotropic thermoelastic moduli by solving the equations-of-state for a mixture of minerals defined by the user. The user may select from a list of minerals applicable to the lower mantle included or easily define one of their own.

Primary Developers: Timo Heister, Clemson University; Ian Rose, UC Berkeley; Sanne Cottaar, University of Cambridge; Robert Myhill, Bayerische Geoinstitut

Status: D_CONTRIB
Created: November 2012
Last Release: 0.7, 2014-06-24
# of Releases: 1
# of Commits: 1208
# of Contributors: 7

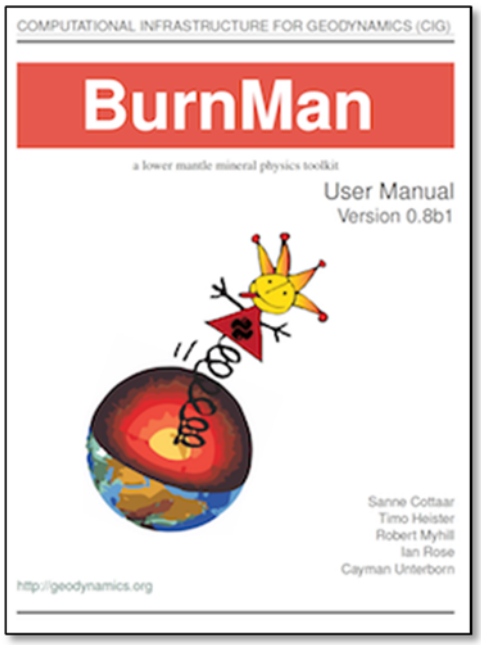

SW4 *NEW

Description:

SW4 implements substantial capabilities for 3-D seismic modeling, with a free surface condition on the top boundary, absorbing super-grid conditions on the far-field boundaries, and an arbitrary number of point force and/or point moment tensor source terms. Each source time function can have one of many predefined analytical time dependencies, or interpolate a user defined discrete time series.

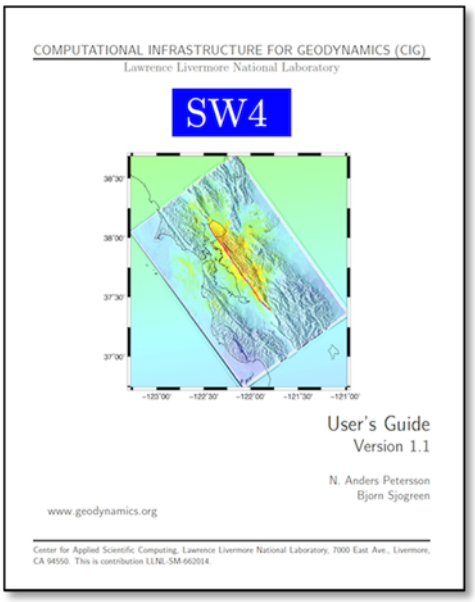

Primary Developers: N. Anders Petersson and Bjorn Sjogreen, Lawrence Livermore National Laboratory

Status:	D_CONTRIB
Created:	January 2012
Last Release:	1.1, 2014-10-22
# of Releases:	1
# of Commits:	32
# of Contributors:	3

AxiSEM *NEW

Description:

AxiSEM is a parallel spectral-element method for 3D (an-)elastic, anisotropic and acoustic wave propagation in spherical domains. It requires axisymmetric background models and runs within a 2D computational domain, thereby reaching all desired highest observable frequencies (up to 2Hz) in global seismology.

Primary Developers: Tarje Nissen-Meyer, Oxford University; Martin van Driel, ETH Zurich; Simon Stahler, LMU München; Kasra Hosseini, LMU München

Status: D_CONTRIB
Created: November 2011
Last Release: 1.1, 2014-08-27
# of Releases: 4
# of Commits: 1,451
# of Contributors: 5

SEISMIC_CPML

Description:

SEISMIC_CPML is a set of eleven open-source Fortran90 programs to solve the two-dimensional or three-dimensional isotropic or anisotropic elastic, viscoelastic or poroelastic wave equation using a finite-difference method with Convolutional or Auxiliary Perfectly Matched Layer (C-PML or ADE-PML) conditions.

Primary Developers: Dimitri Komatitsch, CNRS/University of Aix-Marseille, France
Status: S_CONTRIB
Created: April 2007
Last Release: *available as pull from github*
# of Releases: 6
# of Commits: 75
# of Contributors: 3

SPECFEM1D
Description:
SPECFEM1D simulates seismic wave propagation in a one-dimensional heterogeneous medium. It is a small code that allows users to learn how a spectral-element program is written.
Primary Developers: Dimitri Komatitsch, CNRS/University of Aix-Marseille, France; Elliot Sales de Andrade, University of Toronto
Status: S_CONTRIB
Created: February 2004
Last Release: *pull from github*
# of Releases: 1
# of Commits: 93
# of Contributors: 6

Flexwin
Description:
The FLEXWIN software package automates the time-window selection problem for seismologists.
Primary Developers: Alessia Maggi, University of Strasbourg; Carl Tape, University of Alaska, Fairbanks
Status: A
Created: June 2008
Last Release: 1.0.1, 2012-08-17
# of Releases: 0
# of Commits: 38
# of Contributors: 5

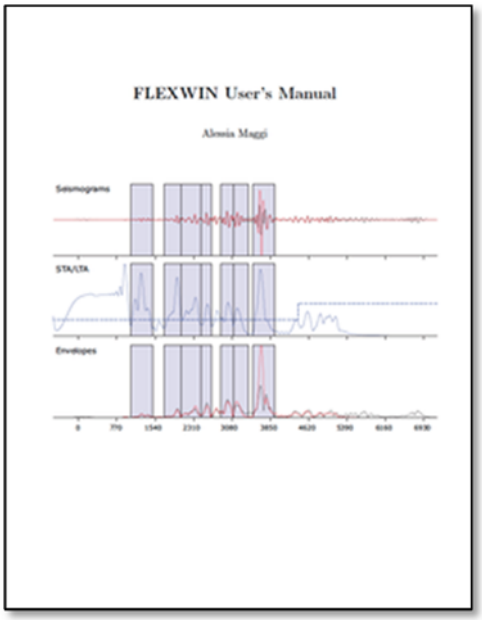

Mineos

Description:

Mineos computes synthetic seismograms in a spherically symmetric non-rotating Earth by summing normal modes.

Primary Developers: Guy Masters, California Institute of Technology

Status:	A
Created:	July 2006
Last Release:	1.0.2, 2011-07-06
# of Releases:	2
# of Commits:	67
# of Contributors:	2

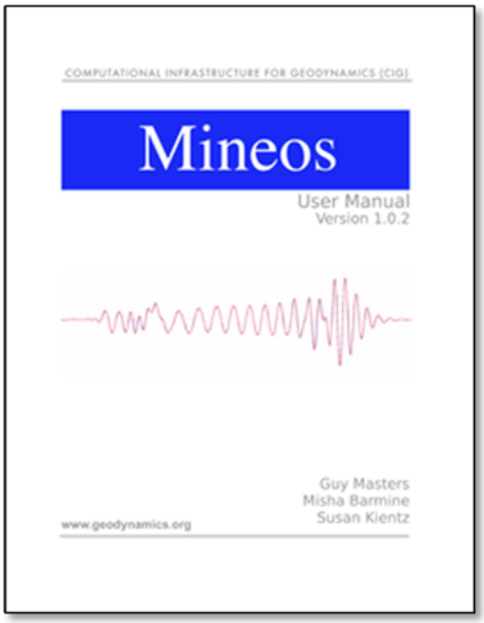

GEODYNAMO

Calypso
Description:
Calypso is a set of codes for MHD dynamo simulation in a rotating spherical shell using spherical harmonics expansion methods.
Primary Developers: Hiroaki Matsui, UC Davis
Status: D_CIG
Created: September 2013
Last Release: 1.1.1, 2014-03-24
# of Releases: 7
# of Commits: 138
# of Contributors: 2

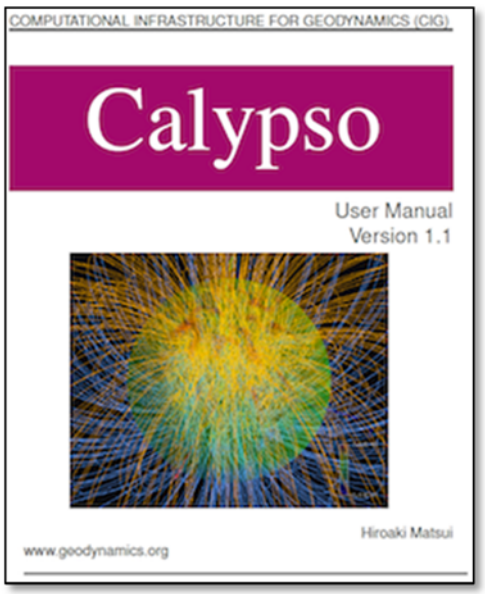

MAG
Description:
MAG is a serial version of a rotating spherical convection/magnetoconvection/dynamo code
Primary Developers: Gary Glatzmaier, UC Santa Cruz; Uli Christensen; Peter Olson, John Hopkins University
Status: A
Created: September 2013
Last Release: 1.0.2. 2007-05-18
# of Releases: 3
# of Commits: 137
# of Contributors: 1

COMPUTATIONAL SCIENCE

Nemesis
Description:
Required for Pylith. Nemesis simply installs a pair of Python interpreters ('nemesis' and 'mpinemesis') which incorporate MPI and include Pythia's "_mpi" module.
Primary Developers: Brad Aagaard, US Geological Survey
Status: S_CIG
Created: July 2007
Last Release: 1.1.0, 2013-0-9-26
# of Releases: 3
# of Commits: 14
# of Contributors: 1

Pythia
Description:
Pythia refers to the Pyre framework and a collection of packages that interact with it, such as an interface to the ACIS solid modeling package.
Primary Developers: Brad Aagaard, US Geological Survey
Status: S_CIG
Created: July 2006
Last Release: 0.8.1.16, 2013-09-26
# of Releases: 14
# of Commits: 154
# of Contributors: 3

Cigma
Description:
The CIG Model Analyzer (Cigma) is a suite of tools that facilitates the comparison of numerical models, and performs error analysis, benchmarking, and code verification.
Primary Developers: Luis Armendariz, California Institute of Technology
Status: A
Created: November 2007
Last Release: 1.0.0, 2009-05-04
# of Releases: 1
# of Commits: 594
# of Contributors: 2
Exchanger
Description:

Exchanger is a package containing several C++ base classes. These classes, when customized for a solver, can provide communication channels between solvers. This packaged is used by CitcomS for solver coupling.

Primary Developers: Eh Tan, California Institute of Technology

Status: A

Created: May 2004

Last Release: 1.0.1, 2009-06-04

# of Releases: 3

# of Commits: 61

# of Contributors: 3

D. Governance and Management

D.1 2015 Elected Committees

Executive Committee
Scott King, Virginia Tech, *Chairperson*
David Bercovici, Yale University
Bruce Buffett, UC Berkeley
Claire Currie, University of Alberta
Omar Ghattas, University of Texas, Austin

Science Steering Committee
Brad Aagaard, USGS chair
Tim Ahern, IRIS
Jon Aurnou, UCLA
Jed Brown, Argonne National Laboratory and University of Colorado, Boulder
Magali Billen, UC Davis
Dave May, ETH
Carl Tape, University of Alaska, Fairbanks
Jolante van Wijk, New Mexico Tech

D.2. Bylaws

By-Laws of Computational Infrastructure for Geodynamics (CIG)

As approved by the Electorate, February 28, 2005
As amended by the Electorate, December 12, 2006
As amended by the Electorate, January 9, 2012

PREAMBLE

The By-Laws of the Computational Infrastructure for Geodynamics (CIG) are adopted by the Member Institutions for the purpose of conducting CIG business in a collegial manner. They should not be construed as overriding the standard responsibilities and prerogatives of Principal Investigators or their respective institutions. However, situations and issues may arise from time to time for which resolution through standard procedures cannot be achieved. Consequently, should the Director and the Executive Committee not be able to reach agreement on any given issue, the Director, as Principal Investigator on the core CIG grants/contracts, will ultimately retain full authority to make and implement decisions on core CIG programs and policies.

Article I Name

Section 1. Name: The name of the Organization is Computational Infrastructure for Geodynamics (abbreviated as CIG).

Article II Member Institutions

Section 1. Membership: Institutions that are both educational and not-for-profit, chartered in the United States, with a major commitment to research in Earth Science with a particular emphasis on geodynamics and computational geophysics, and related fields, including single or multiple campuses of multi-campus university systems, may become Members of the Organization. Governmental research laboratories with a close link to the academic research community in geodynamics and computational geophysics are also eligible for Membership. The current list of member institutions shall be maintained by the Director.

Section 2. Election: An institution applying for membership must be qualified as an educational and not-for-profit institution according to criteria adopted by the Electorate. Qualified institutions may be elected as members by the affirmative vote of two-thirds of the members of the entire Electorate, or by unanimous vote of the Executive Committee of CIG. The rights and privileges of Members with respect to participation in the scientific activities of CIG will be according to policies established by the Electorate.

Section 3. Foreign Affiliation: Institutions not chartered in the United States may be elected as Foreign Affiliates for an indefinite term by the affirmative vote of two-thirds of the members of the entire Electorate or by a unanimous vote of the Executive Committee of the Electorate. A Foreign Affiliate will be entitled to designate a nonvoting representative to the Electorate, and will be able to participate in all activities in the governance of CIG other than voting at business meetings as a regular CIG Member or serving in a position specifically restricted to Electors. The rights and privileges of Foreign Affiliates with respect to participation in the scientific activities of CIG will be according to policies established by the Electorate.

Section 4. Resignation or Removal: Any Member or Affiliate may resign at any time by giving written notice to the Chairperson of the Executive Committee or the Director of the Organization. Such resignation shall take effect at the time of receipt of the notice, or at any later time specified therein. Given sufficient cause, any Member may be removed by the affirmative vote of two-thirds of the Members of the entire Electorate.

Article III Electorate

Section 1. Powers: So long as they do not conflict with the responsibilities of Principal Investigators, power in the management of the affairs of the Organization is vested in the Electorate. To this end and without limitation of the foregoing or of its powers expressly conferred by these By-Laws, the Electorate shall have power to authorize such action on behalf of the Organization, make such rules or regulations for its management, create such additional offices or special committees and select, employ or remove such of its officers, agents or employees as it shall deem best. The Electorate shall have the power to fill vacancies in, and change the membership of, such committees as are constituted by it.

Section 2. Power of Appointment: The term "Executive Officer" referred to in Sections 3-6 shall mean a Senior Officer of a Member institution above or at the level of Department Head.

Section 3. Composition: The Electorate shall be composed of one person from each of the Member institutions. An Executive Officer of each such Member institution shall designate one Elector, who shall be the holder of an academic or permanent research staff appointment, with major responsibilities for instruction and/or research in the earth sciences, in a department, program or other organizational unit of such member institution.

Section 4. Term of Office: Each Elector shall continue in office until a successor is chosen and qualifies or until he or she dies, resigns or is removed by an Executive Officer of the member institution.

Section 5. Resignation: Any Elector may resign at any time giving written notice to the Chairperson of the Executive Committee or the Director of CIG. Such resignation shall take effect at the time of receipt of the notice, or at any later time specified therein.

Section 6. Alternate Electors: An Executive Officer of each Member institution may appoint from within the Member institution an alternate Elector to serve for the term specified by such appointment. In the absence of an Elector from any meeting of the Electorate, his or her alternate may, upon written notice to the Director of the Organization from the Elector or from a duly authorized representative of the Member institution of the Electorate, attend such meeting and exercise all the rights, powers and privileges of the absent Elector.

Article IV Meetings of the Electorate

Section 1. Annual Meeting: A meeting of the Electorate for the transaction of such other business as may properly come before it, shall be held once per year.

Section 2. Special Meetings: Special meetings of the Electorate may be called by the Chairperson of the Executive Committee or by the Director upon written request of at least four Electors or one-fifth (1/5) of the membership of the Electorate, whichever is greater.

Section 3. Place of Meetings: The Chairperson of the Executive Committee or the Director shall designate the place of the annual meeting or any special meeting and which shall be specified in the notice of meeting or waiver of notice thereof.

Section 4. Notice of Meetings: Notice of such meeting of the Electorate shall be given to each Elector by the Director, or by an officer directed by the Chairperson of the Executive Committee or the Director to give such notice, by delivering to him or her personally, by electronic means, or by first-class mail, postage prepaid, addressed to him or her at the address of his or her Member institution, a written or printed notice not less than thirty nor more than sixty days before the date fixed for the meeting. Notice of any meeting need not be given to any Elector, however, who submits a signed waiver of notice, whether before or after the meeting. The attendance of any Elector at a meeting without protesting prior to the conclusion of the meeting the lack of notice thereof shall constitute a waiver of notice by him or her. When a meeting is adjourned to another place or time, it shall not be necessary to give any notice of the adjourned meeting if the time and place to which the meeting is adjourned are announced at the meeting at which the adjournment is taken.

Section 5. Quorum: At all meetings of any committee of the Electorate a majority of the members of that committee shall constitute a quorum. For the purposes of election of Officers and Executive Committee members, a quorum shall be determined in accordance with Article VIII. If a quorum is not present, a majority of the Electors present may adjourn the meeting without notice other than by announcement at said meeting, until a quorum is present. At any duly adjourned meeting at which a quorum is present, any business may be transacted which might have been transacted at the meeting as originally called.

Section 6. Voting: Each Elector shall be entitled to one vote. Except as otherwise expressly required by law or these By-Laws, all matters shall be decided by the affirmative vote of a majority of the Electors present at the time of the vote, if a quorum is then present.

Section 7. Action without a Meeting: Any action required or permitted to be taken by the Electorate, or the Executive Committee, may be taken without a meeting if all Electors or the Executive Committee consent in writing to the adoption of a resolution authorizing the action. The resolution and the written consents thereto shall be filed with the minutes of the proceedings of the Electorate or the Executive Committee.

Section 8. Participation by Conference Telephone or Video Conference: In any meeting of the Electorate or any committee thereof, any one or more Electors or members of any such committee may participate by means of a conference telephone or similar communications equipment allowing all persons participating in the meeting to hear each other at the same time. Participation by such means shall constitute presence in person at a meeting.

Article V Officers

Section 1. Officers and Qualifications: The officers of the Organization shall consist of a Chairperson and a Vice Chairperson of the Executive Committee, and a Director and such other officers as the Electorate may from time to time establish and appoint. Unless otherwise specified by Electorate action, officers need not be Electors.

Section 2. Chairperson: The Chairperson of the Executive Committee shall, when

present, preside at all meetings of the Electorate and shall perform such other duties and exercise such other powers as shall from time to time be assigned by the Electorate. The Chairperson of the Executive Committee shall be an ex officio member of all CIG committees.

Section 3. Vice Chairperson: The Vice Chairperson of the Executive Committee shall preside, in the absence of the Chairperson, at all meetings of the Electorate and shall perform such other duties and exercise such other powers as shall from time to time be assigned by the Electorate.

Section 4. Director: Except as otherwise provided by the Electorate, the Director shall be the Chief Executive Officer of the Organization, and unless authority is given Electorate to other officers or agents to do so, he or she shall execute all contracts and agreements on behalf of the Organization. The Director shall be the Principal Investigator on proposals which fund the core CIG facility. It shall be his or her duty, insofar as the facilities and funds furnished to him or her by the Organization permit, to see that the orders and votes of the Electorate and the purposes of the Organization are carried out. In the absence of the Chairperson or the Vice Chairperson of the Executive Committee, the Director shall preside at meetings of the Electorate. The Director shall be a non-voting member of the Executive Committee.

Section 5. Election and Term of Office: The Chairperson and Vice Chairperson of the Executive Committee shall each be elected by the Electorate for a term not to exceed three years or until his or her successor is chosen and qualifies. The Chairperson of the Executive Committee shall not be eligible for reelection until another person shall have served an intervening term, or a portion of a term of more than one year, as Chairperson. All other officers of the Organization, with the exception of the Director, shall be elected by the Electorate for terms not to exceed three years or until their successors are chosen and qualify, and they shall be eligible for reelection. The Director shall be appointed by the Executive Committee.

Section 6. Resignation: Any officer may resign at any time by giving written notice to the Chairperson, the Vice Chairperson or the Director of the Organization. Such resignation shall take effect at the time of receipt of the notice, or at any later time specified therein.

Section 7. Vacancies: Any vacancy in any office may be filled for the unexpired portion of the term of such office by a vote of the Electorate.

Section 8. Removal: Any officer may be removed at any time either with or without cause by vote of the Electorate.

Article VI Executive and Other Committees

Section 1. Executive Committee of CIG: There shall be established an Executive Committee of CIG comprised of five voting members (the Chairperson, the Vice Chairperson, and three additional members elected by the Electorate) and two nonvoting members (the Director, and the Chairperson of the Science Steering Committee). The elected members of the Executive Committee shall have terms not to exceed three years or until his or her successor is chosen and qualified. Members of the Executive Committee may not simultaneously serve on of the Science Steering Committee.

Section 2. Powers of the Executive Committee of CIG: Unless otherwise provided by resolution adopted by the affirmative vote of a majority of the entire Electorate, the

Executive Committee may have and may exercise all the powers of the Electorate, except that it shall not have authority as to the following matters:

(a) the amendment or repeal of the By-Laws, or the adoption of new By-Laws;

(b) the amendment or repeal of any resolution of the Electorate, which by its terms shall not be so amendable or repealable; and

(c) the levying or assessment of fees and dues.

The responsibilities of the Executive Committee include coordination of activities, meetings, and workshops. The Executive Committee shall review and approve priorities for software development undertaken by CIG. In establishing these priorities, the Executive Committee will consider input obtained from the Electorate directly and from recommendations made by the Science Steering Committee.

At all meetings of the Executive Committee, the presence of a simple majority of its members then in office shall constitute a quorum for the transaction of business.

Section 3. Special Committees: The Electorate may create such special committees as may be deemed desirable, the members of which shall be appointed by the Chairperson of the Executive Committee from among the Electors, with the approval of the Executive Committee. Each such committee shall have only the lawful powers specifically delegated to it by the Electorate.

Section 4. Science Steering Committee: There will be standing committees as defined in Article VII for overseeing the major scientific and research programs to which the Organization provides scientific counsel and advice or management direction and fiscal recommendations.

Section 5. Other Committees: The Executive Committee may create committees other than Standing or Special committees to be Committees of the Organization. Such committees shall be appointed in such a manner as may be determined by the Executive Committee and shall have such lawful duties as may be specified by the Executive Committee. An individual or an institution may be a member of any such committee whether or not they are an Elector or officer of the Organization.

Article VII Science Steering Committee

In order to carry out and oversee CIG operations, a Science Steering Committee (SSC) shall be established. The members will be selected by the Electors and will serve terms up to three years duration. A committee will be formed according to Article VI, section 4 to determine and prioritize software development from the perspective of the Earth science and Computational science disciplines represented by the Electorate. This committee will evaluate the utility of software developed and delivered to the community by CIG. This committee will consider the community's needs and recommend changes in the levels of support of CIG development resources. The committee will formulate policies for evaluation of user proposals for CIG software development. At least twice per year, the committee shall report in writing to the Executive Committee priorities for software development and resource allocation.

Article VIII Elections

Section 1. Officers, Executive Committee, and Standing Committees: Officers, Executive Committee members, and Science Steering Committee members may be

elected by the Electorate at the Annual Meeting or by an E-mail Election, in accordance with the procedures established in this Article.

Section 2. Nominating Committee: No less than 90 days before the Annual Meeting or the E-mail Election, the Executive Committee shall appoint a Nominating Committee, which shall prepare a slate of one or more nominees for each position to be filled. The Nominating Committee shall solicit the Electors for the names of suggested nominees. Any candidate shall be placed on the slate by the Committee upon receipt of written nomination signed by three Electors at least 40 days before the Annual Meeting.

Section 3. Mailed notice of election and ballot: If the election is to be held at the Annual Meeting, the ballot prepared by the Nominating Committee shall be included in the Notice of Meeting. If the election is to be held by E-mail, then a copy of the ballot shall be mail to the Electorate not less than thirty nor more than sixty days before the date fixed for the E-mail Election.

Section 4. Election: If the election shall take place at the Annual Meeting, it shall include the opportunity for nominations to be made from the floor. Election shall be by written ballot, which may be cast in person by an Elector at the meeting, or may be submitted by mail, email, or facsimile, if received by the Vice-Chairman before the meeting. If the Election is by E-mail, then the ballot shall be sent to the Electorate ten (10) days before the date of the Election. Election shall be valid if ballots are received from one-half of the membership of the entire Electorate in accordance with this Article, even if a quorum is not present for the purpose of conducting other business.

Section 5. Method of Voting: In the election of officers, a valid ballot shall contain at most one vote for each office; election shall be decided in favor of the nominee receiving a plurality of votes. In the election of Executive and Science Steering Committee members, a valid ballot shall contain no more votes than vacancies being filled; election to each vacancy shall be determined in sequence in favor of those qualified nominees with the most votes.

Section 6. Counting of ballots: Ballots shall be counted by the Vice- Chairman and the Chair of the Nominating Committee.

Article IX Compensation

Section 1. Compensation: No Elector shall be paid any compensation for serving as Elector. All Electors may be reimbursed for the actual expenses incurred in performing duties assigned to them by the Electorate.

Article X Amendments to the By-Laws

Section 1. Amendments: All By-Laws of the Organization shall be subject to amendment or repeal and new By-Laws may be made by the affirmative vote of two-thirds of the entire Electorate at any annual or special meeting, the notice or waiver of notice of which shall have specified or summarized the proposed amendment, repeal or new By-Laws.

D.3. Organizational Chart